Determining the epigenetic synergy of a repurposed drug and identification of prognosis-related lncRNAs in liver cancer and hematologic malignancies

Doctoral thesis

to obtain a doctorate (MD/PhD)

from the Faculty of Medicine

of the University of Bonn

Yulu Wang

from Jiangxi/(PR) China

2023

Table of Contents

List of abbreviations

DNA	Deoxyribonucleic acid
DNMT	DNA methyltransferase
lncRNAs	long non-coding RNAs
ncRNAs	non-coding RNAs
sncRNAs	small non-coding RNAs
HBV	hepatitis B virus
HCV	hepatitis C virus
NASH	non-alcoholic steatohepatitis
NAFLD	nonalcoholic fatty liver disease
AFB1	aflatoxin B1
HCC	hepatocellular carcinoma
CCA	cholangiocarcinoma
AML	acute myeloid leukemia
CML	Chronic myeloid leukemia
ALL	Acute lymphocytic leukemia
CLL	Chronic lymphocytic leukemia
HDAC	Histone deacetylases
GPCRs	G protein-coupled receptors
RGS20	Regulator of G protein signaling 20

1. Abstract

Background: Epigenetics is crucial in cancer research, revealing its impact on diverse cancer types' development and progression. Epigenetic-targeting drugs show promise in improving patient outcomes, but addressing their potential side effects is also important. Liver cancer and hematological malignancies pose a significant global health burden with high incidence and mortality rates. Further research is needed to explore new treatments and targets for them. Drug repurposing, such as metformin, offers a promising approach by leveraging non-oncology drugs with anticancer effects and low side effects. This strategy holds potential for discovering new therapeutic options.

Aims: This dissertation explores the role of epigenetics in cancer by investigating two primary research objectives: 1) the potential benefits of repurposing market-available drugs for epigenetic therapy as novel anticancer treatments; 2) the identification of long non-coding RNAs (lncRNAs) in cancers for prognosis prediction and the identification of potential therapeutic targets.

Method: In the first publication, we investigated the anticancer properties of meticrane, a diuretic medication, in liver cancer and hematological malignancies. Additionally, we assessed the synergistic effects of meticrane when combined with epigenetic drugs for cancer treatment. In our subsequent publications, we employed bioinformatic analysis to identify potential lncRNAs associated with the survival of cancer patients.

Results: Meticrane demonstrated anticancer effects in liver cancer and leukemia. Furthermore, it exhibited additive or synergistic effects when used in combination with epigenetic drugs against both liver cancer and leukemia. In addition, our research identified several lncRNAs that are associated with the prognosis of cancer patients.

Conclusion: The non-oncology drug meticrane exhibited an anticancer effect and demonstrated additive or synergistic effects when combined with epigenetic drugs in the treatment of cancers (liver cancer and leukemia). Additionally, our research identified prognosis-related lncRNAs with potential applications as prognostic predictors and therapeutic targets, thereby enhancing our knowledge of cancer biology and expanding the scope of therapeutic possibilities.

2. Introduction

2.1 Background:

2.1.1 Epigenetics

Conrad Hal Waddington coined the term "epigenetics" to describe the mechanisms of inheritance that go beyond standard genetics (Waddington, 2012). Epigenetics encompasses heritable traits that are independent of DNA sequence and involves three primary forms of regulation: DNA methylation, histone modification, and noncoding RNA activity (Loscalzo & Handy, 2014), and linked with cancers (Dhabhai, Sharma, Maciaczyk, & Dakal, 2022; Sharma, Liu, Herwig-Carl, Chand Dakal, & Schmidt-Wolf, 2021). DNA methylation, a extensively studied modification, is mediated by the enzymatic activity of DNA methyltransferase (DNMT), which adds a methyl group to the 5'-carbon of the cytosine pyrimidine ring in DNA (Miller & Grant, 2013). This process relies on three main methyltransferases: DNMT1, DNMT3A, and DNMT3B (Nishiyama & Nakanishi, 2021). In addition, the association between DNMTs (DNA methyltransferases) and cancers has been well-established (Chen et al., 2023; W. Zhang & Xu, 2017). In eukaryotic cells, DNA is structured into chromatin, which is composed of nucleosomes as the fundamental units. These nucleosomes consist of an octamer comprising four core histones (H3, H4, H2A, and H2B), with approximately 147 base pairs of DNA coiled around them (Audia & Campbell, 2016). Histone modifications, facilitated by specific enzymes, play a pivotal role in chromatin compaction, nucleosome dynamics, and transcriptional regulation. Perturbations in these processes can disrupt the balance of gene expression and are commonly observed in human cancers, resulting from various mechanisms such as gain or loss of function, overexpression, promoter hypermethylation, chromosomal translocation, mutations in histone-modifying enzymes/complexes, or even modifications in the histone modification sites themselves (Z. Zhao & Shilatifard, 2019). Our current understanding suggests that non-coding RNAs (ncRNAs) make up approximately 98% of the human genome, yet the exploration of this vast amount of information remains limited, with only a small fraction having been investigated to date (Le, Romano, Nana-Sinkam, & Acunzo, 2021). Non-coding RNAs (ncRNAs) encompass a broad range of lengths, varying from a few nucleotides to several thousands. Small non-coding RNAs (sncRNAs) are typically shorter than 200

nucleotides in length, while long non-coding RNAs (lncRNAs) form a separate category of RNA molecules that exceed 200 nucleotides in length. LncRNAs, exhibiting high heterogeneity, play a crucial role in regulating gene expression through diverse mechanisms, and their differential expression in tumors is directly associated with the transition from normal cells to tumor cells (Huarte, 2015). Some lncRNAs have been proved in the proliferation, growth or survival of cancers (Ghafouri-Fard, Ahmadi Teshnizi, Hussen, Taheri, & Zali, 2023; Salman et al., 2023; Su, Huang, & Li, 2023; H. Zhang et al., 2023). Moreover, the intriguing interplay between different epigenetic factors, such as miRNA/DNA methylation or miRNAs/lncRNAs, has garnered considerable attention (Bhattacharjee et al., 2023; Saviana et al., 2023). Therefore, the significance of epigenetics in human diseases, particularly cancer, cannot be overstated.

2.1.2 Liver cancer and hematologic malignancy

Deaths caused by liver cancer ranked fourth cancer death in the world and risk factors include hepatitis B virus (HBV), hepatitis C virus (HCV), alcohol, and non-alcoholic steatohepatitis (NASH) (Huang et al., 2022). NAFLD has emerged as the most prevalent liver disease worldwide, impacting approximately 38% of the global population, and while only a minority of NAFLD patients develop cirrhosis or hepatocellular carcinoma, the growing size of this population puts an increasing number of individuals at risk for these severe outcomes (Wai-Sun Wong, Ekstedt, Lai-Hung Wong, & Hagstrom, 2023). HBV and HCV as the main risk factors for liver cancer will might be replaced by NAFLD/NASH, and Aflatoxin B1 (AFB1) will be a predominant risk factor in the future (McGlynn, Petrick, & El-Serag, 2021). According to a study (Yoo et al., 2023), smoking has been demonstrated to increase the incidence of HCC in individuals with NAFLD. A recent investigation in England (Liao et al., 2023) reveal the following observations: 1) men exhibit a higher risk of liver cancer diagnosis compared to women. 2) Asian and Black African populations show a higher likelihood of HCC diagnosis compared to white British individuals. 3) Survival rates were worse in patients with CCA and other specified/unspecified liver cancers compared to HCC patients. Though, increasing studies revealed that more and more targets were found for liver cancer (Shu, Luo, Zhang, & Gao, 2023; Tang et al., 2023), the escalating incidence, mortality rates, and low survival rates of liver cancer pose a significant burden on the NHS, patients, and

caregivers (Liao et al., 2023). Therefore, additional researches on liver cancer are still required.

Hematologic malignancies, encompassing leukemia (such as ALL, CLL, AML, and CML), myeloma, and lymphoma (both Hodgkin's and non-Hodgkin's), represent a diverse group of malignant disorders affecting the blood, bone marrow, and lymph nodes, and they play a substantial role in contributing to the global burden of cancer (Keykhaei et al., 2021). A survey revealed the number of newly diagnosed cases and deaths for various hematologic malignancies in 2018: leukemia (437,033 new cases and 309,004 deaths), Non-Hodgkin lymphoma (509,590 new cases and 248,724 deaths), Multiple myeloma (159,985 new cases and 106,105 deaths), and Hodgkin lymphoma (79,990 new cases and 26,167 deaths) (Bray et al., 2018). These statistics clearly demonstrate the substantial impact of these diseases on both incidence and mortality rates, indicating their status as global health burden issues. Therefore, it is crucial to implement additional efforts/measures to prevent the occurrence of these diseases and enhance the survival rates of patients affected by them.

Recently, there has been growing evidence highlighting the promising relationship between epigenetics and liver cancer as well as hematological malignancies (Fernandez-Barrena, Arechederra, Colyn, Berasain, & Avila, 2020; Jasielec, Saloura, & Godley, 2014; Wang, Malnassy, & Qiu, 2021; A. Zhao, Zhou, Yang, Li, & Niu, 2023). These findings suggest that exploring the role of epigenetic mechanisms/targets in the development, progression and treatment of these diseases is of great importance, emphasizing the need for further research and investigation in this area.

2.1.3 Non oncology drug

The well-established understanding is that while anti-cancer/chemotherapy drugs are capable of eliminating cancer cells, they can also inflict damage on healthy cells, resulting in a plethora of side effects. Special attention has been devoted to testing non-oncology drugs, leading to the strategy of "drug repurposing," wherein drugs approved for other diseases are identified as potential cancer therapies to mitigate collateral damage (Papapetropoulos & Szabo, 2018; Z. Zhang et al., 2020). A recent article of interest presents a summary of various small molecule non-oncology drugs with therapeutic potential in cancer, providing insights into their putative targets and key

pathways pertinent to cancer treatment (Fu et al., 2022). Metformin, a well-known anti-diabetic drug, serves as a prominent example of non-oncology drug repurposing, with extensive research conducted across various cancer types (Kasznicki, Sliwinska, & Drzewoski, 2014; Zi et al., 2018). It has demonstrated its therapeutic potential in hepatocellular carcinoma (Cheng et al., 2023) and various hematological malignancies, including leukemia, myeloma, and lymphoma (Y. Zhang, Zhou, Guan, Zhou, & Chen, 2023). Therefore, exploring non-oncology drugs for the treatment of liver cancer and hematological malignancies holds promise in identifying additional potential therapeutic options that can benefit patients. Besides, studies (Bezu, Kepp, & Kroemer, 2022; Bridgeman, Ellison, Melton, Newsholme, & Mamotte, 2018) have demonstrated that certain non-oncology drugs with anticancer effects can influence epigenetic processes. Combining non-oncology drugs, which possess anticancer properties, with established epigenetic-targeting treatments for cancers represents a promising and innovative approach to enhance therapeutic efficacy and improve patient outcomes.

2.2 Aims

This dissertation aims to address two primary questions related to the role of the epigenetics in cancers. Firstly, it aims to investigate the potential benefits of novel anticancer treatments through drug repositioning focused on epigenetic therapy using market-available drugs. Secondly, it seeks to identify additional lncRNAs in cancers to improve the prediction of cancer patient prognosis and discover potential cancer targets. By exploring these areas, the study contribute to the advancement of epigenetic-based therapies and expand our understanding of cancer biology.

2.3 References

Audia, J. E., & Campbell, R. M. (2016). Histone Modifications and Cancer. *Cold Spring Harb Perspect Biol, 8*(4), a019521. doi:10.1101/cshperspect.a019521

Bezu, L., Kepp, O., & Kroemer, G. (2022). Impact of local anesthetics on epigenetics in cancer. *Front Oncol, 12*, 849895. doi:10.3389/fonc.2022.849895

Bhattacharjee, R., Prabhakar, N., Kumar, L., Bhattacharjee, A., Kar, S., Malik, S., . . . Kesari, K. K. (2023). Crosstalk between long noncoding RNA and microRNA in Cancer. *Cell Oncol (Dordr)*. doi:10.1007/s13402-023-00806-9

Bray, F., Ferlay, J., Soerjomataram, I., Siegel, R. L., Torre, L. A., & Jemal, A. (2018). Global cancer statistics 2018: GLOBOCAN estimates of incidence and mortality worldwide for 36 cancers in 185 countries. *CA Cancer J Clin, 68*(6), 394-424. doi:10.3322/caac.21492

Bridgeman, S. C., Ellison, G. C., Melton, P. E., Newsholme, P., & Mamotte, C. D. S. (2018). Epigenetic effects of metformin: From molecular mechanisms to clinical implications. *Diabetes Obes Metab, 20*(7), 1553-1562. doi:10.1111/dom.13262

Chen, M., Fang, Y., Liang, M., Zhang, N., Zhang, X., Xu, L., . . . Li, X. (2023). The activation of mTOR signalling modulates DNA methylation by enhancing DNMT1 translation in hepatocellular carcinoma. *J Transl Med, 21*(1), 276. doi:10.1186/s12967-023-04103-9

Cheng, Y., Zhan, P., Lu, J., Lu, Y., Luo, C., Cen, X., . . . Yin, Z. (2023). Metformin synergistically enhances the antitumour activity of Lenvatinib in hepatocellular carcinoma by altering AKT-FOXO3 signalling pathway. *Liver Int*. doi:10.1111/liv.15611

Dhabhai, B., Sharma, A., Maciaczyk, J., & Dakal, T. C. (2022). X-Linked Tumor Suppressor Genes Act as Presumed Contributors in the Sex Chromosome-Autosome Crosstalk in Cancers. *Cancer Invest, 40*(2), 103-110. doi:10.1080/07357907.2021.1981364

Fernandez-Barrena, M. G., Arechederra, M., Colyn, L., Berasain, C., & Avila, M. A. (2020). Epigenetics in hepatocellular carcinoma development and therapy: The tip of the iceberg. *JHEP Rep, 2*(6), 100167. doi:10.1016/j.jhepr.2020.100167

Fu, L., Jin, W., Zhang, J., Zhu, L., Lu, J., Zhen, Y., . . . Yu, H. (2022). Repurposing non-oncology small-molecule drugs to improve cancer therapy: Current situation and future directions. *Acta Pharm Sin B, 12*(2), 532-557. doi:10.1016/j.apsb.2021.09.006

Ghafouri-Fard, S., Ahmadi Teshnizi, S., Hussen, B. M., Taheri, M., & Zali, H. (2023). A review on the role of GHET1 in different cancers. *Pathol Res Pract, 247*, 154545. doi:10.1016/j.prp.2023.154545

Huang, D. Q., Singal, A. G., Kono, Y., Tan, D. J. H., El-Serag, H. B., & Loomba, R. (2022). Changing global epidemiology of liver cancer from 2010 to 2019: NASH is the fastest growing cause of liver cancer. *Cell Metab, 34*(7), 969-977 e962. doi:10.1016/j.cmet.2022.05.003

Huarte, M. (2015). The emerging role of lncRNAs in cancer. *Nat Med, 21*(11), 1253-1261. doi:10.1038/nm.3981

Jasielec, J., Saloura, V., & Godley, L. A. (2014). The mechanistic role of DNA methylation in myeloid leukemogenesis. *Leukemia, 28*(9), 1765-1773. doi:10.1038/leu.2014.163

Kasznicki, J., Sliwinska, A., & Drzewoski, J. (2014). Metformin in cancer prevention and therapy. *Ann Transl Med, 2*(6), 57. doi:10.3978/j.issn.2305-5839.2014.06.01

Keykhaei, M., Masinaei, M., Mohammadi, E., Azadnajafabad, S., Rezaei, N., Saeedi Moghaddam, S., . . . Farzadfar, F. (2021). A global, regional, and national survey on burden and Quality of Care Index (QCI) of hematologic malignancies; global burden of disease systematic analysis 1990-2017. *Exp Hematol Oncol, 10*(1), 11. doi:10.1186/s40164-021-00198-2

Le, P., Romano, G., Nana-Sinkam, P., & Acunzo, M. (2021). Non-Coding RNAs in Cancer Diagnosis and Therapy: Focus on Lung Cancer. *Cancers (Basel), 13*(6). doi:10.3390/cancers13061372

Liao, W., Coupland, C. A. C., Innes, H., Jepsen, P., Matthews, P. C., Campbell, C., . . . Hippisley-Cox, J. (2023). Disparities in care and outcomes for primary liver cancer in England during 2008-2018: a cohort study of 8.52 million primary care population using the QResearch database. *EClinicalMedicine, 59*, 101969. doi:10.1016/j.eclinm.2023.101969

Loscalzo, J., & Handy, D. E. (2014). Epigenetic modifications: basic mechanisms and role in cardiovascular disease (2013 Grover Conference series). *Pulm Circ, 4*(2), 169-174. doi:10.1086/675979

McGlynn, K. A., Petrick, J. L., & El-Serag, H. B. (2021). Epidemiology of Hepatocellular Carcinoma. *Hepatology, 73 Suppl 1*(Suppl 1), 4-13. doi:10.1002/hep.31288

Miller, J. L., & Grant, P. A. (2013). The role of DNA methylation and histone modifications in transcriptional regulation in humans. *Subcell Biochem, 61*, 289-317. doi:10.1007/978-94-007-4525-4_13

Nishiyama, A., & Nakanishi, M. (2021). Navigating the DNA methylation landscape of cancer. *Trends Genet, 37*(11), 1012-1027. doi:10.1016/j.tig.2021.05.002

Papapetropoulos, A., & Szabo, C. (2018). Inventing new therapies without reinventing the wheel: the power of drug repurposing. *Br J Pharmacol, 175*(2), 165-167. doi:10.1111/bph.14081

Salman, I. T., Abulsoud, A. I., Abo-Elmatty, D. M., Fawzy, A., Mesbah, N. M., & Saleh, S. M. (2023). The long non-coding RNA ZFAS1 promotes colorectal cancer progression via miR200b/ZEB1 axis. *Pathol Res Pract, 247*, 154567. doi:10.1016/j.prp.2023.154567

Saviana, M., Le, P., Micalo, L., Del Valle-Morales, D., Romano, G., Acunzo, M., . . . Nana-Sinkam, P. (2023). Crosstalk between miRNAs and DNA Methylation in Cancer. *Genes (Basel), 14*(5). doi:10.3390/genes14051075

Sharma, A., Liu, H., Herwig-Carl, M. C., Chand Dakal, T., & Schmidt-Wolf, I. G. H. (2021). Epigenetic Regulatory Enzymes: mutation Prevalence and Coexistence in Cancers. *Cancer Invest, 39*(3), 257-273. doi:10.1080/07357907.2021.1872593

Shu, J., Luo, P., Zhang, G., & Gao, Y. (2023). Identification of glutamyl-prolyl-tRNA synthetase as a new therapeutic target in hepatocellular carcinoma via a novel bioinformatic approach. *J Gastrointest Oncol, 14*(2), 636-649. doi:10.21037/jgo-23-247

Su, M., Huang, P., & Li, Q. (2023). Long noncoding RNA SNHG6 promotes the malignant phenotypes of ovarian cancer cells via miR-543/YAP1 pathway. *Heliyon, 9*(5), e16291. doi:10.1016/j.heliyon.2023.e16291

Tang, B., Wang, Y., Zhu, J., Song, J., Fang, S., Weng, Q., . . . Ji, J. (2023). TACE responser NDRG1 acts as a guardian against ferroptosis to drive tumorgenesis and metastasis in HCC. *Biol Proced Online, 25*(1), 13. doi:10.1186/s12575-023-00199-x

Waddington, C. H. (2012). The epigenotype. 1942. *Int J Epidemiol, 41*(1), 10-13. doi:10.1093/ije/dyr184

Wai-Sun Wong, V., Ekstedt, M., Lai-Hung Wong, G., & Hagstrom, H. (2023). Changing epidemiology, global trends and implications for outcomes of NAFLD. *J Hepatol*. doi:10.1016/j.jhep.2023.04.036

Wang, F., Malnassy, G., & Qiu, W. (2021). The Epigenetic Regulation of Microenvironment in Hepatocellular Carcinoma. *Front Oncol, 11*, 653037. doi:10.3389/fonc.2021.653037

Yoo, J. J., Park, M. Y., Cho, E. J., Yu, S. J., Kim, S. G., Kim, Y. J., . . . Yoon, J. H. (2023). Smoking Increases the Risk of Hepatocellular Carcinoma and Cardiovascular Disease in Patients with Metabolic-Associated Fatty Liver Disease. *J Clin Med, 12*(9). doi:10.3390/jcm12093336

Zhang, H., Ma, B., Li, N., Zhang, L., Xu, J., Zhang, S., . . . Zhang, B. (2023). SNHG1, a KLF4-upregulated gene, promotes glioma cell survival and tumorigenesis under endoplasmic reticulum stress by upregulating BIRC3 expression. *J Cell Mol Med*. doi:10.1111/jcmm.17779

Zhang, W., & Xu, J. (2017). DNA methyltransferases and their roles in tumorigenesis. *Biomark Res, 5*, 1. doi:10.1186/s40364-017-0081-z

Zhang, Y., Zhou, F., Guan, J., Zhou, L., & Chen, B. (2023). Action Mechanism of Metformin and Its Application in Hematological Malignancy Treatments: A Review. *Biomolecules, 13*(2). doi:10.3390/biom13020250

Zhang, Z., Zhou, L., Xie, N., Nice, E. C., Zhang, T., Cui, Y., & Huang, C. (2020). Overcoming cancer therapeutic bottleneck by drug repurposing. *Signal Transduct Target Ther, 5*(1), 113. doi:10.1038/s41392-020-00213-8

Zhao, A., Zhou, H., Yang, J., Li, M., & Niu, T. (2023). Epigenetic regulation in hematopoiesis and its implications in the targeted therapy of hematologic malignancies. *Signal Transduct Target Ther, 8*(1), 71. doi:10.1038/s41392-023-01342-6

Zhao, Z., & Shilatifard, A. (2019). Epigenetic modifications of histones in cancer. *Genome Biol, 20*(1), 245. doi:10.1186/s13059-019-1870-5

Zi, F., Zi, H., Li, Y., He, J., Shi, Q., & Cai, Z. (2018). Metformin and cancer: An existing drug for cancer prevention and therapy. *Oncol Lett, 15*(1), 683-690. doi:10.3892/ol.2017.7412

3. Publications

3.1 Publication 1: Non-oncology drug (meticrane) shows anti-cancer ability in synergy with epigenetic inhibitors and appears to be involved passively in targeting cancer cells

Yulu Wang[1], Amit Sharma[1,2], Fangfang Ge[1], Peng Chen[1], Yu Yang[3], Hongjia Liu[3], Hongde Liu[3], Chunxia Zhao[4], Lovika Mittal[5], Shailendra Asthana[5] and Ingo G.H. Schmidt-Wolf [1] *

[1]Department of Integrated Oncology, Center for Integrated Oncology (CIO), University Hospital Bonn, Bonn, Germany
[2]Department of Neurosurgery, University Hospital Bonn, Bonn, Germany
[3]State Key Laboratory of Bioelectronics, School of Biological Science and Medical Engineering, Southeast University, Nanjing, China
[4]School of Nursing, Nanchang University, Nanchang, China
[5]Translational Health Science and Technology Institute (THSTI), NCR Biotech Science Cluster, Faridabad, Haryana, India

Check for updates

Non-oncology drug (meticrane) shows anti-cancer ability in synergy with epigenetic inhibitors and appears to be involved passively in targeting cancer cells

Yulu Wang[1], Amit Sharma[1,2], Fangfang Ge[1], Peng Chen[1], Yu Yang[3], Hongjia Liu[3], Hongde Liu[3], Chunxia Zhao[4], Lovika Mittal[5], Shailendra Asthana[5] and Ingo G. H. Schmidt-Wolf[1*]

[1]Department of Integrated Oncology, Center for Integrated Oncology (CIO), University Hospital Bonn, Bonn, Germany, [2]Department of Neurosurgery, University Hospital Bonn, Bonn, Germany, [3]State Key Laboratory of Bioelectronics, School of Biological Science and Medical Engineering, Southeast University, Nanjing, China, [4]School of Nursing, Nanchang University, Nanchang, China, [5]Translational Health Science and Technology Institute (THSTI), NCR Biotech Science Cluster, Faridabad, Haryana, India

Emerging evidence suggests that chemotherapeutic agents and targeted anticancer drugs have serious side effects on the healthy cells/tissues of the patient. To overcome this, the use of non-oncology drugs as potential cancer therapies has been gaining momentum. Herein, we investigated one non-oncology drug named meticrane (a thiazide diuretic used to treat essential hypertension), which has been reported to indescribably improve the therapeutic efficacy of anti-CTLA4 in mice with AB1 HA tumors. In our hypothesis-driven study, we tested anti-cancer potential meticrane in hematological malignance (leukemia and multiple myeloma) and liver cancer cell lines. Our analysis showed that: 1) Meticrane induced alteration in the cell viability and proliferation in leukemia cells (Jurkat and K562 cells) and liver cancer (SK-hep-1), however, no evidence of apoptosis was detectable. 2) Meticrane showed additive/synergistic effects with epigenetic inhibitors (DNMT1/5AC, HDACs/CUDC-101 and HDAC6/ACY1215). 3) A genome-wide transcriptional analysis showed that meticrane treatment induces changes in the expression of genes associated with non-cancer associated pathways. Of importance, differentially expressed genes showed favorable correlation with the survival-related genes in the cancer genome. 4) We also performed molecular docking analysis and found considerable binding affinity scores of meticrane against PD-L1, TIM-3, CD73, and HDACs. Additionally, we tested its suitability for immunotherapy against cancers, but meticrane showed no response to the cytotoxicity of cytokine-induced killer (CIK) cells. To our knowledge, our study is the first attempt to identify and experimentally confirm the anti-cancer potential of meticrane, being also the first to test the suitability of any non-oncology drug

in CIK cell therapy. Beyond that, we have expressed some concerns confronted during testing meticrane that also apply to other non-oncology drugs when considered for future clinical or preclinical purposes. Taken together, meticrane is involved in some anticancer pathways that are passively targeting cancer cells and may be considered as compatible with epigenetic inhibitors.

Introduction

It has been well established that while anti-cancer/ chemotherapy drugs kill cancer cells, they can also damage the healthy cells, causing a plethora of side effects. To avoid this collateral damage, special attention has been paid to the concept of testing non-oncology drugs, prompting the strategy of "drug repurposing," i.e., drugs already approved for other diseases being identified as potential cancer therapies (1, 2). One of the best examples demonstrating the use of non-oncology drug repurposing is metformin, a classic anti-diabetic drug, that has been under intense investigation across multiple cancer types (3, 4). Of interest is a recent article summarizing several small molecule non-oncology drugs with therapeutic potential in cancer and discussing their putative targets and key pathways relevant to cancer treatment (5).

Notwithstanding all this new progress, it is still too early to definitively assess the success of these proposed potential drugs, although early indications point to positive results. Pushpakom and colleagues recently discussed the challenges being faced by the repurposing community and recommended some innovative ways to address them (6). As a broader concept, the testing of selective (computationally/dockings, high throughput screenings) non-oncology drugs in diverse cancer models, and how they may respond to individual epi(genomic) characteristics remain to be carefully evaluated. In particular, if they can be well combined with other clinically proven drugs/active compounds for cancer. For instance, the combination of epigenetic drugs with chemotherapeutic regimens has proven to be a synergistically relevant as treatment approach (7, 8). More importantly, if the newly selective drug is compatible with cancer immunotherapy related approach.

Considering this, herein, we investigated one non-oncology drug named meticrane (a thiazide diuretic used to treat essential hypertension), which undescribably improved the therapeutic efficacy of anti-CTLA4 in AB1-HA tumor-bearing mice (9). In this hypothesis-driven study, we tested the anti-cancer potential meticrane in hematological malignance (leukemia and multiple myeloma) and liver cancer cell lines. We further extend our analyses by assessing the additive/synergistic potential of meticrane with two epigenetic inhibitors (DNMT1/5AC and HDAC/CUDC-101) in these cells, which was further supported by the molecular docking analysis. Besides, we evaluated the compatibility of meticrane with cytokine-induced killer (CIK) cells, a clinically established effective adoptive immunotherapy approach. To our knowledge, our study is the first attempt to identify and experimentally confirm the anticancer potential of meticrane.

Materials and methods

Generation of PBMCs and CIKs

Both Peripheral Blood Mononuclear Cells (PBMCs) and Cytokine-induced killer (CIK) cells were generated, as described previously (10–13). To isolate PBMCs from healthy donors by gradient density centrifugation, Pancoll (Pan-Biotech, Aidenbach, Bavaria, Germany) was used. All donors included in our study were from the blood bank of the University Hospital Bonn. To generate CIK cells, fresh PBMCs were seeded at 3×10^6 cells/mL in a 75 cm^2 flask and 1000 U/ml IFN-γ (ImmunoTools GmbH, Aidenbach, Bavaria, Germany) was added after 2 hours. On the following day, 50 ng/ml anti-CD3 antibody (OKT, eBioscience, Thermo Fisher Scientific, Inc. San Diego, CA, USA), 600 U/ml IL-2 (ImmunoTools GmbH, Aidenbach, Bavaria, Germany) and 100 U/ml IL-1β (ImmunoTools GmbH, Aidenbach, Bavaria, Germany) were supplemented. Both PBMCs and CIK cells were cultured in RPMI-1640 medium (Pan-Biotech, Aidenbach, Bavaria, Germany) supplemented with 10% FBS (Sigma-Aldrich Chemie GmbH, Munich, Germany) and 1% penicillin/streptomycin (P/S) (Gibco, Schwerte, Germany), at 37°C, 5% CO$_2$, and humidified atmosphere. CIK cells were subcultured every 2-3 days with fresh medium supplemented with 600U/ml IL-2 (1×10^6 cells/ml). On completion of 14 days of expansion, the CIK cells were collected for the experiments.

Cell culture, meticrane compound and epigenetic inhibitors

We utilized seven cell lines in this study. The cell lines K562, SK-hep-1, HepG2, and CCD18co were purchased from the American Type Culture Collection (ATCC, Manassas, Virginia,

USA). Whereas the cell lines Jurkat, U266 and OPM2 were acquired from the German Collection of Microorganisms and Cell Cultures (DSMZ, Braunschweig, Germany). We cultured K562, U266, Jurkat, and OPM2 in RPMI1640 medium (Pan-Biotech, Aidenbach, Bavaria, Germany) supplemented with 10% FBS (Sigma-Aldrich Chemie GmbH, Munich, Germany) and 1% penicillin/streptomycin (P/S) (Gibco, Schwerte, Germany). While SK-hep-1, HepG2, and CCD18co cells were maintained in EMEM medium (Pan-Biotech, Aidenbach, Bavaria, Germany) supplemented with 10% FBS (Sigma-Aldrich Chemie GmbH, Munich, Germany) and 1% penicillin/streptomycin (P/S) (Gibco, Schwerte, Germany). Meticrane (Sigma-Aldrich Chemie GmbH, Munich, Germany) was dissolved in DMSO and stored at -20°C at a concentration of 200mM. The HDAC inhibitor CUDC-101 (Selleck Chemicals GmbH, Munich, Germany) and the selective HDAC6 inhibitor ACY1215 (Cayman Chemical, Ann Arbor, Michigan, US) was dissolved in DMSO and stored at -20°C at a concentration of 50mM. Also, DNMT1 inhibitor 5-Azacytidine (5AC) (STEMCELL Technologies Germany GmbH, Cologne, Germany) was dissolved in DMSO and stored at -20°C at a concentration of 25mM.

Cell viability assay and cells number counting assay

In case of suspension cells (K562, U266, OPM2, Jurkat, and PBMCs), the cells were seeded in 96-well flat-bottom plates and then immediately mixed with compounds (meticrane, CUDC-101, 5AC and ACY1215). For adherent cells (SK-hep-1, HepG2, and CCD18co), the drugs were added 4 hours later allowing the cells to adhere first. Considering the different growth rates of tumor cells, 0.5×10^4 K562 cells, 2×10^4 U266 cells, 2×10^4 OPM2 cells, 10×10^4 PBMCs, 0.5×10^4 Jurkat cells, 0.25×10^4 CCD18co cells, 0.3×10^4 SK-hep-1 cells, and 0.3×10^4 HepG2 cells were seeded. CCK8 assay (Dojindo EU GmbH, Munich, Germany) was used to determine the cell viability according to its manufacturer's instructions. In addition, based on the CCK8 results, the combined effects of meticrane and HDAC inhibitors (CUDC101, 5AC and ACY1215) were evaluated using the formula, as described elsewhere (14):

Combination index Q

$$= KE(a+b)/(KEa + KEb - KEa \times KEb)$$

KE represents the killing effect of drugs on cells, while a and b represent drug a and drug b. KE(a+b) means the killing effect of combination drug a and drug b.

According to the combination index Q value, the combined effects of meticrane and epigenetic inhibitors on tumor cells were classified as antagonism (< 0.85), additive (0.85 - 1.15) or synergism (> 1.15). The live cell count was performed using the Canto II flow cytometer (BD Biosciences, Heidelberg, Germany). Hoechst 33258 (Cayman Chemical, Ann Arbor, Michigan, US) was used to stain dead cells, and then precision count beads (BioLegend GmbH, Koblenz, Germany) were used to count the number of live cells.

Cell proliferation and apoptosis assays

To assess cell proliferation, 0.25μM CFSE (Cell Trace carboxyfl fluorescein succinimidyl ester) (Thermo Fisher Scientific, Eugene, USA) was used to stain 1×10^6 cells in PBS for 20 minutes at room temperature. While 1ul FITC-annexin (BioLegend GmbH, Koblenz, Germany) and 1ul eBioscience[TM] 7-AAD Viability Staining Solution (Thermo Fisher Scientific, Eugene, USA) were added to stain tumor cells (100ul volume) for 15mins at room temperature and then were used to assay cell apoptosis. In addition, CellEvent[TM] Caspase-3/7 Green Flow Cytometry Assay Kit (Thermo Fisher Scientific, Eugene, USA) was used to further evaluate the apoptosis and caspase 3/7 activation level. 0.5μM CellEvent[TM] Caspase-3/7 Green Detection Reagent and 1μM SYTOX[TM] AADvanced[TM] Dead Cell Stain were utilized to stain tumor cells at room temperature for 1h and 5 mins respectively. In these three experiments, 0.5×10^4 K562 cells, 0.5×10^4 Jurkat cells and 0.3×10^4 SK-hep-1 cells were seeded in 96-well flat-bottom plates for 3 days. Of note, adherent cells (SK-hep-1) were added to the wells and meticrane was added 4 hours afterwards. Flow cytometry was performed for these three experiments.

Cytotoxicity assay of CIK cells

0.25μM CFSE was used to stain tumor cells (1×10^6) in 1ml PBS, 20 min at room temperature. Subsequently, 1×10^4 cells of K562 were seeded in 96-well flat-bottom plates and then meticrane and 10×10^4 CIK cells (4h co-culture time), 10×10^4 CIK cells (24h co-culture time) and 20×10^4 CIK cells (24h co-culture time) were added respectively. Likewise, 1×10^4 SK-hep-1 cells were seeded in 96-well flat-bottom plates and 4 hours later meticrane and 40×10^4 CIK cells (4h coculture time), 10×10^4 CIK cells (24h coculture time) and 20×10^4 CIK cells (24h coculture time) were added. Flow cytometry was used to test the cytotoxicity of CIKs against tumors at 4 and 24 hours of coculture. The cytotoxicity was calculated as following formula: cytotoxicity (%) = ((TC-TT)/TC)×100. TC: percentage of live tumor cells in control tubes (tumor cells alone), TT: percentage of live tumor cells in test tubes (tumor cells + CIK cells).

RNA isolation and whole transcriptome analysis

K562 (1×10^5 cells), Jurakt (1×10^5 cells) and SK-hep-1 (0.6×10^5 cells) were seeded in six well plates. As previous described, meticrane was added promptly in K562 and Jurkat cells but in SK-hep-1 cells, it was introduced 4h later. RNA isolation was performed using the RNeasy plus mini kit (QIAGEN GmbH, Hilden, Germany) following the manufacturer's instructions. Whole transcriptome analysis (3'-mRNA sequencing) was performed at the NGS Core Facility in Bonn, Germany. The data was analyzed using Histat2 (mapping tool) and EdgeR2 (differential analysis tool). The cutoff value (logFC > 2 and FDR< 0.05) was

applied to select the differential genes between the untreated and treated meticrane groups. KEGG pathway enrichment analysis (R package: clusterProfiler) were performed on the basis of based on differential genes. The heatmap (R package: pheatmap) was used to show the comparative analysis of differential genes between the untreated and treated meticrane groups.

Identification of the potential targets of meticrane

To identify potential targets of meticrane, we used previously described methodology (15). Briefly, AML (Acute Myeloid Leukemia) and HCC (Hepatocellular carcinoma) specific gene expression data (log2 (FPKM+1)) (TCGA data from TCGA database, https://portal.gdc.cancer.gov/, project:TCGA-LAML and TCGA-LIHC) and survival data (TCGA data from Ucsc Xena database, https://xenabrowser.net/datapages/, cohort: GDC TCGA Liver Cancer (LIHC) and GDC TCGA Acute Myeloid Leukemia (LAML)) were utilized to imitate the clinical model. Using the TCGA data, we identified genes relevant to survival based on the following criteria: KM curve ($p< 0.001$), Cox regression ($p< 0.001$) and the difference in five-year survival between the low and high gene expression groups of more than 10%. Based on the HR (hazard ratio) value from the Cox regression, we further distinguish between genes with a high risk (poor prognosis) (HR > 1) and those with a low risk (good prognosis) (HR< 1). We then overlap differentially expressed genes (RNA-sequence data) with prognostic genes from TCGA patients' data. In particular, overlapping of low risk group with up-regulated genes and a high-risk group with down-regulated genes induced by meticrane treatment. All the overlapping genes were used to build protein-protein interaction (string: https://string-db.org/) and KEGG analysis (R package: clusterProfiler).

Molecular docking and molecular dynamics (MD) simulation

In addition, molecular docking was used to further explore the potential targets of meticrane, particularly focusing on known immune checkpoint (CTLA-4, PD-1, PD-L1, LAG-3, TIM-3, B7-H4, TIGIT, CD73) and epigenetic targets (DNMT1, HDACs). For this purpose, the crystal structures of the corresponding proteins were first extracted from the protein database (www.rcsb.org) and the respective proteins CTLA-4/1I8L, PD-1/4ZQK, PD-L1/6R3K, LAG-3/7TZH, TIM-3/7M3Z, B7-H4/4GOS, TIGIT/5V52, CD73/6TWA, DNA methyltransferase 1/3PTA, and Histone deacetylases (HDAC2/7JS8, HDAC3/4A69, HDAC4/2VQJ, HDAC6/5EDU, HDAC7/3ZNR, HDAC8/7JVU and HDAC10/7U3M were identified. Since for HDACs, three small molecules bound crystal structures were available, therefore, we used all of them to comprehensively analyze different binding modes of ligands in their respective pockets. The protein structures were prepared by using the protein preparation wizard (PPW) module of maestro (Schrodinger LLC, New York, NY, USA) was used to pre-process the structures (16–20). Then, the ligand (meticrane) was prepared

using Schrödinger suite (LLC, New York, NY, 2020) LIGPREP (module of maestro), which generates tautomers, and possible ionization states at the pH range 7 ± 2 using Epik (21) and also generates all the stereoisomers of the compound, if necessary (16). The optimization was done using the OPLS3 (Optimized Potentialsfor Liquid Simulations) force field (22). Finally, Glide module of Schrodinger was used to perform the molecular docking and Prime MM-GBSA for binding free energy quantification. The grids were generated using the centroid of co-crystals by using the Receptor Grid Generation panel in Glide. The most favorable ligand-receptor conformations for a drug complex provided by a docking study (18). Glide is a comprehensive and systematic search tool for the molecule of interest from the virtual libraries. The obtained docked poses were then subjected to short MD simulations to study their dynamicity in the pocket. Desmond v3.6 module from Schrodinger suite was used to perform the MD simulations. The systems were built *via* Systems builder using OPLS3 force field and solvated with TIP3P water solvent model. All the complexes were placed in the orthorhombic periodic boundary conditions with a size of repeating buffered units at 10Å. Counter ions were also added to neutralize the systems. An energy minimization step was done for each system for 100ps. The NPT ensemble was employed for the simulations with the Nose-Hover chain thermostat and the martyna-tobias-klein barostat. RESPA integrator was used with a time step of 0.002ps. For short range coulombic interactions, a 9.0 Å cut-off was considered. Bonds to hydrogen were constrained using the MSHAKE algorithm of Desmond. The coordinates were saved at intervals of 10 ps.

Statistical analysis

All experiments were performed in triplicate and repeated thrice. Besides, the experiments involving CIK cells were performed with three independent donors. FACS data were analyzed using FlowJo V10.6 software (FlowJo, LLC, Ashland, Oregon, U.S.A.). The mean values and standard deviations were used in the figures to demonstrate the experimental data. Also, figures and statistical analyses including one-way or two-way analyses of variance (ANOVA) with Bonferroni's *post-hoc* test and T-tests were performed using GraphPad Prism v.8.0 (GraphPad Soft-ware, Inc., San Diego, CA, U.S.A.). For bioinformatic data, the statistical analyses and figures were performed by R software. A $p< 0.05$ was considered as significant. *$p< 0.05$; **$p< 0.01$; ***$p< 0.001$; ****$p< 0.0001$; ns: not significant.

Results

Meticrane-induced alteration in the cell viability and proliferation is independent from the apoptosis signaling pathway

To investigate the anticancer effect of meticrane, all cancer cells were co-cultured with meticrane at a concentration of 0.06 to 1 mM at 72 h. The leukemia cells (K562 and Jurkat) were found to be more
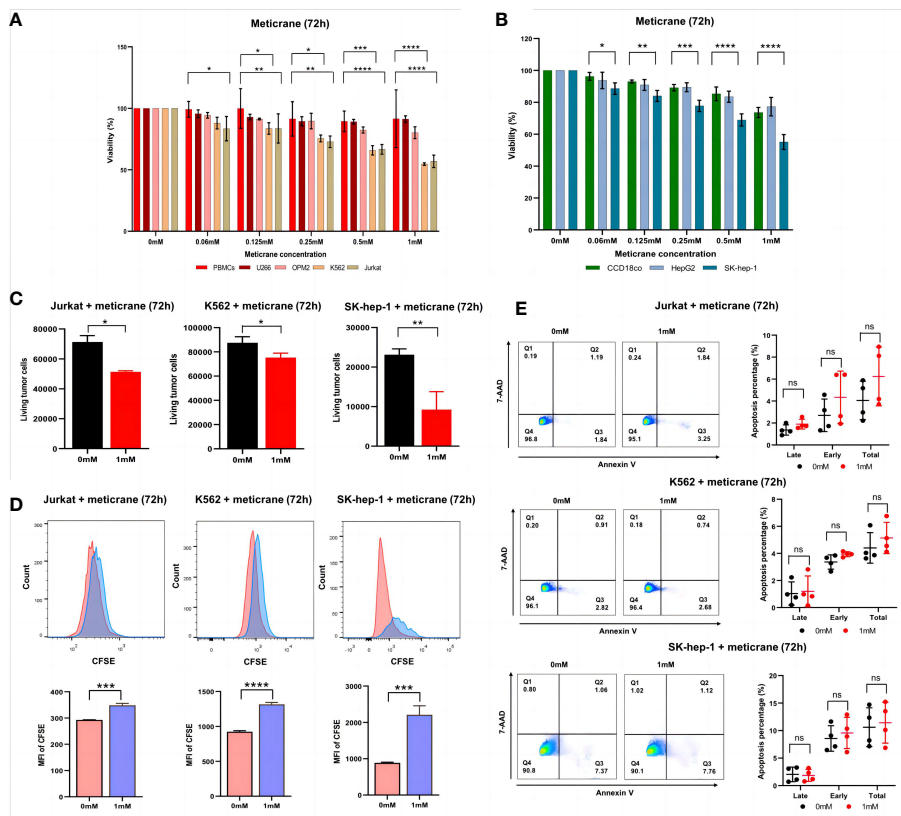
FIGURE 1

Effect of meticrane on the cell viability, alive cell number, proliferation and apoptosis of tumor cells. **(A)** CCK8 assay for cell viability for leukemia cell lines, myeloma cell lines and control cells. PBMCs (control cells), myeloma (U266 and OPM2) and leukemia (K562 and Jurkat) cells. P value were calculated by two-way ANOVA and Bonferroni's *post-hoc* test. All data were representative of at least three independent experiments (n≥3). **(B)** CCK8 assay for cell viability for liver cancer cell lines and control cells. CCD18co (control cells), and liver cancer (HepG2 and SK-hep-1) cells. P value were calculated by two-way ANOVA and Bonferroni's *post-hoc* test. All data were representative of at least three independent experiments (n≥3). **(C)** FASC assay for the relative alive cell number for Jurkat (left), K562 cells (middle) and SK-hep-1 cells (right). All data were representative of three independent experiments (n=3). P value were calculated by T tests. **(D)** Proliferation of Jurkat (left), K562 cells (middle) and SK-hep-1 cells (right). Data are mean ± SD of triplicate measurements; data are one representative of three independent experiments. T test were applied to calculate the p values. MFI, Mean Fluorescent Intensity. **(E)** The apoptosis of K562, Jurkat and SK-hep-1 cells. All data were representative of at four independent experiments (n=4). P value were calculated by two-way ANOVA and Bonferroni's *post-hoc* test. *p< 0.05, **p< 0.01, ***p< 0.001, ****p< 0.0001, ns, no significant.

sensitive to meticrane from 0.125 mM to 1 mM compared to the control cells (PBMCs) (Figure 1A). The cell viability was found to be decrease with increase in meticrane concentration in K562 (0.06mM: *p*=0.2384, 0.125mM: *p*=0.0264, 0.25mM: *p*=0.0323, 0.5mM: *p*=0.0005, 1mM: *p*<0.0001) and Jurkat (0.06mM: *p*=0.0103, 0.125mM: *p*=0.0073, 0.25mM: *p*=0.0017, 0.5mM: *p*<0.0001, 1mM: *p*<0.0001). However, myeloma cells (U266 and OPM2) (Figure 1A) showed no significant difference at any concentration compared to the controls (all *p* values at each concentration were more than 0.05). Likewise, in liver cells, SK-hep-1 cells showed significantly lower viability compared to the control cells (CCD18co cells), whereas HepG2 cells showed no significant difference (Figure 1B). The cell viability was found to be decrease with increase in meticrane concentration in SK-hep-1 (0.06mM: *p*=0.011, 0.125mM: *p*=0.0025, 0.25mM: *p*=0.0001, 0.5mM: *p*<0.0001, 1 mM: *p*<0.0001) and HepG2 (all *p* values at each concentration were more than 0.05) (Figure 1B). Considering cell viability is directly correlated to the viable/alive cells, we next investigated and found that the number of alive K562 cells

(*p*=0.026), Jurkat cells (*p*=0.0013), and SK-hep-1 cells (*p*=0.0011) significantly decreased in the meticrane (1mM)-treated group compared with the untreated group after 72 h (Figure 1C), suggesting that meticrane could reduce the number of tumor cells. In addition, the MFI (Mean fluorescent intensity) of CFSE (Cell Trace carboxyfl fluorescein succinimidyl ester) of K562 cells (*p*<0.0001), Jurkat cells (*p*=0.0002), and SK-hep-1 cells (*p*=0.0007) was also found to be higher in the presence of meticrane (Figure 1D), suggesting that the proliferation of these cell were inhibited due to meticrane. Interestingly, no significant difference was observed between early and late apoptosis in all observed groups of K562 cells, Jurkat cells and SK-hep-1 cells by using Annexine V and 7AAD dyes (Figure 1E). Besides, we checked both apoptosis and caspase 3/7 activation level potentially caused by meticrane, and found no alterations by using CellEvent™ Caspase-3/7 Green Flow Cytometry Assay Kit (Supplementary Figure 1). Both two apoptosis experiments suggested that the strongly reduced cell viability is independent of the apoptosis-related signaling pathway. It can therefore be concluded that meticrane may

induce the alteration of cell viability and proliferation in selected hematologic and liver cancer cells, through independent of the apoptosis signaling pathway.

Meticrane showed additive/synergistic effect with epigenetic inhibitors

Whether the effects of meticrane led to the alteration in cell viability and proliferation in leukemia cells (K562 and Jurkat) and liver cancer cells (SK-hep-1) can be enhanced with known epigenetic inhibitors, we assayed both the DNMT1 inhibitor (5AC) and HDAC inhibitor (CUDC-101) in these cells for 72 h using CCK8 assay (Figures 2A, B). To ensure consistency, meticrane (125μM) was combined with 5AC (31.25nM-1000nM) and CUDC -101 (6.25nM-200nM) against K562 and Jurkat cells, whereas CUDC -101 (0.125μM-4μM) or 5AC (0.313μM-10μM) was optimized against SK-hep-1 cells. Of interest, in all cell lines, the

addition of 5AC in combination with meticrane showed significant differences in Jurkat cells (all $p<0.0001$), K562 cells (1000nm: $p=0.0033$, 31.25-500nM: all p values< 0.0001) and SK-hep-1 cells (0.313-1.25μM: all $p<0.05$, 2.5μM: $p=0.0014$) compared to the 5AC alone. Notably, in Jurkat cells, meticrane (125μM) in combination with 5AC (250nM: $p=0.0499$, 500nM: $p=0.001$ and 1000nM: $p<0.0001$) showed higher inhibitory effect than meticrane alone (Figure 2A). This effect was also observed in K562 (125nM: $p=0.0104$, 250nM: $p=0.0004$, 500nM: $p<0.0001$ and 1000nM: $p<0.0001$) and SK-hep-1 cells (0.625μM: $p=0.0006$, 1.25μM-10μM: all $p<0.0001$). Like 5AC, CUDC -101 also in combination with meticrane showed significant differences in Jurkat cells (6.25nM: $p=0.0005$, 12.5nM: $p=0.0019$, 25nM: $p=0.0018$, 50nM: $p=0.0221$), K562 cells (6.25nM-25nM: all $p<0.0001$, 50nM: $p=0.0002$, 100nM: $p<0.0001$, 200nM: $p=0.0016$), and SK-hep-1 cells (0.125μM: $p<0.0001$, 0.25μM: $p=0.0001$, 0.5μM: $p=0.0116$) compared to the CUDC-101 alone. The higher inhibitory effect of meticrane in combination with CUDC-101 was observed in Jurkat
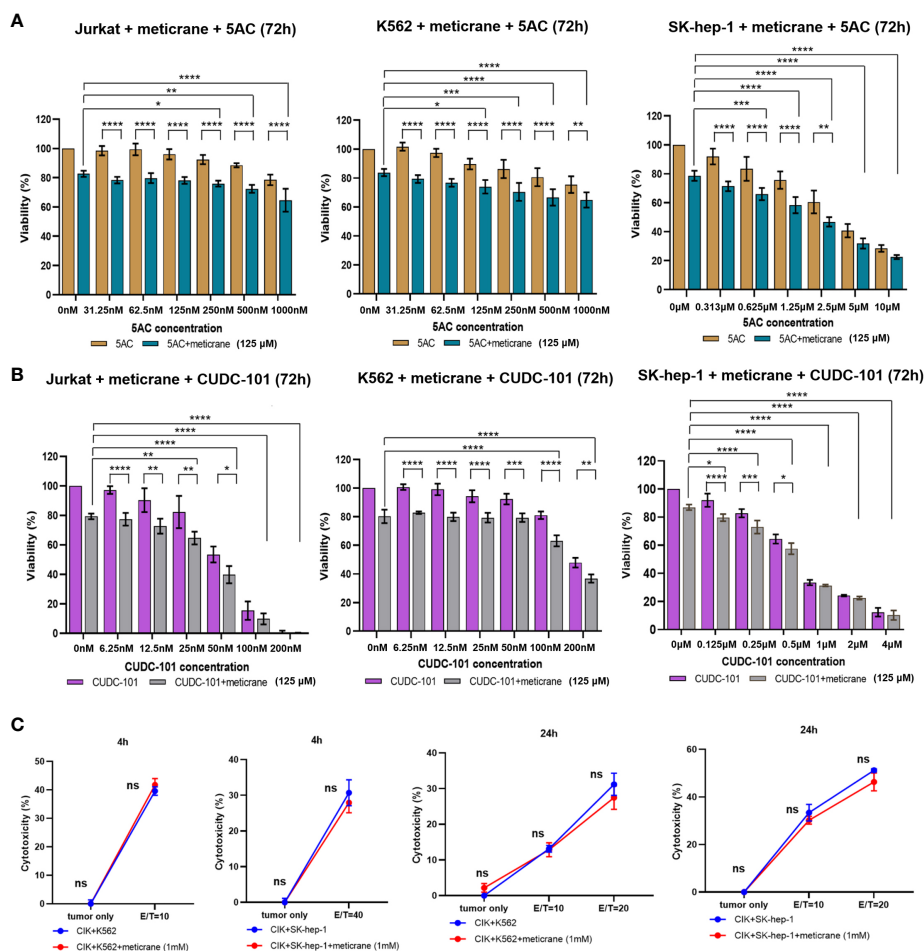

FIGURE 2

The combination effect of meticrane with epigenetic inhibitors or CIK cells. 5AC **(A)** or CUDC-101 **(B)** were used to test the cell viability (CCK8 assay) in Jurkat, K562 and SK-hep-1 cells. All data were representative of at least three independent experiments (n≥3). When comparing these two groups (no meticrane group vs. combined meticrane group), p-values were calculated using two-way ANOVA and Bonferroni's *post-hoc* test. When comparing the different dose in the group with meticrane, the p-value was calculated using a one-way ANOVA and the Bonferroni *post-hoc* test. **(C)** Cytotoxicity of CIK cells with/without meticrane against K562 and SK-hep-1 cells at 4 hours (left) and 24 hours (right) point time. Data are mean ± SD of triplicate measurements; data are one representative of three independent experiments. T test (4h) and two-way ANOVA (Bonferroni's *post-hoc* test) (24h) were applied to calculate the *p* values. *p<0.05, **p<0.01, ***p<0.001, ****p<0.0001. ns, no significant.

cells (25nM: p=0.0033, 50nM-200nM: all p<0.0001), K562 (100nM: p<0.0001, 200nM: p<0.0001) and Sk-hep-1 cells (0.125μM: p=0.0126, 0.25μM-4μM: p<0.0001) compared to meticrane alone. We also calculated the combination index Q values of meticrane with different concentrations of CUDC101 or 5AC on tumor cells (K562, Jurkat and SK-hep-1), and found mainly the additive/synergetic effects (Tables 1, 2).

Meticrane showed no compatibility with cytokine-induced killer cells

To further investigate the potential effect of meticrane with immunotherapy, cytokine-induced killer cells (CIKs) were assessed with meticrane. Meticrane (1mM) in combination with CIK cells was tested against K562 cells and SK-hep-1 cells. In particular, meticrane did not change the cytotoxicity of CIKs against K562 cells (p=0.2391) and SK-hep-1 cells (p=0.424) tested at time point 4h (Figure 2C). Due to this different sensitivity of CIKs against K562 and SK-hep-1 cells at 4h, we applied a different E/T ratio for K562 (E/T=10) and SK-hep-1 (E/T=40). Likewise, meticrane did not change the cytotoxicity of CIKs against K562 cells (E/T=10 p=1, E/T=20 p=0.1548) and SK-hep-1 cells (E/T=10 p=0.344, E/T=20 p=0.0673) tested at time point 24h (Figure 2C). Of note, as shown in the tumor only group in Figure 2C at 4h and 24 time point, meticrane alone (without CIKs) did not show cytotoxicity against

K562 (4 hours p=1, 24 hours p=0.6757) or SK-hep-1 cells (4 hours p=1, 24 hours p=1) at either 4 hours or 24 hours (Figure 2C). Overall, meticrane showed no compatibility with cytokine-induced killer cells.

Meticrane exerts no effect on cancer-associated signaling pathways in cancer cells

A genome-wide transcriptional analysis was performed to investigate the transcriptional changes in the cells treated with meticrane (Figures 3A-C). Based on differential genes between untreated and treated meticrane groups, we obtained meticrane induced significantly upregulated/downregulated genes from leukemia cell lines (Jurkat: 1500 up-regulated and 1519 down-regulated, Supplementary Table 1; K562: 1521 up-regulated and 1237 down-regulated, Supplementary Table 2) and liver cancer cell line (SK-hep-1: 1195 up-regulated and 1557 down-regulated, Supplementary Table 3). Using KEGG enrichment analysis to identify the ten most enriched metabolic pathways, we found that the leukaemia cell lines (Jurkat and K562) were highly enriched in oxidative phosphorylation, mTOR signalling, RNA degradation and regulation of cancer-related metabolic pathways. For the liver cancer cell line (SK-hep-1), there was significant enrichment in ferroptosis, focal adhesion and signaling pathways that play an

TABLE 1 Combination index Q of meticrane with CUDC101 in K562, Jurkat and SK-hep-1 cells.

Jurkat			K562			SK-hep-1		
meticrane	CUDC101	Index Q	meticrane	CUDC101	Index Q	meticrane	CUDC101	Index Q
125μM	0nM	1.00	125μM	0nM	1.00	125μM	0μM	1.00
125μM	6.25nM	0.99	125μM	6.25nM	0.90	125μM	0.125μM	1.02
125μM	12.5nM	0.96	125μM	12.5nM	0.98	125μM	0.25μM	0.96
125μM	25nM	1.02	125μM	25nM	0.85	125μM	0.5μM	0.96
125μM	50nM	1.05	125μM	50nM	0.80	125μM	1μM	0.97
125μM	100nM	1.03	125μM	100nM	1.05	125μM	2μM	0.98
125μM	200nM	1.00	125μM	200nM	1.03	125μM	4μM	1.01

TABLE 2 Combination index Q of meticrane with 5AC in K562, Jurkat and SK-hep-1 cells.

Jurkat			K562			SK-hep-1		
meticrane	5AC	Index Q	meticrane	5AC	Index Q	meticrane	5AC	Index Q
125μM	0nM	1.00	125μM	0nM	1.00	125μM	0μM	1.00
125μM	31.25nM	1.17	125μM	31.25nM	1.39	125μM	0.313μM	1.03
125μM	62.5nM	1.14	125μM	62.5nM	1.26	125μM	0.625μM	0.99
125μM	125nM	1.06	125μM	125nM	1.05	125μM	1.25μM	1.03
125μM	250nM	1.02	125μM	250nM	1.07	125μM	2.5μM	1.02
125μM	500nM	1.03	125μM	500nM	1.03	125μM	5μM	1.00
125μM	1000nM	1.01	125μM	1000nM	0.95	125μM	10μM	1.00

important role in cancer regulation, such as protein processing in the ribosome and endoplasmic reticulum. Thus, meticrane showed no direct/predominant effect on cancer-related signaling pathways in leukemia cell lines, and a distant impact (i.e., pathways not directly involved in cancer) to cancer in liver cancer cells.
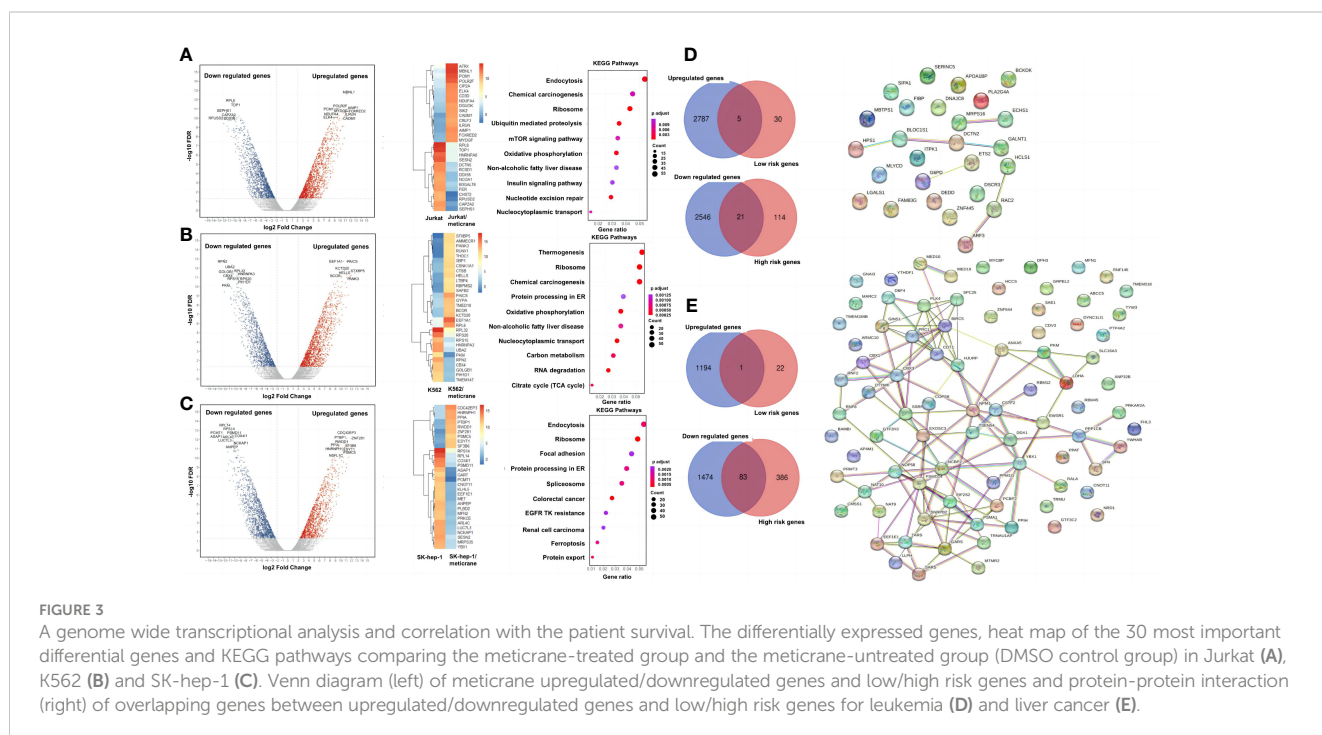
Meticrane induced differentially expressed genes showed association with survival-related genes in cancer

We identified survival relevant genes for AML (high risk genes: n=135 and low risk genes: n=35; Supplementary Table 4) and HCC (high risk genes: n=469 and low risk genes: n=23; Supplementary Table 5) were found using TCGA datasets. Subsequently, the low-risk genes were correlated with the up-regulated genes induced by meticrane (RNA-sequence) and the high-risk genes were correlated with the down-regulated genes induced by meticrane. In this pattern, we identified groups of overlapping genes in for AML (low-risk/up-regulated genes: n=5; high-risk/down-regulated genes: n=21) and HCC (low-risk/up-regulated genes: n=1; high-risk/down-regulated genes: n=83) (Figures 3D, E; Supplementary Table 6). By combining our *in vitro* data and information from TCGA's publicly available clinical portal, we described 110 genes (AML=26 genes; HCC=84 genes) (Supplementary Table 6) as potential targets of meticrane in these two cancers. We then established PPI (protein-protein interaction, cutoff interaction value: 0.4.) on these genes and found moderate to weak interactions in HCC and AML, respectively (Figures 3D, E). Using KEGG analysis of these selective genes, we also found that they are specifically involved in non-cancer pathways (Supplementary Figure 2).

Molecular docking and molecular dynamics (MD) simulation analysis confirmed the binding affinity of meticrane with known oncological targets

To further explore the potential targets of meticrane, we performed a molecular docking analysis by aligning Meticrane against known immune checkpoints (CTLA-4, PD-1, PD-L1, LAG-3, TIM-3, B7-H4, TIGIT, CD73) and epigenetic targets (DNMT1, HDACs) (Figure 4; Supplementary Figure 3). On the basis of molecular docking followed by MM-GBSA scores, it is evident that meticrane has considerable binding affinity against some oncological targets such as PD-L1, TIM-3, CD73, and HDACs (HDAC2, HDAC3, HDAC4, HDAC6, HDAC7, HDAC8 and HDAC10) (Figure 4). Given the small size of meticrane, the binding affinity score is considerable, suggesting that these proteins may be possible targets. As proof of principle, we selected HDAC6 for further analysis. Interestingly, when HDAC6 inhibitor (ACY1215) was combined with meticrane, a significantly high impact on the viability of tumor cells (K562, Jurkat and SK-hep-1) were observed (Supplementary Figures 4A-C). Additionally, we found that meticrane with ACY1215 has additive/synergistic effects against tumor cells, based on the combination index Q values (Supplementary Figure 4D).

To extend the analysis, we also performed MD simulations and investigated the dynamic behavior of the protein and ligands using the RMSD parameter, in which the structural deviations in the molecule are calculated over time with respect to the initial structure (docked pose). The RMSD of the ligands (plateau reached) confirms the stability of the meticran in the pocket of each protein, suggesting that these proteins may be of interest as

FIGURE 3
A genome wide transcriptional analysis and correlation with the patient survival. The differentially expressed genes, heat map of the 30 most important differential genes and KEGG pathways comparing the meticrane-treated group and the meticrane-untreated group (DMSO control group) in Jurkat **(A)**, K562 **(B)** and SK-hep-1 **(C)**. Venn diagram (left) of meticrane upregulated/downregulated genes and low/high risk genes and protein-protein interaction (right) of overlapping genes between upregulated/downregulated genes and low/high risk genes for leukemia **(D)** and liver cancer **(E)**.
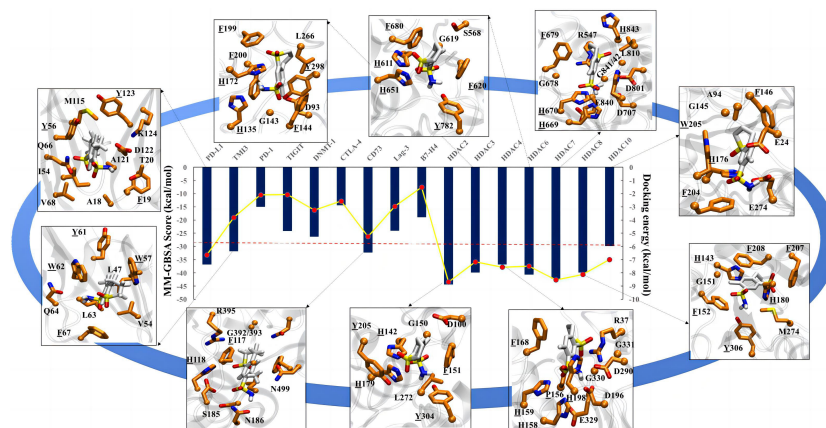
FIGURE 4
Molecular docking analysis for meticrane. Molecular docking of meticrane on established oncological targets is shown. The bi-axis docking energy and MM-GBSA scores (in kcal/mol) are marked. The cut-off is shown in a red dotted line. The interaction mapping of all targets with significant docking energy and MM-GBSA scores (>= to cut-off) are highlighted. In the interaction map, the meticrane and amino acids of each protein are shown in licorice color and colored by atoms as C: white/orange, O: red, N: blue, S: yellow, respectively. From the interaction map the aromatic residues that appear to be essential for the binding and stability of the metachrane have been identified (highlighted with underlining).

potential targets for thorough experimental validation in the future (Supplemental Figure 5).

Discussion

Certainly, there are enormous number of chemotherapeutic agents and targeted anti-cancer drugs, however, their side effects on the patient's healthy cells/tissues are not negligible. Given that the development of new anti-tumor drugs requires extensive preclinical and clinical studies, drug repositioning (also known as "drug repurposing") has emerged as a rapid alternative strategy, particularly related to non-oncology drugs (23). Moreover, several putative non-oncology drugs have been predicted, but their potential as future cancer therapeutics is unknown (24). Broadly, metformin is currently a typical example of a non-oncology anticancer drug (25), driven by the hypothesis of reducing the availability of glucose and insulin to slow down the tumor growth and progression. Herein, we tested another non-oncological drug named as meticrane, a thiazide diuretic commonly used to treat essential hypertension. Previously, meticrane in combination with CTLA-4 treatment was reported to improve the survival of mesothelioma mice (9), however, the anticancer effect of meticrane in tumors remained unexplored. In the current study, for the first time, we investigated the anti-cancer ability of meticrane in hematologic malignancies (myeloma and leukemia) and liver cancer cell lines.

We first cultured meticrane with cancer cells and found that leukemia cells (K562 and Jurkat) were more sensitive, whereas myeloma cells (U266 and OPM2) lacked a similar response. Similarly, some liver cancer cells (SK-hep-1) responded more effectively to meticrane, whereas others did not (HepG2). Notably, all the cell lines included in this study have a very distinctive (epi-)genetic profile, e.g., K562 (adult female/53 years, TP53 mutation), Jurkat (young male/14 years, TP53, BAX,

NOTCH1, MSH1/6, INPP5D mutations), U266 (adult male/53 years, TP53, BRAF, TRAF3, MSH6 mutations), OPM2 (adult female/56 years, TP53, SMAD2, CDKN2A, FGFR3 mutations), SK-hep-1 (adult male/52 years, BRAF, CDKN2A mutations), and HepG2 (young male/15 years, TERT, NRAS mutations). Thus, we confirmed that meticrane indeed has an anti-cancer potential that specifically targets certain genetic constellations. Certainly, some discrepancies in the experiments are expected owing to heterogeneity among cancer cell lines in addition to (epi-) genomic factors (26). In addition, we also tested and confirmed that meticrane has the potential to significantly reduce the number of tumor cells and proliferation. Particularly, these effects were validated in three cell lines (K562, Jurakt and SK-hep-1). We also examined whether apoptosis-related signaling pathways (cell death) might contribute to this noticeable cytotoxic effect, but confirmed that no evidence of apoptosis was detectable in K562, Jurkat, or SK-hep-1 cells, suggesting that it may inhibit cancer cell proliferation in an apoptosis-independent manner. In fact, some previous evidence suggests that a few compounds can cause cancer cell death *via* an apoptosis-independent pathway (27, 28). Whether meticrane would be of greater benefit to patients, who do not respond to clinical drugs due to apoptosis resistance, will be of future interest.

Next, we combined meticrane with the established epigenetic inhibitors CUCD-101 (HDACi) and 5AC (DNMTi), as epigenetic alterations are also known to influence numerous aspects of cancer and such inhibitors have already been tested in multiple cancer/ clinical studies (29). Noticeably, meticrane in combination with CUDC-101 or 5AC showed a higher inhibitory effect in hematological malignancies (K562 and Jurkat cells) and in liver cancer (SK-hep-1) cells compared to meticrane or epigenetic inhibitors alone. The combination of meticrane and epigenetic inhibitors (CUDC-101 or 5AC) showed additive/synergistic effects on K562, Jurkat and SK-hep-1 cells. Therefore, this combo (meticrane+epigenetic inhibitors) might be a possible replacement for toxic substances used for cancer treatment, however, *in-vivo*

studies are warranted in this context. Motivated by the optimistic results attained with a cocktail of meticrane and epigenetic inhibitors for anticancer efficacy, we subsequently tested its suitability for immunotherapy against cancers, in particular, cytokine-induced killer (CIK) cell therapy. Being a pioneer of CIK cell therapy (30), we have already demonstrated the favorable effect of CIK cells with known cancer inhibitors (e.g. PD-1/PD-L1) (31) and even epigenetic compounds (e.g. HDAC) (32). Intriguingly, meticrane showed no response to the cytotoxicity of CIKs against K562 cells and Sk-hep-1 cells over 4-24 hours of treatment. At this point, we cannot conclude whether similar effect will also prevail for other immunomodulatory effects of CIK cells when used under *in vivo* conditions. To our knowledge, this is the very first study to test any non-oncology drug against CIK cells. To gain better insight into the transcriptional role of meticrane, we performed genome-wide transcriptional analyses in both untreated and treated groups of meticrane in Jurkat, K562 and SK-hep-1 cells. Interestingly, we identified both up-regulated and down-regulated genes in all experimental groups, showed no direct/predominant effect on cancer-related signaling pathways in leukemia cell lines, and a distant impact to cancer in liver cancer cells. This suggests that meticrane can induce changes in cancer cells (as confirmed by the changes in cell viability and proliferation), but in a passive manner. As a proof of concept, we also overlap the obtained meticrane induced differentially expressed genes with the cancer specific survival data from the publicly available TCGA dataset and found a correlation among them. Therefore, it is reasonable to speculate that meticrane is involved in some anticancer pathways that are passively involved in targeting cancer cells and may be considered as compatible with other clinically safe drugs, particularly epigenetic inhibitors. These findings also prompted us to conduct molecular docking analysis in order to further explore the potential targets of meticrane. We specifically focused on known immune checkpoints (CTLA-4, PD-1, PD-L1, LAG-3, TIM-3, B7-H4, TIGIT, CD73) and epigenetic targets (DNMT1, HDACs). Of interest, we found considerable binding affinity scores of meticrane against PD-L1, TIM-3, CD73, and HDACs. To validate, we focused on HDAC6 for further analysis, and found a significantly high impact on the viability of tumor cells when HDAC6 inhibitor (ACY1215) was combined with the meticrane. Since meticrane showed additive/synergistic effects with CUDC101, 5AC and ACY1215 in our analysis, this could partly explain its positive molecular binding affinity with these epigenetic target proteins. Certainly, additional analyses for other putative targets are warranted. On a broader view, it is reasonable to speculate that meticrane may not alter any specific cancer-related pathway, but may exert its distant effects on the cancer cells (passively) *via* well-known immune-regulatory/epigenetic signaling pathways, preferably *via* targeting PD-L1, TIM-3, CD73, and HDACs.

It is equally important to address the limitations and future prospects of our (similar) studies, for instance, 1) As we have observed in case of meticrane, other non-oncology drugs may also not have direct targets associated with cancer, and therefore experiments like RNA sequencing (whole transcriptome analysis) studies following co-cultures in cancer cells may not be sufficient to draw any conclusions. 2) It is entirely possible that these drugs show anticancer activity only at high doses, so screening with variable concentrations (min to max) is recommended. At least in the case of meticrane, synthesis of other next-generation compounds (based on its structure) with a stronger tendency to inhibit the proliferation of cancer cells may solve this problem to some extent. 3) The genetic/epigenetic background of the cancer type and even gender differences may lead to different outcomes with these drugs in clinics. Specifically, when it is also known about the considerable overlapping between gene expression variation and the association of altered mutational pathways across the cancer genome (33, 34). Therefore, larger panels of cancer cell lines with multiple genetic constellations are necessary to confirm their potential mode of action. 4) Considering that cancer patients have a limited therapeutic window, it will be a significant question to follow whether non-oncology drugs (presumably alone) are sufficient to prolong the survival, especially in patients without any signs of cancer for a certain period of time after the treatment. 5) Such drugs may not be appropriate for all cancer immunotherapy types, hence, a critical selection of specific immunotherapy (broadly activating the immune system and/or precisely targets of the tumor) should be pre-addressed. Overall, we were able to show that meticrane, a non-oncology drug, exhibits anticancer potential with epigenetic inhibitors *in-vitro*, but not with cytokine-induced killer (CIK) cells.

Conclusions

Non-oncology drug (meticrane) effectively synergizes with epigenetic inhibitors in leukemia and liver cancer cells. Though we have demonstrated its anticancer ability, its mechanistic inference is still unclear. In the current study, we also expressed some important concerns encountered during the meticrane testing, which are also relevant to other non-oncology drugs when considering their future clinical or preclinical use.

Data availability statement

The data supporting the findings of this study are available from the corresponding author [I.G.H.S-W] on request.

Author contributions

Conceptualization, YW, AS, and IS-W; methodology, YW, YY, HJL, HDL, LM, SA, and CZ; validation, YW, FG and PC; writing—original draft preparation, YW, AS, and IS-W, project administration, AS and IS-W; funding acquisition, IS-W. All authors contributed to the article and approved the submitted version.

Funding

Conflict of interest

The authors declare that the research was conducted in the absence of any commercial or financial relationships that could be construed as a potential conflict of interest.

Publisher's note

All claims expressed in this article are solely those of the authors and do not necessarily represent those of their affiliated organizations, or those of the publisher, the editors and the reviewers. Any product that may be evaluated in this article, or claim that may be made by its manufacturer, is not guaranteed or endorsed by the publisher.

Supplementary material

The Supplementary Material for this article can be found online at: https://www.frontiersin.org/articles/10.3389/fonc.2023.1157366/full#supplementary-material

SUPPLEMENTARY FIGURE 1

Evaluating apoptosis and Caspase3/7 activation by using CellEvent™ Caspase-3/7 Green Flow Cytometry Assay Kit

SUPPLEMENTARY FIGURE 2

KEGG enrichment analysis of overlapping genes found between meticrane induced differentially expressed genes and survival-related genes in cancer.

SUPPLEMENTARY FIGURE 3

Molecular docking analysis.

SUPPLEMENTARY FIGURE 4

The combination effect of meticrane with ACY1215 (selective HDAC6 inhibitor). The viability of Jurkat (A), K562 (B) and SK-hep-1 (C) cells in presence of ACY1215 with/without meticrane. D) Combination index Q of Meticrane and ACY1215 on K562, Jurkat and SK-hep-1 cells.

SUPPLEMENTARY FIGURE 5

Molecular dynamics

SUPPLEMENTARY TABLE 1

Meticrane induced differentially expressed genes in Jurkat.

SUPPLEMENTARY TABLE 2

Meticrane induced differentially expressed genes in K562.

SUPPLEMENTARY TABLE 3

Meticrane induced differentially expressed genes in SK-hep-1.

SUPPLEMENTARY TABLE 4

Survival-related genes in AML.

SUPPLEMENTARY TABLE 5

Survival-related genes in HCC.

SUPPLEMENTARY TABLE 6

Overlapping genes between meticrane induced differentially expressed genes and survival-related genes in cancers.

References

1. Zhang Z, Zhou L, Xie N, Nice EC, Zhang T, Cui Y, et al. Overcoming cancer therapeutic bottleneck by drug repurposing. *Signal transduction targeted Ther* (2020) 5 (1):113. doi: 10.1038/s41392-020-00213-8

2. Papapetropoulos A, Szabo C. Inventing new therapies without reinventing the wheel: the power of drug repurposing. *Br J Pharmacol* (2018) 175(2):165–7. doi: 10.1111/bph.14081

3. Kasznicki J, Sliwinska A, Drzewoski J. Metformin in cancer prevention and therapy. *Ann Trans Med* (2014) 2(6):57. doi: 10.3978/j.issn.2305-5839.2014.06.01

4. Zi F, Zi H, Li Y, He J, Shi Q, Cai Z. Metformin and cancer: an existing drug for cancer prevention and therapy. *Oncol Lett* (2018) 15(1):683–90. doi: 10.3892/ol.2017.7412

5. Fu L, Jin W, Zhang J, Zhu L, Lu J, Zhen Y, et al. Repurposing non-oncology small-molecule drugs to improve cancer therapy: current situation and future directions. *Acta Pharm Sin B* (2022) 12(2):532–57. doi: 10.1016/j.apsb.2021.09.006

6. Pushpakom S, Iorio F, Eyers PA, Escott KJ, Hopper S, Wells A, et al. Drug repurposing: progress, challenges and recommendations. *Nat Rev Drug Discovery* (2019) 18(1):41–58. doi: 10.1038/nrd.2018.168

7. Majchrzak-Celińska A, Warych A, Szoszkiewicz M. Novel approaches to epigenetic therapies: from drug combinations to epigenetic editing. *Genes* (2021) 12 (2). doi: 10.3390/genes12020208

8. Sharma A, Liu H, Herwig-Carl MC, Chand Dakal T, Schmidt-Wolf IGH. Epigenetic regulatory enzymes: mutation prevalence and coexistence in cancers. *Cancer Invest* (2021) 39(3):257–73. doi: 10.1080/07357907.2021.1872593

9. Lesterhuis WJ, Rinaldi C, Jones A, Rozali EN, Dick IM, Khong A, et al. Network analysis of immunotherapy-induced regressing tumours identifies novel synergistic drug combinations. *Sci Rep* (2015) 5:12298. doi: 10.1038/srep12298

10. Schmidt-Wolf IG, Negrin RS, Kiem HP, Blume KG, Weissman IL. Use of a scid Mouse/Human lymphoma model to evaluate cytokine-induced killer cells with potent antitumor cell activity. *J Exp Med* (1991) 174(1):139–49. doi: 10.1084/jem.174.1.139

11. Pinho MP, Lepski GA, Rehder R, Chauca-Torres NE, Evangelista GCM, Teixeira SF, et al. Near-complete remission of glioblastoma in a patient treated with an allogenic dendritic cell-based vaccine: the role of tumor-specific Cd4+T-cell cytokine secretion pattern in predicting response and recurrence. *Int J Mol Sci* (2022) 23(10). doi: 10.3390/ijms23105396

12. Zhang Y, Wu X, Sharma A, Weiher H, Schmid M, Kristiansen G, et al. Anti-Cd40 predominates over anti-Ctla-4 to provide enhanced antitumor response of dc-cik cells in renal cell carcinoma. *Front Immunol* (2022) 13:925633. doi: 10.3389/fimmu.2022.925633

13. Garofano F, Sharma A, Abken H, Gonzalez-Carmona MA, Schmidt-Wolf IGH. A low dose of pure cannabidiol is sufficient to stimulate the cytotoxic function of cik cells without exerting the downstream mediators in pancreatic cancer cells. *Int J Mol Sci* (2022) 23(7). doi: 10.3390/ijms23073783

14. Sun X, Fan T, Sun G, Zhou Y, Huang Y, Zhang N, et al. 2-Deoxy-D-Glucose increases the sensitivity of glioblastoma cells to bcnu through the regulation of glycolysis, ros and ers pathways: In vitro and in vivo validation. *Biochem Pharmacol* (2022) 199:115029. doi: 10.1016/j.bcp.2022.115029

15. Wang Y, Setiawan MF, Liu H, Dakal TC, Liu H, Ge F, et al. Regulator of G protein signaling 20 correlates with long intergenic non-coding rna (Lincrnas) harboring oncogenic potential and is markedly upregulated in hepatocellular carcinoma. *Biology* (2022) 11(8). doi: 10.3390/biology11081174

16. Mittal L, Kumari A, Srivastava M, Singh M, Asthana S. Identification of potential molecules against covid-19 main protease through structure-guided virtual screening approach. *J biomol structure dynamics* (2021) 39(10):3662–80. doi: 10.1080/07391102.2020.1768151

17. Mittal L, Tonk RK, Awasthi A, Asthana S. Targeting cryptic-orthosteric site of pd-L1 for inhibitor identification using structure-guided approach. *Arch Biochem biophys* (2021) 713:109059. doi: 10.1016/j.abb.2021.109059

18. Panwar S, Kumari A, Kumar H, Tiwari AK, Tripathi P, Asthana S. Structure-based virtual screening, molecular dynamics simulation and in vitro evaluation to

identify inhibitors against nampt. *J biomol structure dynamics* (2022) 40(20):10332–44. doi: 10.1080/07391102.2021.1943526

19. Tyagi R, Srivastava M, Jain P, Pandey RP, Asthana S, Kumar D, et al. Development of potential proteasome inhibitors against mycobacterium tuberculosis. *J biomol structure dynamics* (2022) 40(5):2189–203. doi: 10.1080/07391102.2020.1835722

20. Srivastava M, Mittal L, Kumari A, Asthana S. Molecular dynamics simulations reveal the interaction fingerprint of remdesivir triphosphate pivotal in allosteric regulation of sars-Cov-2 rdrp. *Front Mol Biosci* (2021) 8:639614. doi: 10.3389/fmolb.2021.639614

21. Greenwood JR, Calkins D, Sullivan AP, Shelley JC. Towards the comprehensive, rapid, and accurate prediction of the favorable tautomeric states of drug-like molecules in aqueous solution. *J computer-aided Mol design* (2010) 24(6-7):591–604. doi: 10.1007/s10822-010-9349-1

22. Harder E, Damm W, Maple J, Wu C, Reboul M, Xiang JY, et al. Opls3: a force field providing broad coverage of drug-like small molecules and proteins. *J Chem Theory Comput* (2016) 12(1):281–96. doi: 10.1021/acs.jctc.5b00864

23. Turabi KS, Deshmukh A, Paul S, Swami D, Siddiqui S, Kumar U, et al. Drug repurposing-an emerging strategy in cancer therapeutics. *Naunyn-Schmiedeberg's Arch Pharmacol* (2022) 395(10):1139–58. doi: 10.1007/s00210-022-02263-x

24. Corsello SM, Nagari RT, Spangler RD, Rossen J, Kocak M, Bryan JG, et al. Discovering the anti-cancer potential of non-oncology drugs by systematic viability profiling. *Nat Cancer* (2020) 1(2):235–48. doi: 10.1038/s43018-019-0018-6

25. Skuli SJ, Alomari S, Gaitsch H, Bakayoko A, Skuli N, Tyler BM. Metformin and cancer, an ambiguanidous relationship. *Pharm (Basel Switzerland)* (2022) 15(5). doi: 10.3390/ph15050626

26. Sharma A, Reutter H, Ellinger J. DNA Methylation and bladder cancer: where genotype does not predict phenotype. *Curr Genomics* (2020) 21(1):34–6. doi: 10.2174/1389202921666200102163422

27. Yang J, Zhou Y, Cheng X, Fan Y, He S, Li S, et al. Isogambogenic acid induces apoptosis-independent autophagic cell death in human non-Small-Cell lung carcinoma cells. *Sci Rep* (2015) 5:7697. doi: 10.1038/srep07697

28. O'Sullivan-Coyne G, O'Sullivan GC, O'Donovan TR, Piwocka K, McKenna SL. Curcumin induces apoptosis-independent death in oesophageal cancer cells. *Br J Cancer* (2009) 101(9):1585–95. doi: 10.1038/sj.bjc.6605308

29. Cheng Y, He C, Wang M, Ma X, Mo F, Yang S, et al. Targeting epigenetic regulators for cancer therapy: mechanisms and advances in clinical trials. *Signal transduction targeted Ther* (2019) 4:62. doi: 10.1038/s41392-019-0095-0

30. Sharma A, Schmidt-Wolf IGH. 30 years of CIK cell therapy: recapitulating the key breakthroughs and future perspective. *J Exp Clin Cancer Res CR* (2021) 40(1):388. doi: 10.1186/s13046-021-02184-2

31. Li Y, Sharma A, Bloemendal M, Schmidt-Wolf R, Kornek M, Schmidt-Wolf IGH. Pd-1 blockade enhances cytokine-induced killer cell-mediated cytotoxicity in b-cell non-Hodgkin lymphoma cell lines. *Oncol Lett* (2021) 22(2):613. doi: 10.3892/ol.2021.12874

32. Stephan D, Weiher H, Schmidt-Wolf IGH. Cik cells and hdac inhibitors in multiple myeloma. *Int J Mol Sci* (2017) 18(5). doi: 10.3390/ijms18050945

33. Liu H, Li H, Luo K, Sharma A, Sun X. Prognostic gene expression signature revealed the involvement of mutational pathways in cancer genome. *J Cancer* (2020) 11(15):4510–20. doi: 10.7150/jca.40237

34. Sharma A, Wüllner U, Schmidt-Wolf IGH, Maciaczyk J. Marginalizing the genomic architecture to identify crosstalk across cancer and neurodegeneration. *Front Mol Neurosci* (2023) 16:1155177. doi: 10.3389/fnmol.2023.1155177

3.2 Publication 2: Regulator of G Protein Signaling 20 Correlates with Long Intergenic Non-Coding RNA (lincRNAs) Harboring Oncogenic Potential and Is Markedly Upregulated in Hepatocellular Carcinoma

Yulu Wang[1,†], Maria F. Setiawan[1,†], Hongde Liu[2,†], Tikam Chand Dakal[3], Hongjia Liu[2], Fangfang Ge[1], Oliver Rudan[1], Peng Chen[1], Chunxia Zhao[4], Maria A. Gonzalez-Carmona[5], Miroslaw T. Kornek[5], Christian P. Strassburg[5], Matthias Schmid[6], Jarek Maciaczyk[7], Amit Sharma[7,*] and Ingo G.H. Schmidt-Wolf [1,*]

[1]Department of Integrated Oncology, Center for Integrated Oncology (CIO), University Hospital Bonn, 53127 Bonn, Germany
[2]State Key Laboratory of Bioelectronics, School of Biological Science & Medical Engineering, Southeast University, Nanjing 210096, China
[3]Genome and Computational Biology Lab, Department of Biotechnology, Mohanlal Sukhadia University, Udaipur 313001, India
[4]School of Nursing, Nanchang University, Nanchang 330006, China
[5]Department of Internal Medicine I, University Hospital Bonn, 53127 Bonn, Germany
[6]Institute of Medical Biometry, Informatics and Epidemiology, University Hospital Bonn, 53127 Bonn, Germany
[7]Department of Neurosurgery, University Hospital Bonn, 53127 Bonn, Germany

Article

Regulator of G Protein Signaling 20 Correlates with Long Intergenic Non-Coding RNA (lincRNAs) Harboring Oncogenic Potential and Is Markedly Upregulated in Hepatocellular Carcinoma

Yulu Wang [1,†], **Maria F. Setiawan** [1,†], **Hongde Liu** [2,†], **Tikam Chand Dakal** [3], **Hongjia Liu** [2], **Fangfang Ge** [1], **Oliver Rudan** [1], **Peng Chen** [1], **Chunxia Zhao** [4], **Maria A. Gonzalez-Carmona** [5], **Miroslaw T. Kornek** [5], **Christian P. Strassburg** [5], **Matthias Schmid** [6], **Jarek Maciaczyk** [7], **Amit Sharma** [7,*] **and Ingo G. H. Schmidt-Wolf** [1,*]

1 Department of Integrated Oncology, Center for Integrated Oncology (CIO), University Hospital Bonn, 53127 Bonn, Germany
2 State Key Laboratory of Bioelectronics, School of Biological Science & Medical Engineering, Southeast University, Nanjing 210096, China
3 Genome and Computational Biology Lab, Department of Biotechnology, Mohanlal Sukhadia University, Udaipur 313001, India
4 School of Nursing, Nanchang University, Nanchang 330006, China
5 Department of Internal Medicine I, University Hospital Bonn, 53127 Bonn, Germany
6 Institute of Medical Biometry, Informatics and Epidemiology, University Hospital Bonn, 53127 Bonn, Germany
7 Department of Neurosurgery, University Hospital Bonn, 53127 Bonn, Germany
* Correspondence: ingo.schmidt-wolf@ukbonn.de (I.G.H.S.-W.); amit.sharma@ukbonn.de (A.S.); Tel.: +49-(0)-228-287-17050 (I.G.H.S.-W.)
† These authors contributed equally to this work.

Simple Summary: Clinical and molecular advances have improved knowledge and treatment prospects for cancer, yet hepatocellular carcinoma (HCC), the most common form of liver cancer, still ranks significantly higher in terms of the global cancer burden. Herein, we investigated the role of RGS20 as a potential prognostic marker in 28 different cancers with a particular focus on HCC.

Abstract: Hepatocellular carcinoma (HCC) is at the forefront of the global cancer burden, and biomarkers for HCC are constantly being sought. Interestingly, RGS (Regulators of G protein signaling) proteins, which negatively regulate GPCR signaling, have been associated with various cancers, with some members of the RGS family being associated with liver cancer as well. Considering this, we investigated the role of RGS20 as a potential prognostic marker in 28 different cancer types with special emphasis on HCC. By using the Cancer Genome Atlas (TCGA) and Gene Expression Omnibus (GEO) data, our analysis revealed that (a) RGS20 was strongly upregulated in tumor tissue compared with adjacent normal tissue of HCC patients; (b) RGS20 was strongly associated with some important clinical parameters such as alpha-fetoprotein and tumor grade in the HCC patients; (c) besides HCC ($p < 0.001$), RGS20 was found to be an important factor for survival in four other cancers (clear renal cell carcinoma: $p < 0.001$, lung adenocarcinoma: $p = 0.004$, mesothelioma: $p = 0.039$, ovarian serous cystadenocarcinoma: $p = 0.048$); (d) RGS20 was found to be significantly associated with some tumor-related signaling pathways and long intergenic non-coding RNAs (lincRNAs: LINC00511, PVT1, MIR4435-2HG, BCYRN1, and MAPKAPK5-AS1) that exhibit oncogenic potential. Taken together, we showed that RGS20 correlates with a few HCC-associated lincRNAs harboring oncogenic potential and is markedly upregulated in HCC patients. Our analysis further supports the putative function of RGS proteins, particularly RGS20, in cancer.

1. Introduction

Liver cancer is the fourth leading cause of cancer-related deaths [1], and remains a global health concern among prevalent cancers, being hepatocellular carcinoma (HCC) the most common form of liver cancer. In the last few decades, the number of liver cancer cases has also increased, primarily due to hepatitis C infection and nonalcoholic fatty liver disease (NAFLD).

Indeed, clinical and molecular advances have improved the knowledge and treatment perspective, still, HCC ranks significantly higher in terms of global cancer burden. While many approaches have been applied to the treatment of HCC, cancer immunotherapy has been at the forefront of respective clinical trials and patient care [2,3]. There has been a constant search for identifying HCC-related biomarkers, however, most of them showed association with poor prognosis, either in early or advanced HCC [4]. Notably, two members of the ubiquitin C-terminal hydrolases (UCHs) family, BRCA1-associated protein-1 (BAP1) [5] and UCH-L3 [6] have been implicated in the survival rate of this particular cancer. More recently, authors established immuno-autophagy-related long non-coding RNA (IARlncRNA) signature with a prognostic ability in HCC [7]. Recently, the crucial role of G protein-coupled receptors (GPCRs) in tumorigenesis and HCC development has been discussed [8]. Interestingly, RGS (Regulators of G protein signaling) proteins, which negatively regulate GPCR signaling, have been implicated in various cancers including lung, prostate, breast, and ovarian cancers [9–12]. To date, 20 canonical RGS genes (RGS1-RGS20) have been reported and a few members of the RGS family (RGS3, RGS5, RGS17) have also been associated with liver cancer [13–18].

Considering this, herein, we focused our analysis on RGS20, which is solely associated with the occurrence and progression of several cancers, including breast cancer, bladder cancer, oral squamous cell carcinoma, and metastatic melanoma [19–22]. With special emphasis on HCC, we investigated the role of RGS20 as a potential prognostic marker. Furthermore, we also evaluated the survival probability of RGS20 in 28 different cancer types. In addition, we correlate its expression with putative HCC-related long intergenic non-coding RNAs (lincRNAs). To our knowledge, our study is the first to expand the clinical relevance and molecular significance of RGS20 in the cancer spectrum, especially HCC.

2. Materials and Methods

2.1. Gene Expression Data and Clinical Data

Gene expression data (workflow type: HTSeq—FPKM) was obtained from the TCGA-LICH dataset in the Cancer Genome Atlas Program (TCGA) database, which contains 374 tumor samples and 50 normal samples. The clinical data of HCC patients were downloaded from the GDC TCGA Liver Cancer (LIHC) dataset in the UCSC XENA database. The clinical data parameters included age, sex, Child-Pugh classification, alpha-fetoprotein (AFP), fibrosis, grade, and stage. Of note, 371 primary HCC samples were included in our analysis by excluding 3 recurrent samples. Among them, 365 samples contained survival data (survival time and survival status) and gene expression data, while 163 samples contained survival data, clinical characteristics and gene expression data. In addition, the gene expression data and clinical data of HCC in the GSE76427 dataset from the Gene Expression Omnibus (GEO) database were used for validation, which contains 115 tumor samples and 52 normal samples. Besides gene expression data, all 115 tumor samples also contained survival data. In addition, gene expression data (TPM) and cancer samples with overall survival data for 28 cancer types were obtained from TCGA database as well. These 28 cancer types include adrenocortical carcinoma (ACC, 73 samples), bladder urothelial carcinoma (BLCA, 400 samples), breast invasive carcinoma (BRCA, 1033 samples), cervical

squamous cell carcinoma and endocervical adenocarcinoma (CESC, 292 samples), cholangiocarcinoma (CHOL, 33 samples), colon adenocarcinoma (COAD, 261 samples), lymphoid neoplasm diffuse large B-cell lymphoma (DLBC, 46 samples), esophageal carcinoma (ESCA, 182 samples), glioblastoma multiforme (GBM, 162 samples), head and neck squamous cell carcinoma (HNSC, 518 samples), kidney chromophobe (KICH, 60 samples), kidney renal clear cell carcinoma (KIRC, 509 samples), kidney renal papillary cell carcinoma (KIRP, 281 samples), acute myeloid leukemia (LAML, 102 samples), liver hepatocellular carcinoma (LIHC, 344 samples), lung adenocarcinoma (LUAD, 477 samples), lung squamous cell carcinoma (LUSC, 482 samples), mesothelioma (MESO, 79 samples), ovarian serous cystadenocarcinoma (OV, 418 samples), pancreatic adenocarcinoma (PAAD, 178 samples), pheochromocytoma and paraganglioma (PCPG, 179 samples), prostate adenocarcinoma (PRAD, 460 samples), stomach adenocarcinoma (STAD, 377 samples), testicular germ cell tumors (TGCT, 135 samples), thyroid carcinoma (THCA, 508, samples), thymoma (THYM, 118 samples), uterine corpus endometrial carcinoma (UCEC, 172 samples), uterine carcinosarcoma (UCS, 56 samples). The cutoff values for grouping patients into high and low RGS20 gene expression were based on the median value of RGS20 gene expression in each kind of cancer, respectively.

2.2. Gene Set Enrichment Analysis

Gene set enrichment analysis (GSEA) was used to determine a defined set of genes that exhibit statistical significance and consistent differences between the two biological states (e.g., phenotypes). In GSEA analysis, RGS20 expression was divided into low and high groups, and the cut-off value was considered as the median value of its expression. Gene set permutations were performed 1000 times for each analysis in the h.all.v7.4.symbols.gmt [Hallmarks] set. The expression level of RGS20 was set as a phenotype label. The enrichment of pathways in each phenotype was selected according to the *p* value < 0.05 and false discovery rate (FDR) < 0.25.

2.3. Prediction of RGS20 Interaction with lincRNAs

Both RGS20 gene expression (FPKM) and lincRNAs gene expression (FPKM) in LIHC were obtained from TCGA data and a total of 1193 lincRNAs were involved in this analysis. The averages of gene expression no more than 0 were excluded. Log2 was further applied to the gene expression data (FPKM) in order to obtain a suitable normalized distribution. Subsequently, gene expression (log2 (FPKM+1)) was used to investigate the correlation between RGS20 and lincRNAs using the Spearman correlation test. Statistical significance was determined using Spearman correlation coefficient | R | > 0.4 and *p* value < 0.05.

The prediction of physical and functional interaction between five lincRNAs and the RGS20 protein was performed in RNA-Protein Interaction Prediction (RPISeq, http://pridb. gdcb.iastate.edu/RPISeq/, accessed on 5 January 2022) using the protein sequence of RGS20 and RNA sequence of the lincRNAs. The output, i.e., prediction probability of possible interactions were obtained in terms of RF and SVM classifiers. Interaction probabilities range from 0 to 1, wherein the higher the probability is better. In general, prediction probabilities with scores of more than 0.5 are considered "positive," i.e., expressing the likelihood of interaction between given lincRNA and protein.

LincRNAs and RGS20 mRNA Interaction and Tissue-specific Expression Profile were investigated. The prediction of physical and functional interaction between five lincRNAs and the mRNA of RGS20 was performed using LncRRIsearch web server (http://rtools.cbrc. jp/LncRRIsearch/, accessed on 5 January 2022), which also gives tissue-specific expression level of lincRNAs and mRNA based on RNA-seq data from the Genotype-Tissue Expression (GTEx) Project (E-MTAB-2919).

2.4. Statistical Analysis

The statistical analyses were performed using R. The relationship between clinical characteristics and RGS20 was analyzed using Wilcoxon Rank Sum and logistic regression.

The Kaplan–Meier method was used to demonstrate the association between RGS20 expression and overall survival (OS). Clinical variables and RGS20 were associated with survival using Cox regression. Multivariable Cox analysis was used to find independent factors based on the clinical characteristics and RGS20 gene. The cutoff value for RGS20 expression was determined by its median value. Spearman analysis was used to find lincRNAs related to RGS20. *p* values of less than 0.05 were considered statistically significant.

3. Results

3.1. RGS20 Gene Expression, Clinical Features Relevant and Survive Probability in HCC

We first sought to analyze the difference in RGS20 gene expression between normal and tumor tissue samples from the TCGA database. In the panel of 421 samples (tumor = 371, normal = 50) and paired samples (tumor = 50, normal = 50), we observed elevated expression of RGS20 in tumor samples compared to the controls (Figure 1A,B) using Wilcoxon Rank Sum test. To assess the survival pattern according to the RGS20 expression, we next divided the data into high and low expression groups (based on their median value) and analyzed them using Kaplan–Meier survival analysis (Figure 1C). The analysis showed that patients with higher RGS20 expression had a worse prognosis ($p = 0.005$), suggesting that RGS20 may be predictive of survival in liver cancer patients. Next, we correlate the patient-specific clinical parameters with the RGS20 expression. We specifically distinguished these clinical parameters in groups such as age ($\geq$65 vs. <65), AFP ($\geq$400 vs. <400), Child-pugh (B + C vs. A), fibrosis (no fibrosis vs. fibrosis), sex (male vs. female), grade (G3 + G4 vs. G1 + G2), stage (III + IV vs. I + II). Using Wilcoxon Rank Sum test, we found that RGS20 expression significantly correlated with AFP ($p = 0.04$) and grade ($p = 0.003$) (Figure 1D). Likewise, logistic regression analysis also confirmed this in the case of AFP ($p = 0.043$) and grade ($p = 0.009$) (Table 1). To verify the predictive function, we also used the independent dataset GSE76427 from the GEO database. The analysis clearly showed that the expression of RGS20 varied significantly between tumor and normal samples ($p = 0.023$) (Figure 1E). Importantly, the KM curve result also indicated that the group with higher RGS20 expression had a lower survival rate than the group with low expression (Figure 1F).

Table 1. Logistic regression assessment of RGS20 expressions between the clinical variable groups using TCGA data.

| Clinical Characteristics	Odd Ratio (OR)	*p*-Value
Age ($\geq$65 vs. <65)	0.923 (0.494–1.722)	0.801
Gender (male vs. female)	0.780 (0.398–1.518)	0.465
Grade (G3 + G4 vs. G1 + G2)	2.358 (1.245–4.539)	0.009 **
Stage (III + IV vs. I + II)	0.743 (0.337–1.612)	0.454
AFP ($\geq$400 vs. <400)	2.360 (1.048–5.619)	0.043 *
Child-pugh (B + C vs. A)	0.767 (0.262–2.166)	0.617
Fibrosis (no fibrosis vs. fibrosis)	0.808 (0.412–1.573)	0.531

* $p < 0.05$, ** $p < 0.01$.

3.2. RGS20 Survive Probability Spectrum in 28 Cancers

To investigate the survival potential of RGS20 in other cancer types, we extend our analysis to 28 cancer types (Figure 2). Interestingly, only five cancers, namely KIRC ($p < 0.001$), LIHC ($p < 0.001$), LUAD ($p = 0.004$), MESO ($p = 0.039$), and OV ($p = 0.048$), showed a difference in survival between the high and low RGS20 expression groups. Of these, KIRC, LIHC, LUAD, and MESO cancers demonstrated poorer survival in the high RGS20 expression group, while OV cancers were observed to have poorer survival in the low RGS20 expression group.
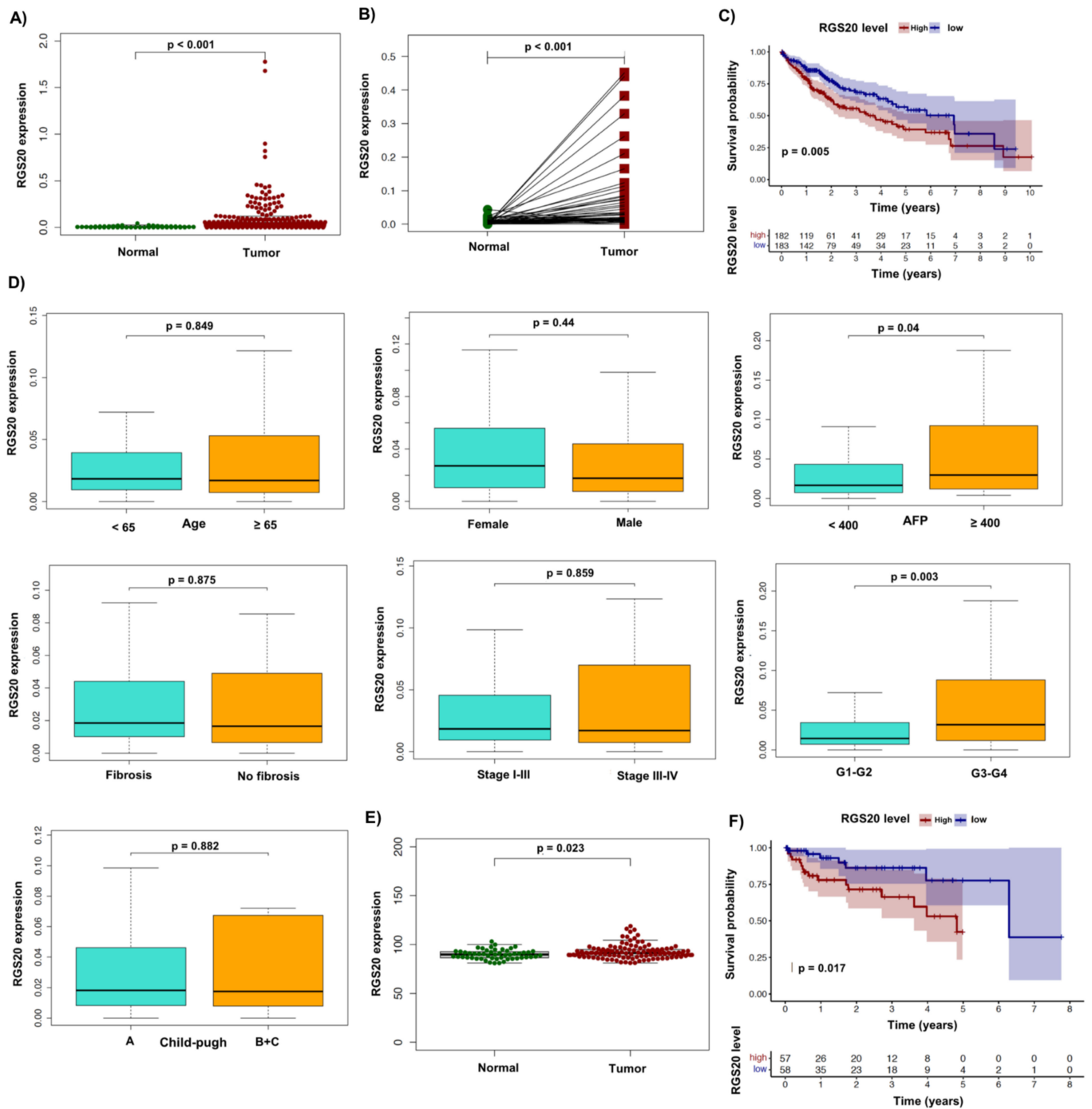
Figure 1. RGS20 analysis in HCC patients (TCGA and GEO analysis). (**A**) All samples, (**B**) and paired samples from TCGA data were analyzed using Wilcoxon Rank Sum test. (**C**) The impact of RGS20 expression level on overall survival time in HCC patients calculated using Kaplan–Meier method. (**D**) Relationship between RGS20 expression and clinical features using Wilcoxon Rank Sum test. (**E**) RGS20 gene expression between tumor and normal samples (Wilcoxon Rank Sum test), (**F**) and KM curve was used to assess the survival rate between high and low RGS20 expression group using GEO data.
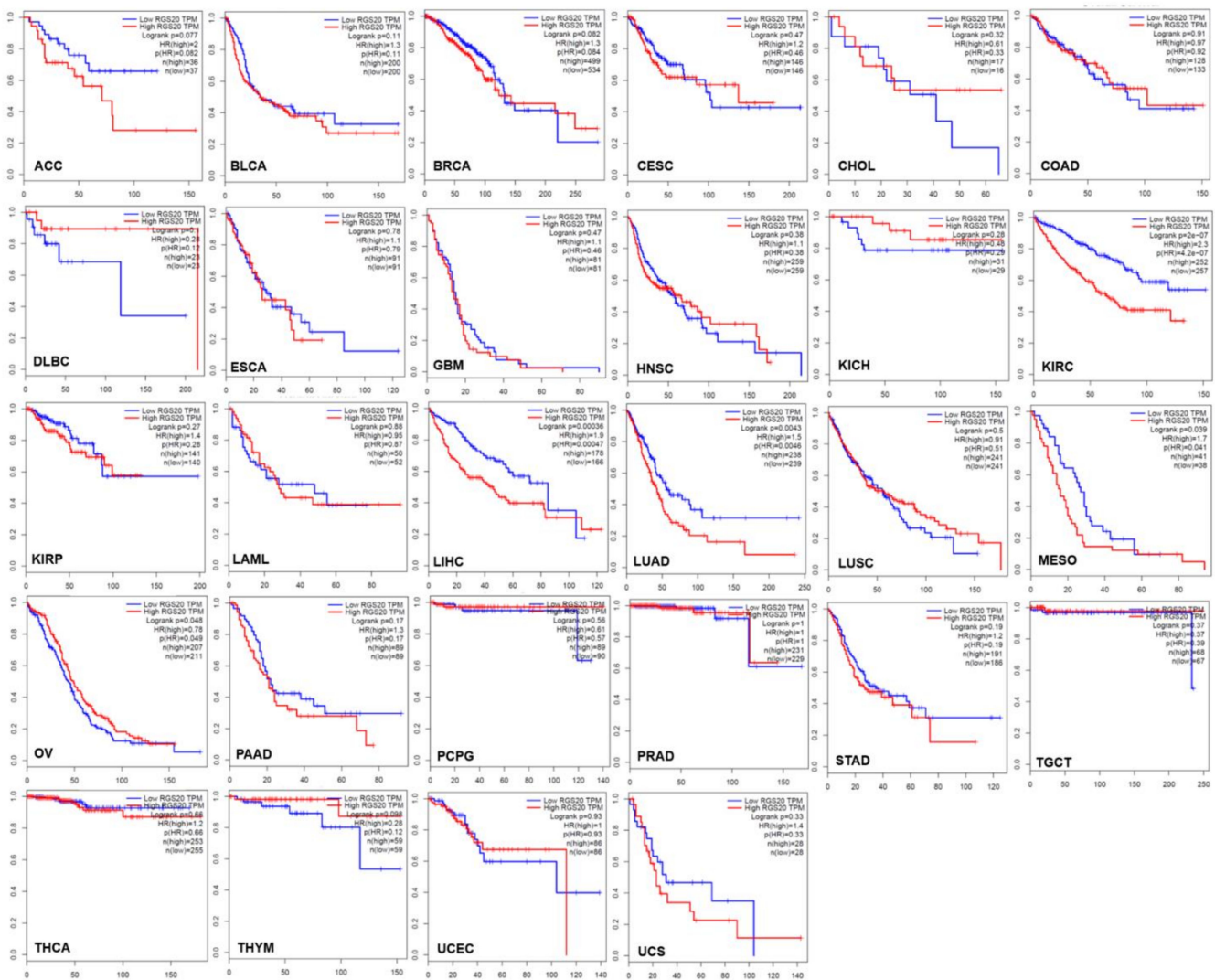
Figure 2. RGS20 survival probability in 28 cancers. KM curves show data from 28 cancers. Patients were classified into low and high expression groups based on the median value of RGS20 in each cancer.

3.3. Identification of Independent Factors and GSEA Enrichment Results

In the context of overall survival (OS), univariate analysis also revealed that age ($p = 0.022$), stage ($p = 0.017$), and RGS20 ($p < 0.001$) were related to OS. (Table 2). In addition, multivariable Cox regression confirmed that age, stage, and RGS20 were independent factors associated with survival (Figure 3A). In the above part, each clinical feature was classified into two subgroups. However, age (continuous value), AFP (continuous value), RGS20 gene expression (continuous value), Child-pugh (A, B and C), fibrosis (no fibrosis and fibrosis), sex (female and male), grade (G1, G2, G3 and G4) and stage (I, II, III and IV) were applied in this part.

To determine whether RGS20 is involved in established biological pathways, we performed gene set enrichment analysis (GSEA) using the TCGA dataset. We first divided the RGS20 data into high and low cohorts and investigated them using hallmark gene sets. GSEA revealed that 20 gene signatures were enriched in patients with high RGS20 expression (FDR < 0.25, normalized p-value < 0.05) (Figure 3B). Some tumor-related pathways were included such as mTORC1, MYC TARGETS V1, MYC TARGETS V1, DNA REPAIR, P53, G2M CHECKPOINT, PI3K/AKT/MTOR, IL2/STAT5, and APOPTOSIS. Of which,

DNA REPAIR, mTORC1, MYC TARGETS V1 signaling were the top three enriched terms with NES values > 2. These three enrichment plots are shown in Figure 3C.

Table 2. Univariate survival prediction of RGS20 expression and the clinical factors using TCGA data.

|	Univariate Cox Regression	
	HR (95% CI of HR)	**p Value**
Age (continuous)	1.029 (1.004–1.054)	0.022 *
Gender	0.761 (0.420–1.379)	0.368
Grade	1.405 (0.912–2.164)	0.123
Stage	1.463 (1.072–1.997)	0.017 *
Child-pugh	1.447 (0.611–3.426)	0.401
AFP (continuous)	1.000 (1.000–1.000)	0.615
Fibrosis	0.686 (0.380–1.239)	0.212
RGS20 (continuous)	77.931 (5.954–1019.956)	<0.001 ***

* $p < 0.05$, *** $p < 0.001$.
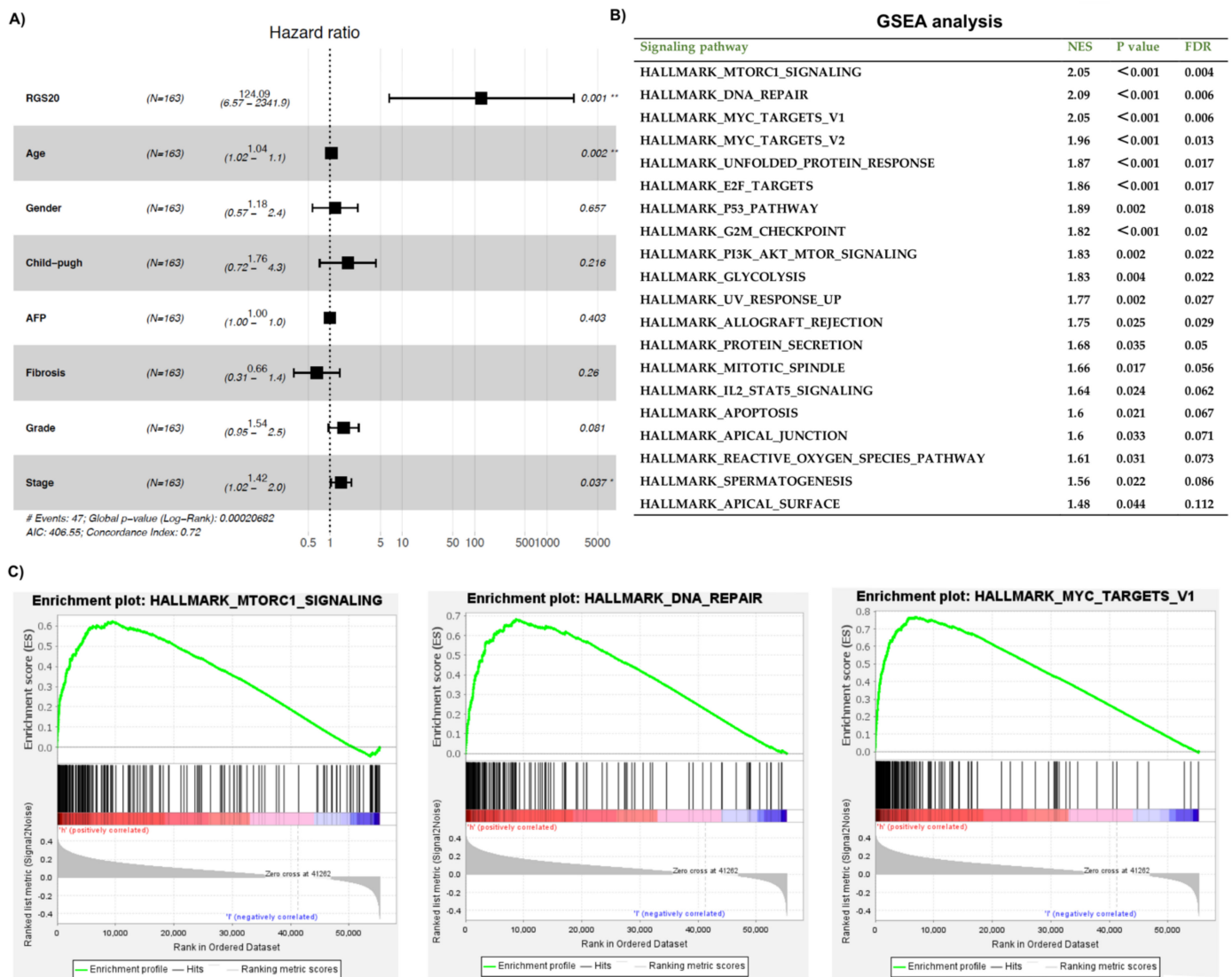
Figure 3. Multivariable Cox regression and GSEA enrichment analysis. (**A**) Multivariable Cox survival model including RGS20 and clinical features. The hazard ratio values are represented by squares. The

horizontal bars depict the 95% CI of the hazard ratio estimation. * $p < 0.05$, ** $p < 0.01$. (**B**) GSEA enrichment results. (**C**) Top 3 Enrichment plots from GSEA (NES > 2). The green curves depict the enrichment score curve obtained from GSEA software. NES: normalized enrichment score; *p*-value: normalized *p*-value; FDR: false discovery rate.

3.4. Prediction of RGS20 Interaction with lincRNAs

Given that the non-coding genome has been suggested to contribute to the regulation of RGS protein in oral squamous cell carcinoma [22], cervical cancer [23], ovarian cancer [24] and lung cancer [25]. We therefore investigated the possible links of RGS20 to lincRNAs implicated in HCC. Using TCGA data, we performed Spearman correlation analysis ($|R| > 0.4$ and $p < 0.05$) and identified five lincRNAs, including LINC00511, PVT1, MIR4435-2HG, BCYRN1, and MAPKAPK5-AS1 in this category (Figure 4A).
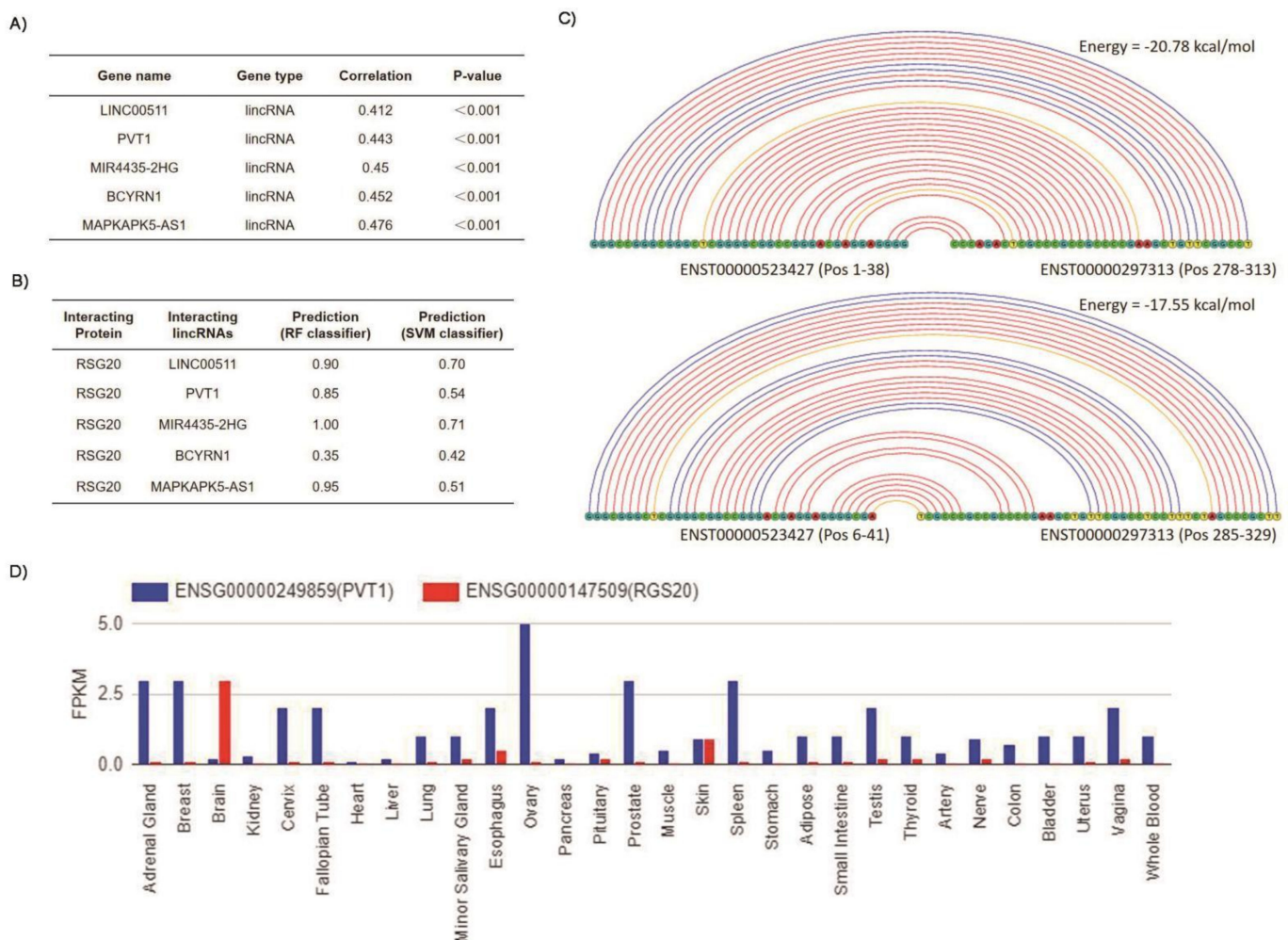
Figure 4. Prediction of RGS20 interaction with lincRNAs and gene expression in human tissues. (**A**) Correlation of RGS20 with five lincRNAs. (**B**) Interaction of five lincRNAs with RGS20 protein. (**C**) Two physical interactions of lincRNA PVT1 and mRNA of RGS20. (**D**) Gene expression level of the lincRNA PVT1 and the RGS20 mRNA in different tissues of humans.

Further investigations for the possible interaction of RGS20 with the obtained five lincRNAs were performed using two kinds of web tools. First, the prediction of physical and functional interaction between five lincRNAs and the RGS20 protein was performed using the RPISeq webtool of the Iowa State University [26]. The prediction probabilities in terms of RF and SVM classifiers of individual interaction of lincRNAs with the

RGS20 protein have been shown in Figure 4B. The prediction probabilities indicate that all five obtained lincRNAs are likely to interact with RGS20 protein, except the lincRNA BCYRN1 (prediction probability less than the threshold value). Then, we subjected the five lincRNAs and RGS20 to the LncRRIsearch web server to predict possible physical and functional interaction. However, the information on lincRNA BCYRN1 was not available in this web tool which means it cannot predict the interaction of lincRNA BCYRN1 with mRNA of RGS20. For the remaining four lincRNAs, we found that only lincRNA PVT1 (Transcript ID: ENST00000523427) interacts with the mRNA of RGS20 (Transcript ID: ENST00000297313). The genomic locus of PVT1 (transcript length 938 nt) is chr8(+) 127,794,575–127,890,952 based on the UCSC Genome Browser (https://genome.ucsc.edu/, accessed on 5 January 2022). The genomic locus of RGS20 (transcript length 2104 nt) is chr8(+) 53,851,808–53,959,303. The total genomic distance is 73,835,271 bp. Figure 4C shows that two physical interactions of LincRNA PVT1 and RGS20 mRNA are possible with energy −20.78 and −17.55 kcal/mol, respectively. Of note, the energy threshold was set as −16 kcal/mol. In addition, we also checked the RNA expression level of the lincRNA PVT1 and the RGS20 mRNA. We generated the RNA-seq expression profile using the database E-MTAB-2919, which encompasses the expression profile of RNAs from different tissues in humans. The RNA-seq expression profile shows that the expression of PVT1 is very high in the ovary (FPKM ~5.0) and high in some other tissues such as the adrenal gland, breast, prostate and spleen (FPKM ~3.0) (Figure 4D). Compared to this the expression levels of RGS20 mRNA is almost negligible (FPKM~0.1–0.2) in these five tissues (Figure 4D). However, in brain tissue the expression of RGS20 mRNA is high (FPKM ~3.0) and the expression of lincRNA PVT1 is very low (FPKM ~0.2–0.3) (Figure 4D).

4. Discussion

There has been a plethora of evidence to suggest that each cancer is unique and that there is considerable overlap in altered mutational pathways across the cancer genome [27–29]. Liver cancer is no different from other cancers in this respect, exhibiting shared molecular mechanisms. Interestingly, alterations in this particular gene have also been observed in numerous other cancers [30]. Due to clinical and molecular heterogeneity, stratification of patients remains a difficult task, especially in HCC, the predominant form of liver cancer. Of interest, several abnormally regulated signaling pathways [31], and the frequently mutated drivers [32] have been associated with HCC; however, their transformation as molecular therapy is still pending. Therefore, there is an urgent need to find more effective diagnostic and prognostic markers.

Since there have been recent discussions about the crucial role of G protein-coupled receptors (GPCRs) in tumorigenesis and the development of HCC [8]. Moreover, the possible involvement of RGS (Regulators of G protein signaling) proteins that negatively regulate GPCR signaling in various cancers. Herein, we investigated the potential role of RGS20 in liver cancer. As aforementioned, a few members of the RGS family (RGS3, RGS5, RGS17) have also been associated with liver cancer, however, the putative role of RGS20 as a prognostic indicator in HCC has not yet been investigated. We found that RGS20 was strongly upregulated in tumor tissue compared with adjacent normal tissue of HCC patients. In addition, RGS20 was strongly associated with some important clinical parameters such as AFP and grade in HCC patients. Of interest, RGS20 was found to be an important factor in the survival of HCC patients. Specifically, in TCGA data high RGS20 expression group was associated with a worse survival rate compared to the low RGS20 expression group. Using Cox regression analysis to examine independent HCC survival-related factors, some features including RGS20, age and tumor stage were confirmed. We also validated the prognostic potential of RGS20 in HCC using GEO datasets. GSEA analysis revealed some tumor pathways associated with RGS20, namely DNA REPAIR, mTORC1, MYC TARGETS V1 signaling being predominant. In addition, the RGS20 gene is correlated with five lincRNAs (LINC00511, PVT1, MIR4435-2HG, BCYRN1, and MAPKAPK5-AS1). Besides BCYRN1, the other four lincRNAs present possible interaction with RGS20 protein and only

lincRNA PTV1 showed potential interaction with mRNA of RGS20. This evidence supports that RGS20 was found to be significantly associated with some tumor-related signaling pathways and long non-coding RNAs (lincRNAs) that exhibit oncogenic potential. An interesting study using overexpression and knockdown of RGS20 in different cancer cell lines showed that it may play a role in the regulation of cancer cell migration and invasion, and even perhaps metastasis [19].

Of interest, all of the lincRNAs (LINC00511, PVT1, MIR4435-2HG, BCYRN1, and MAPKAPK5-AS1) that we found associated with RGS20 have previously been implicated in HCC. For instance, a high expression of LINC00511 was found in HCC tissues and cell lines, and blocking the LINC00511 contributed to a lower proliferation, migration, and invasion in HCC cell lines [33]. Similarly, PVT1 has been shown to facilitate the growth of HCC cells via the PVT1/EZH2/miR-214 axis [34]. In the case of MIR4435-2HG, its expression was found to be upregulated in HCC which may promote cancer cell proliferation by upregulating miRNA-487a [35]. The high expression of BCYRN1 was also linked to an unfavorable prognosis in patients with HCC [36]. The expression of MAPKAPK5-AS1 was also significantly increased in HCC, and it was suggested that the MAPKAPK5-AS1/PLAGL2/HIF-1α signaling loop contributes to HCC progression [37]. Since some cancers were not associated with RGS20 and some also did not show a significant difference, despite RGS20 being expressed highly in their respective tissues (e.g., glioblastoma). This can be partially explained by variability in the expression of certain genes in different tissues. Furthermore, a cumulative effect of (epi-) genomics and oncogenic networks/mechanisms might be contributing to this. Recently, a novel immunodiagnostic assay was developed to screen tumor-associated antigens (TAAs) associated with HCC, that includes RGS20 in a panel of eleven TAAs (AAGAB, C17orf75, CDC37L1, DUSP6, EID3, PDIA2, RGS20, PCNA, TAF7L, TBC1D13, and ZIC2) [38]. Thus, providing further evidence to support our study indicating the distinctive involvement of RGS20 in HCC. Overall, our results suggest that RGS20 is an attractive candidate to predict the prognosis for survival of HCC patients. Further studies in experimental and clinical settings are required to validate our findings.

5. Conclusions

The regulator of G protein signaling 20 correlates with lincRNAs harboring oncogenic potential and is markedly upregulated in hepatocellular carcinoma. Our analysis further supports the putative function of RGS proteins, particularly RGS20, in cancer.

References

1. Villanueva, A. Hepatocellular Carcinoma. *N. Engl. J. Med.* **2019**, *380*, 1450–1462. [CrossRef]
2. Zhong, C.; Li, Y.; Yang, J.; Jin, S.; Chen, G.; Li, D.; Fan, X.; Lin, H. Immunotherapy for Hepatocellular Carcinoma: Current Limits and Prospects. *Front. Oncol.* **2021**, *11*, 589680. [CrossRef] [PubMed]

3. Sharma, A.; Schmidt-Wolf, I.G.H. 30 years of CIK cell therapy: Recapitulating the key breakthroughs and future perspective. *J. Exp. Clin. Cancer Res. CR* **2021**, *40*, 388. [CrossRef] [PubMed]

4. Piñero, F.; Dirchwolf, M.; Pessôa, M.G. Biomarkers in Hepatocellular Carcinoma: Diagnosis, Prognosis and Treatment Response Assessment. *Cells* **2020**, *9*, 1370. [CrossRef] [PubMed]

5. Yan, Y.C.; Meng, G.X.; Ding, Z.N.; Liu, Y.F.; Chen, Z.Q.; Yan, L.J.; Yang, Y.F.; Liu, H.; Yang, C.C.; Dong, Z.R.; et al. Somatic mutation and expression of BAP1 in hepatocellular carcinoma: An indicator for ferroptosis and immune checkpoint inhibitor therapies. *J. Cancer* **2022**, *13*, 88–101. [CrossRef]

6. Sharma, A.; Liu, H.; Tobar-Tosse, F.; Chand Dakal, T.; Ludwig, M.; Holz, F.G.; Loeffler, K.U.; Wüllner, U.; Herwig-Carl, M.C. Ubiquitin Carboxyl-Terminal Hydrolases (UCHs): Potential Mediators for Cancer and Neurodegeneration. *Int. J. Mol. Sci.* **2020**, *21*, 3910. [CrossRef] [PubMed]

7. Wang, Y.; Ge, F.; Sharma, A.; Rudan, O.; Setiawan, M.F.; Gonzalez-Carmona, M.A.; Kornek, M.T.; Strassburg, C.P.; Schmid, M.; Schmidt-Wolf, I.G.H. Immunoautophagy-Related Long Noncoding RNA (IAR-lncRNA) Signature Predicts Survival in Hepatocellular Carcinoma. *Biology* **2021**, *10*, 1301. [CrossRef]

8. Peng, W.T.; Sun, W.Y.; Li, X.R.; Sun, J.C.; Du, J.J.; Wei, W. Emerging Roles of G Protein-Coupled Receptors in Hepatocellular Carcinoma. *Int. J. Mol. Sci.* **2018**, *19*, 1366. [CrossRef]

9. James, M.A.; Lu, Y.; Liu, Y.; Vikis, H.G.; You, M. RGS17, an overexpressed gene in human lung and prostate cancer, induces tumor cell proliferation through the cyclic AMP-PKA-CREB pathway. *Cancer Res.* **2009**, *69*, 2108–2116. [CrossRef]

10. Tso, P.H.; Yung, L.Y.; Wang, Y.; Wong, Y.H. RGS19 stimulates cell proliferation by deregulating cell cycle control and enhancing Akt signaling. *Cancer Lett.* **2011**, *309*, 199–208. [CrossRef]

11. Liang, G.; Bansal, G.; Xie, Z.; Druey, K.M. RGS16 inhibits breast cancer cell growth by mitigating phosphatidylinositol 3-kinase signaling. *J. Biol. Chem.* **2009**, *284*, 21719–21727. [CrossRef]

12. Wang, Y.; Tong, Y.; Tso, P.H.; Wong, Y.H. Regulator of G protein signaling 19 suppresses Ras-induced neoplastic transformation and tumorigenesis. *Cancer Lett.* **2013**, *339*, 33–41. [CrossRef] [PubMed]

13. Lu, S.; Zhou, J.; Sun, Y.; Li, N.; Miao, M.; Jiao, B.; Chen, H. The noncoding RNA HOXD-AS1 is a critical regulator of the metastasis and apoptosis phenotype in human hepatocellular carcinoma. *Mol. Cancer* **2017**, *16*, 125. [CrossRef]

14. Xu, C.; Li, Y.M.; Sun, B.; Zhong, F.J.; Yang, L.Y. ATE1 Inhibits Liver Cancer Progression through RGS5-Mediated Suppression of Wnt/β-Catenin Signaling. *Mol. Cancer Res. MCR* **2021**, *19*, 1441–1453. [CrossRef] [PubMed]

15. Umeno, Y.; Ogasawara, S.; Akiba, J.; Hattori, S.; Kusano, H.; Nakashima, O.; Koga, H.; Torimura, T.; Yamakawa, R.; Yano, H. Regulator of G-protein signaling 5 enhances portal vein invasion in hepatocellular carcinoma. *Oncol. Lett.* **2018**, *15*, 1763–1770. [CrossRef] [PubMed]

16. Hu, M.; Chen, X.; Zhang, J.; Wang, D.; Fang, X.; Wang, X.; Wang, G.; Chen, G.; Jiang, X.; Xia, H.; et al. Over-expression of regulator of G protein signaling 5 promotes tumor metastasis by inducing epithelial-mesenchymal transition in hepatocellular carcinoma cells. *J. Surg. Oncol.* **2013**, *108*, 192–196. [CrossRef] [PubMed]

17. Zhang, W.; Qian, S.; Yang, G.; Zhu, L.; Zhou, B.; Wang, J.; Liu, R.; Yan, Z.; Qu, X. MicroRNA-199 suppresses cell proliferation, migration and invasion by downregulating RGS17 in hepatocellular carcinoma. *Gene* **2018**, *659*, 22–28. [CrossRef] [PubMed]

18. Sokolov, E.; Iannitti, D.A.; Schrum, L.W.; McKillop, I.H. Altered expression and function of regulator of G-protein signaling-17 (RGS17) in hepatocellular carcinoma. *Cell. Signal.* **2011**, *23*, 1603–1610. [CrossRef]

19. Yang, L.; Lee, M.M.; Leung, M.M.; Wong, Y.H. Regulator of G protein signaling 20 enhances cancer cell aggregation, migration, invasion and adhesion. *Cell. Signal.* **2016**, *28*, 1663–1672. [CrossRef]

20. Li, G.; Wang, M.; Ren, L.; Li, H.; Liu, Q.; Ouyang, Y.; He, L.; Li, F. Regulator of G protein signaling 20 promotes proliferation and migration in bladder cancer via NF-κB signaling. *Biomed. Pharmacother. Biomed. Pharmacother.* **2019**, *117*, 109112. [CrossRef]

21. Li, Q.; Jin, W.; Cai, Y.; Yang, F.; Chen, E.; Ye, D.; Wang, Q.; Guan, X. Regulator of G protein signaling 20 correlates with clinicopathological features and prognosis in triple-negative breast cancer. *Biochem. Biophys. Res. Commun.* **2017**, *485*, 693–697. [CrossRef] [PubMed]

22. Huang, G.; He, X.; Wei, X.L. lncRNA NEAT1 promotes cell proliferation and invasion by regulating miR-365/RGS20 in oral squamous cell carcinoma. *Oncol. Rep.* **2018**, *39*, 1948–1956. [CrossRef] [PubMed]

23. Hu, P.; Zhou, G.; Zhang, X.; Song, G.; Zhan, L.; Cao, Y. Long non-coding RNA Linc00483 accelerated tumorigenesis of cervical cancer by regulating miR-508-3p/RGS17 axis. *Life Sci.* **2019**, *234*, 116789. [CrossRef]

24. Wang, S.L.; Dong, X.W.; Zhao, F.; Li, C.X. MiR-203 inhibits cell proliferation, invasion, and migration of ovarian cancer through regulating RGS17. *J. Biol. Regul. Homeost. Agents* **2021**, *35*, 1109–1115. [CrossRef] [PubMed]

25. Su, W.Z.; Ren, L.F. MiRNA-199 inhibits malignant progression of lung cancer through mediating RGS17. *Eur. Rev. Med. Pharmacol. Sci.* **2019**, *23*, 3390–3400. [CrossRef]

26. Muppirala, U.K.; Honavar, V.G.; Dobbs, D. Predicting RNA-protein interactions using only sequence information. *BMC Bioinform.* **2011**, *12*, 489. [CrossRef]

27. Sharma, A.; Liu, H.; Herwig-Carl, M.C.; Chand Dakal, T.; Schmidt-Wolf, I.G.H. Epigenetic Regulatory Enzymes: Mutation Prevalence and Coexistence in Cancers. *Cancer Investig.* **2021**, *39*, 257–273. [CrossRef]

28. Dhabhai, B.; Sharma, A.; Maciaczyk, J.; Dakal, T.C. X-Linked Tumor Suppressor Genes Act as Presumed Contributors in the Sex Chromosome-Autosome Crosstalk in Cancers. *Cancer Investig.* **2022**, *40*, 103–110. [CrossRef] [PubMed]

29. Liu, H.; Li, H.; Luo, K.; Sharma, A.; Sun, X. Prognostic gene expression signature revealed the involvement of mutational pathways in cancer genome. *J. Cancer* **2020**, *11*, 4510–4520. [CrossRef]

30. Sharma, A.; Biswas, A.; Liu, H.; Sen, S.; Paruchuri, A.; Katsonis, P.; Lichtarge, O.; Chand Dakal, T.; Maulik, U.; Gromiha, M.M.; et al. Mutational Landscape of the BAP1 Locus Reveals an Intrinsic Control to Regulate the miRNA Network and the Binding of Protein Complexes in Uveal Melanoma. *Cancers* **2019**, *11*, 1600. [CrossRef]

31. Dimri, M.; Satyanarayana, A. Molecular Signaling Pathways and Therapeutic Targets in Hepatocellular Carcinoma. *Cancers* **2020**, *12*, 491. [CrossRef] [PubMed]

32. Wang, F.; Breslin, S.J.P.; Qiu, W. Novel oncogenes and tumor suppressor genes in hepatocellular carcinoma. *Liver Res.* **2021**, *5*, 195–203. [CrossRef] [PubMed]

33. Wang, R.P.; Jiang, J.; Jiang, T.; Wang, Y.; Chen, L.X. Increased long noncoding RNA LINC00511 is correlated with poor prognosis and contributes to cell proliferation and metastasis by modulating miR-424 in hepatocellular carcinoma. *Eur. Rev. Med. Pharmacol. Sci.* **2019**, *23*, 3291–3301. [CrossRef] [PubMed]

34. Gou, X.; Zhao, X.; Wang, Z. Long noncoding RNA PVT1 promotes hepatocellular carcinoma progression through regulating miR-214. *Cancer Biomark. Sect. A Dis. Markers* **2017**, *20*, 511–519. [CrossRef] [PubMed]

35. Kong, Q.; Liang, C.; Jin, Y.; Pan, Y.; Tong, D.; Kong, Q.; Zhou, J. The lncRNA MIR4435-2HG is upregulated in hepatocellular carcinoma and promotes cancer cell proliferation by upregulating miRNA-487a. *Cell. Mol. Biol. Lett.* **2019**, *24*, 26. [CrossRef] [PubMed]

36. Ding, S.; Jin, Y.; Hao, Q.; Kang, Y.; Ma, R. LncRNA BCYRN1/miR-490-3p/POU3F2, served as a ceRNA network, is connected with worse survival rate of hepatocellular carcinoma patients and promotes tumor cell growth and metastasis. *Cancer Cell Int.* **2020**, *20*, 6. [CrossRef]

37. Wang, L.; Sun, L.; Liu, R.; Mo, H.; Niu, Y.; Chen, T.; Wang, Y.; Han, S.; Tu, K.; Liu, Q. Long non-coding RNA MAPKAPK5-AS1/PLAGL2/HIF-1α signaling loop promotes hepatocellular carcinoma progression. *J. Exp. Clin. Cancer Res. CR* **2021**, *40*, 72. [CrossRef] [PubMed]

38. Wu, J.; Wang, P.; Han, Z.; Li, T.; Yi, C.; Qiu, C.; Yang, Q.; Sun, G.; Dai, L.; Shi, J.; et al. A novel immunodiagnosis panel for hepatocellular carcinoma based on bioinformatics and the autoantibody-antigen system. *Cancer Sci.* **2021**, *113*, 411. [CrossRef]

3.3 Publication 3: Systematic discrimination of the repetitive genome in proximity of ferroptosis genes and a novel prognostic signature correlating with the oncogenic lncRNA CRNDE in multiple myeloma

Jiading Qin[1,2,3†] , Amit Sharma[4,5†], **Yulu Wang**[4†], Fabian Tobar-Tosse[6], Tikam Chand Dakal[7], Hongde Liu[8], Hongjia Liu[8], Bo Ke[2], Chunfang Kong[2], Tingting Liu[2], Chunxia Zhao[9], Ingo G. H. Schmidt-Wolf[4] and Chenghao Jin[1,2,3*]

[1]Medical College of Nanchang University, Nanchang, China
[2]Department of Hematology, Jiangxi Provincial People's Hospital, Nanchang, China,
[3]National Clinical Research Center for Hematologic Diseases, The First Affifiliated Hospital of Soochow University, Soochow China
[4]Department of Integrated Oncology, Center for Integrated Oncology, University Hospital of Bonn, Bonn, Germany,
[5]Department of Neurosurgery, University Hospital of Bonn, Bonn, Germany
[6]Department of Basic Sciences for Health, Pontifificia Universidad Javeriana Cali, Cali, Colombia
[7]Genome and Computational Biology Lab, Department of Biotechnology, Mohanlal Sukhadia University, Udaipur, India
[8]State Key Laboratory of Bioelectronics, School of Biological Science & Medical Engineering, Southeast University, Nanjing, China
[9]School of Nursing, Nanchang University, Nanchang, China

Check for updates

Systematic discrimination of the repetitive genome in proximity of ferroptosis genes and a novel prognostic signature correlating with the oncogenic lncRNA CRNDE in multiple myeloma

Jiading Qin[1,2,3†], Amit Sharma[4,5†], Yulu Wang[4†], Fabian Tobar-Tosse[6], Tikam Chand Dakal[7], Hongde Liu[8], Hongjia Liu[8], Bo Ke[2], Chunfang Kong[2], Tingting Liu[2], Chunxia Zhao[9], Ingo G. H. Schmidt-Wolf[4] and Chenghao Jin[1,2,3*]

[1]Medical College of Nanchang University, Nanchang, China, [2]Department of Hematology, Jiangxi Provincial People's Hospital, Nanchang, China, [3]National Clinical Research Center for Hematologic Diseases, The First Affiliated Hospital of Soochow University, Soochow China, [4]Department of Integrated Oncology, Center for Integrated Oncology, University Hospital of Bonn, Bonn, Germany, [5]Department of Neurosurgery, University Hospital of Bonn, Bonn, Germany, [6]Department of Basic Sciences for Health, Pontificia Universidad Javeriana Cali, Cali, Colombia, [7]Genome and Computational Biology Lab, Department of Biotechnology, Mohanlal Sukhadia University, Udaipur, India, [8]State Key Laboratory of Bioelectronics, School of Biological Science & Medical Engineering, Southeast University, Nanjing, China, [9]School of Nursing, Nanchang University, Nanchang, China

Emerging insights into iron-dependent form of regulated cell death ferroptosis in cancer have opened a perspective for its use in cancer therapy. Of interest, a systematic profiling of ferroptosis gene signatures as prognostic factors has gained special attention in several cancers. Herein, we sought to investigate the presence of repetitive genomes in the vicinity of ferroptosis genes that may influence their expression and to establish a prognostic gene signature associated with multiple myeloma (MM). Our analysis showed that genes associated with ferroptosis were enriched with the repetitive genome in their vicinity, with a strong predominance of the SINE family, followed by LINE, of which the most significant discriminant values were SINE/Alu and LINE/L1, respectively. In addition, we examined in detail the performance of these genes as a cancer risk prediction model and specified fourteen ferroptosis-related gene signatures, which identified MM high-risk patients with lower immune/stromal scores with higher tumor purity in their immune microenvironment. Of interest, we also found that lncRNA CRNDE correlated with a risk score and was highly associated with the majority of genes comprising the signature. Taken together, we propose to investigate the molecular impact of the repetitive genome we have highlighted on the local transcriptome of ferroptosis genes in

cancer. Furthermore, we revealed a genomic signature/biomarker related to ferroptosis that can be used to predict the risk of survival in MM patients.

Highlights

- Ferroptosis-related genes showed enrichment with the repetitive genome in their vicinity, with strong predominance of the SINE family.
- We generated ferroptosis-related prognostic gene signature that can identify high-risk multiple myeloma patients.
- LncRNA CRNDE showed strong association with the majority of genes forming the prognostic signature.

Introduction

Cell death is an essential feature of physiological/pathological processes, and ferroptosis which differs considerably from other cell death types, such as apoptosis, necrosis, and autophagy has recently gained attention. Accumulative studies have shown that dysregulated ferroptosis participates in several cancers, including renal cell carcinoma (1), colorectal carcinoma (2), gastric cancer (3), and multiple myeloma (4, 5). Overall, targeting potential regulatory factors in the ferroptosis pathway is thought to promote or inhibit disease progression in several malignancies.

Over the years, ferroptosis-related genes have been used to generate a prognostic signature in lung adenocarcinoma (6), low-grade glioma (7)., acute myeloid leukemia (8), gastric cancer (9), renal cell carcinoma (10), osteosarcoma (11), skin melanoma (12), and breast cancer (13). However, most of studies focused on the gene expression patterns and correlation with the clinical outcomes, mainly survival rate. None of the above-mentioned studies addressed the impact of genome organization in proximity to these genes, which is known to play a pivotal role in human diseases (14). On this note, the prevalence of repetitive sequences, especially LINEs (Long Interspersed Nuclear Elements), SINEs (Short Interspersed Nuclear Elements), Alu family in the functional parts of genomes and their association with cancers remains undisputed (15–17). Aoki et al. evaluated global methylation levels of four repetitive elements (LINE-1, Alu Ya5, Alu Yb8 and Satellite-α) in MM samples and found the global

hypomethylation of LINE-1 being associated with progression and worse prognosis of multiple myeloma (MM) (18). Using bisulfite treatment followed by sequencing, Bollati et al. investigated the methylation status of repetitive DNA elements to verify a possible correlation with the different molecular subtypes of MM, and found a progressive and significant decrease of methylation in Alu, LINE-1 and SAT-α sequences (19). In a comprehensive study, Lee et al. discussed about various somatic insertions of LINE-1, Alu and ERV in different types of cancer, including colorectal, glioblastoma, ovarian, prostate and multiple myeloma (20). It is also noteworthy to mention that some noncoding RNAs (ncRNAs), particularly long noncoding RNAs, have been found to be involved in biological processes of ferroptosis, thus influencing cancer growth (21, 22). Although the exact regulatory mechanism behind this remains unclear, their potential use as ncRNAs-based ferroptosis targeting has been hypothesized (23) An interesting study examined some lncRNAs closely related to ferroptosis and identified PELATON as a novel ferroptosis suppressor that may also serves as a prognostic signature in glioblastoma patients (24).

Considering this, herein, we investigate the presence of repetitive genomes in the vicinity of ferroptosis genes that may influence their expression. In our comprehensive approach, we considered the analysis of various repeat configurations, e.g., LINEs (L1 and L2), SINEs (Alu and MIR), low complexity (AT and GC) and interspersed elements, across the upstream promoter region of these particular genes, as we reported previously (25). In addition, we used ferroptosis genes to create the first prognostic gene signature (based on risk groups and immune microenvironment) linked to multiple myeloma. Besides, we demonstrated the putative association of the oncogenic lncRNA CRNDE with the obtained MM-specific ferroptosis gene signature.

Materials and methods

Ferroptosis-related genes and repetitive genome analysis

We manually collected 387 genes classified as ferroptosis driver genes, suppressor genes, and markers using available

database (http://www.zhounan.org/ferrdb). Upon removal of duplicates, we retained 269 genes that were used for further analysis like repetitive genomic analysis and determination of the prognostic signature.

To identify repetitive genomic sequence in the proximity of these genes, we retrieved repeats and genomic annotations from the T2T genome assembly (CHM13v2.0) available in the NCBI FTP (ftp://ncbi.nlm.nih.gov). Genomics coordinates were used to identify repeats in the 2kb promoter region of genes, as well as the classification of the repeats, their length, and their order relative to the transcription start site. We then calculated the repeat content for each gene using the n-gram probabilistic model (26) in which each repeat was defined as a unigram with a normalized weight (frequency and length were properties associated with the model). It was calculated as $RC(r) = Log (Nr * Lr/Le)$, where the repeat content (RC) for the repeat (r) is defined by the absolute frequency (Nr) and repeat length (Lr) under a region of exploration with a specific length (Le), here 2kb promoter. A weighted matrix was created with the genes as the index and the repeat content values as the score for each repeat type. To identify discriminative repeats, two clustering methods were applied under the matrix: Hierarchical clustering with a complete linkage method, Manhattan distance metric for the whole data, and k-mean clustering as an unsupervised algorithm for the pair of repeat types with a significant discriminative score defined by hierarchical clustering, mainly implemented by using custom Python algorithms. Finally, gene clusters with associated repeats in k-means clustering were described by functional enrichment analysis in the String database (https://string-db.org), which includes Geneontology, KEGG, and Wikipathways datasets, together with the Enrich Tool and Allen Brain Atlas datasets (27).

Gene expression data and construction/validation of a prognostic signature

Multiple myeloma was selected to establish the prognostic signature based on ferroptosis-related genes. MM gene expression study MMRF-COMMPASS was obtained from the XENA database maintained by UCSC (https://xenabrowser.net/datapages/) and GSE24080 was obtained from the GEO database (https://www.ncbi.nlm.nih.gov/geo/). We used the MICE package to supplement missing values such as ethnicity, race, age, and International Staging System (ISS) stage from the MMRF-COMMPASS study and B2M, CRP, and creatinine from the GSE24080 cohort. We strictly followed the previously described procedure for data processing, and the paired-samples t-test was used to check for the consistency of the distribution between two cohorts. Subsequently, 844 patients from the

MMRF-COMMPASS study were used as the training cohort, while the 556 patients from the GSE24080 dataset served as the validation cohort. Next, Kaplan-Meier and univariate Cox analyses were performed in the training cohort to investigate the prognostic relationship between gene expression and overall survival (OS). A list of prognostic genes with risk correlation coefficients was generated using the Cox regression model LASSO (Least Absolute Shrinkage and Selection Operator) based on the OS in the training cohort with the optimal parameter lambda. Risk score was calculated using following equation, where n, βi and Coefi represented the number of hub genes, regression coefficient values and gene expression levels, respectively. Risk Score $= \sum_{i=1}^{n} Coefi * \beta i$. On the basis of median risk scores, patients were divided into either high or low risk score groups and Kaplan-Meier analysis were used to determine the survival differences between them. In this study, ROC analyses were performed to further evaluate the prognostic power of the ferroptosis-related gene signature. A similar procedure was used for the validation cohort. To mention, the training cohort had only OS status with five years follow-up, while validation cohort contained both OS status and event-free survival (EFS) status with seven years follow-up. We extend our analysis by generating and validating the nomogram-based analysis for predicting the survival probability in our cohorts. The nomogram was validated with the R package "rms" (calibrated for 3 and 5 years) and the C-index was measured to determine the predictive power.

Gene set enrichment analysis and immune infiltration status estimation

The relative cell component of tumor microenvironment in the MMRF-COMMPASS study was calculated using the CIBERSORT algorithm (28, 29). Furthermore, gene set enrichment analysis (GSEA) were used to investigate the pathophysiological mechanisms associated with the ferroptosis-related genes. Based on the median cutoff value, samples were divided into low and high expression groups. KEGG enrichment terms with an adjusted P value<0.05 and false discovery rate (q value)<0.05 were considered statistically significant and ranked accordingly. ESTIMATE algorithm was used to calculate the immune score, stromal score, and tumor purity of each sample. We also quantified the relative infiltration of 28 immune cell types that mark the infiltrating immune cells of MM by single-sample GSEA analysis (ssGSEA) followed previous published methods (30). Each immune cell type of feature gene panels was obtained from a recent article (31). An enrichment score in ssGSEA analysis represented the relative abundance of each immune cell type *via* "GSVA" package (version 1.39.1).

Expression profile of ferroptosis-related signatures in pan-cancer

To explore the expression of obtained signatures in pan-cancer, we downloaded the gene expression data of FPKM from TCGA for 33 cancers, FPKM (Fragments Per Kilobase per Million) i.e. fragments per kilobase of transcription per million mapped reads. We then calculated the average expression levels of these selective genes in all samples and in each cancer type separately to plot heat maps for visualization.

Prediction of ferroptosis and lncRNA interactions

LncRNAs gene expression in myeloma were obtained from MMRF-COMMPASS dataset in XENA database maintained by UCSC (https://xenabrowser.net/datapages/) and GSE24080 dataset in GEO database (https://www.ncbi.nlm.nih.gov/geo/). The correlation of risk score (based on our signature) and lncRNAs were investigated. Statistical significance was determined using Spearman correlation coefficient |R| > 0.3 and p value< 0.05. The prediction of physical and functional interaction between selected lncRNA (CRNDE) and the proteins of our signature genes were performed in RNA-Protein Interaction Prediction (RPISeq, http://pridb.gdcb.iastate.edu/RPISeq/) using the protein sequence of signature genes and RNA sequence of the lncRNAs. The output, i.e., prediction probability of possible interactions was obtained in terms of RF and SVM classifiers. The interaction probabilities ranging from 0 to 1 were considered, being higher probabilities were better. In general, prediction probabilities with score more than 0.5 was considered "positive," i.e., expressing the likelihood of interaction between given lncRNA and proteins. Next, the interaction of CRNDE (lncRNA) and mRNA of signature genes were explored. The prediction of physical and functional interaction between five lincRNAs and the mRNA of RGS20 was done using LncRRIsearch web server (http://rtools.cbrc.jp/LncRRIsearch/).

Statistical analysis

Statistical analyses were performed using R Studio (version 2021.09.1; https://rstudio.com/). Kaplan-Meier analysis was performed using the R packages "survival" and "survminer". Student's t-test was used to compare differences between subgroups where the data were normally distributed, otherwise the Wilcox. Test was applied. Univariate and multivariate Cox proportional hazard regression analyses were performed with the R package "survival", and LASSO analysis was performed with the R package "glmnet." All statistical tests were two-sided and P<0.05 was considered statistically significant.
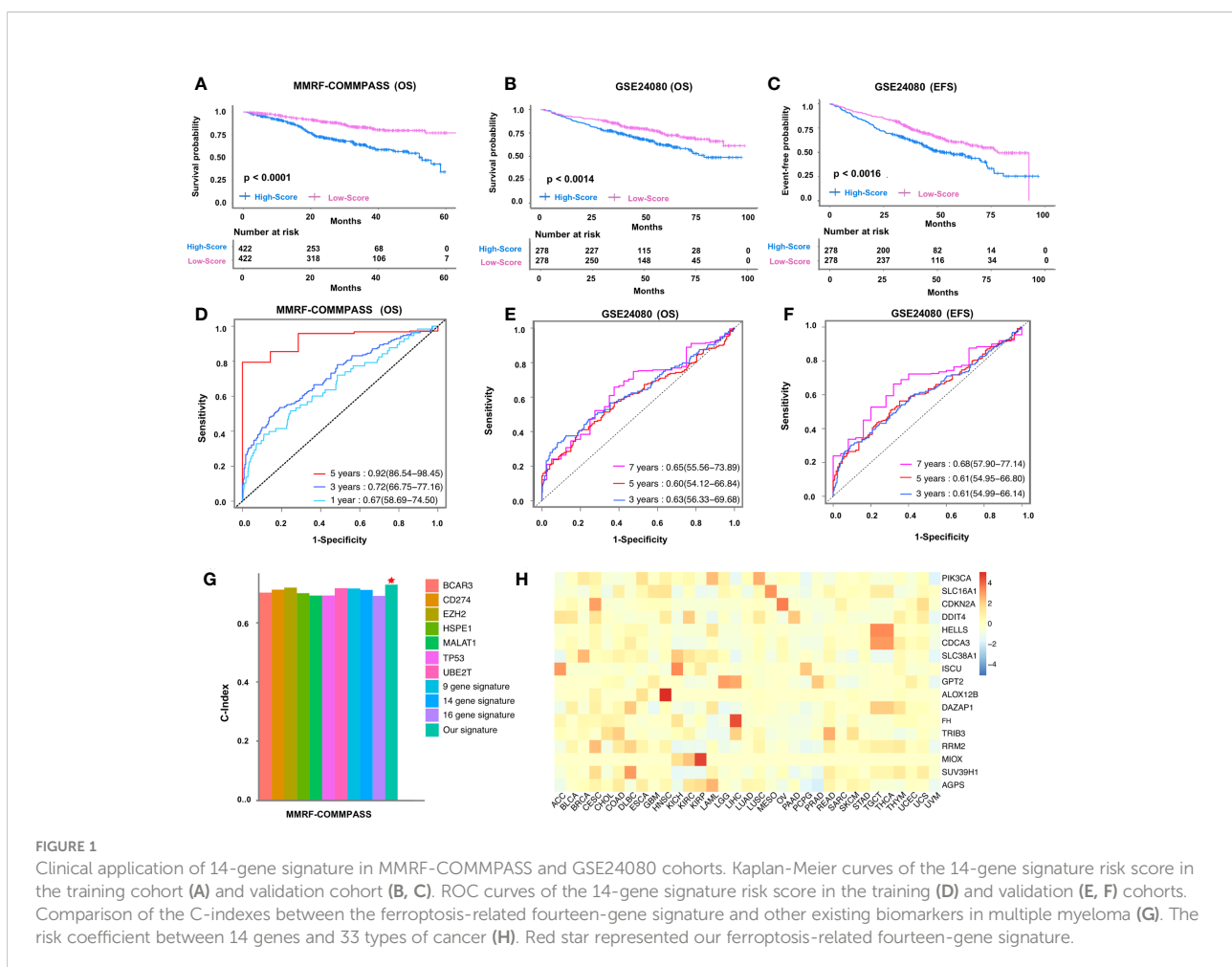
Results

Repetitive genome predominantly distributed in the proximity of ferroptosis genes

We first investigated the occurrence of repetitive genomic elements in the vicinity of ferroptosis genes (Supplementary Figure 1). For this purpose, we first determined the repetitive genome configuration in the promoter regions of these genes (~2KB). We found that Alu, MIR, L1 and L2 were the frequent repeats around 148 ferroptosis genes (Supplementary Figure 1A). Further clustering of these genes revealed high prevalence of LINE/L1, SINE/MIR, and SINE/Alu and low prevalence when these genes were combined or when LINE/L2 or others were included. In addition, the hierarchical distribution of repeats shows SINE/Alu and LINE/L1 as the divergent elements or with a significant discriminative score for gene clustering. To provide evidence for a possible functional relationship between gene clusters and repeats, we applied k-means clustering and functional enrichment analysis (Supplementary Figure 1B). Using this approach, we identified four significant gene clusters: L1-related (16 genes), Alu-related (59 genes), Alu/L1-related (17 genes), and unrelated genes (56 genes). In terms of their functional analysis, this discriminative analysis revealed the weight of each repeat type in the promoter region of gene sets that could define regulatory directions in the cellular and molecular context. We also checked the abilities of these clusters in other available datasets, such as the Allen Brain Atlas datasets, and found that each cluster represented a set of genes for some brain segments, e.g., "anterior cingulate area" for L1 and "paraventricular hypo-thalamic nucleus" for Alu-related repeats. For instance, the gene GABARAPL2 (highly associated to SINE/Alu) and the gene PARK7 (highly associated to LINE/L1) highlighted in our analysis, are known to be expressed highly in brain. In addition, these clusters were analyzed according to key cellular and molecular processes, e.g., the gene cluster more associated with LINE/L1 shows cellular responses to external stimuli (cytokine production, nongenomic effect of vitamin D, metabolic-related processes). Also, the gene cluster more associated with SINE/Alu shows standard metabolic processes and cellular adaptations to endogenous factors (response to starvation, autophagy, ferroptosis, fatty acid metabolism). Of interest, the cluster with Alu/L1-related genes reveals chromatin pathways mainly associated with the sirtulin 1 (SIRT1) and histone lysine methyltransferase (SUV39H1) genes, which could define specific configurations of these repeats for important regulatory processes.

Ferroptosis-related gene signature predicts the survival in multiple myeloma

We described our strategy in a flowchart (Supplementary Figure 2). Using the stringent strategy, the clinical characteristics of the patients involved in the study were outlined (Supplementary Table 1). We primarily used information from 844 patients (in the training cohort) and obtained 1669 survival-related genes (Supplementary Table 2). Thereafter, we intersected these survival-related genes with ferroptosis-related genes (n=269) and generated a list of 17 ferroptosis-related prognostic genes (Supplementary Figure 3A, Supplementary Table 3), which were further narrowed down based on risk coefficient scores (n=14) (Supplementary Figures 3B, C, Supplementary Table 4). Based on their mean risk score derived from the signature of 14 genes, the patients were classified into high-risk and low-risk groups. Notably, twelve signature genes (SLC38A1, CDKN2A, MIOX, AGPS, HELLS, FH, DAZAP1, SLC16A1, SUV39H1, DDIT4, TRIB3, ALOX12B) were found to be upregulated (Supplementary Figures 4A–L), while two (PIK3CA, ISCU) were downregulated

in the high-risk group, based on the training cohort (Supplementary Figures 4M, N). It is important to mention that compared to the low-risk group, the high-risk group showed a worse outcome in the training cohort OS (P< 0.0001, Figure 1A), both in the validation cohort OS (P = 0.0014, Figure 1B), and in the validation cohort EFS (P = 0.00016, Figure 1C). To confirm the prognostic power and independence of the ferroptosis-related gene signature from other clinical characteristics (age, albumin, B2M, creatine, CRP, hemoglobin, isotype, ISS stage, LDH, race, sex, risk), univariate and multivariate Cox analyses were also performed. Our analysis confirmed the robustness of the signature in the OS of the training cohort (univariate, HR = 1.1, 95% = 1.06-1.15, P<0.001; multivariate, HR = 1.06, 95%=1.02-1.1, P=0.005), OS of the validation cohort (univariate, HR = 1. 18, 95%=1.15-1.21, P<0.001; multivariate, HR=1.17, 95%=1.13-1.20, P<0.001) and EFS of the validation cohort (univariate, HR=1.08, 95%=1.05-1.12, P<0.001; multivariate, HR=1.05, 95%=1.02-1.09, P=0.004) (Supplementary Table 5). Thus, the gene signature associated with ferroptosis appears to be a reliable prognostic indicator for MM patients.

FIGURE 1
Clinical application of 14-gene signature in MMRF-COMMPASS and GSE24080 cohorts. Kaplan-Meier curves of the 14-gene signature risk score in the training cohort (A) and validation cohort (B, C). ROC curves of the 14-gene signature risk score in the training (D) and validation (E, F) cohorts. Comparison of the C-indexes between the ferroptosis-related fourteen-gene signature and other existing biomarkers in multiple myeloma (G). The risk coefficient between 14 genes and 33 types of cancer (H). Red star represented our ferroptosis-related fourteen-gene signature.

Prognostic performance and clinical application of ferroptosis-related gene signature

Next, to assess the prognostic performance of the signature, we performed time-dependent (one-year, three-year, and five-year) dynamic AUC comparisons in the OS training cohort and obtain AUC values of 0.67, 0.72, and 0.92, respectively (Figure 1D). Of interest, the AUC value of the multigene risk score compared with ISS stage and sex fared better compared to the independent variables in the training cohort across each time point within 5 years (Supplementary Figure 5A). Likewise, in the GSE24080 training cohort, the AUC value of the multigene risk score was 0.63, 0.6, and 0.65 at 3, 5, and 7 years, respectively (Figure 1E), and each event within 7 years was found to be greater compared to the defined clinical variables (Supplementary Figures 5B–D). Similar results were obtained when the EFS of the validation cohort was used to assess the predictive power of this multigene risk score (AUC: 0.61, 0.61, 0.68 at 3, 5, and 7 years, respectively) (Figure 1F, Supplementary Figures 5E–G). To translate our obtained ferroptosis-related gene signature into clinical application, we integrated the training factors (patient age, sex, ISS stage, and multigene signature) into multivariate Cox analysis and constructed a nomogram to predict the survival probability of patients with MM (Supplementary Figure 6A). Analysis of the calibration curve, which included the nomogram after 3 and 5 years, showed a close resemblance to the diagonal curve at the same defined intervals (Supplementary Figures 6B, C). In addition, the C-index of the training cohort for overall survival was found to be 0.764 (95CI = 0.747-0.781), whereas the C-index of the validation cohort was estimated as 0.703 (95CI = 0.682-0.724), suggesting reliability of the nomogram. Of interest, we found superior performance and better prognostic ability of the obtained ferroptosis-related signature when compared with 10 already known biomarkers (32–41) (Figure 1G). This was also evident in the decision curve analysis (DCA) of the nomogram, where the threshold probability ranged from 14% to 95% and the probability of maximum net benefit exceeded 0.2 (Supplementary Figure 7). Besides, we investigated the reliability of the obtained signature in a panel of 29 cancers and found that these genes are relatively highly expressed in most cancers, especially in HNSC (squamous cell carcinoma of the head and neck), CESC (squamous cell carcinoma of the cervix and endocervical adenocarcinoma), and COAD (adenocarcinoma of the colon) (Figure 1H).

Gene enrichment and immunofiltration analysis confirmed the relevance of the signature in high-risk MM patients

The result of CIBERSORT indicated that the plasma cells accounted for more than 85% (Supplementary Figure 8A), which was consistent with the experimental protocol of the GSE24080 or MMRF-COMMPASS study. To our surprise, non-plasma cells together, including memory B cells, CD4+ T cells, and activated NK cells (Supplementary Figure 8B), could account for more than 10% of the tumor microenvironment. These immune cells should not be ignored despite low absolute content (42). Considering the negative correlation between the risk score of ferroptosis-related gene signature and the clinical outcome of MM, KEGG enrichment analysis was performed between the high-risk and low-risk groups. We found that 22 KEGG terms were significantly enriched in the high-risk group (Figure 2A), with DNA replication being the highly enriched (Enrichment score = 0.8046), while the mRNA surveillance pathway had the lowest enrichment (Enrichment score = 0.5593) (Figure 2B). Notably, four ferroptosis-related pathways, including proteasome (NES = 1.6748, adjusted p-value = 0.0263, 5q-value = 0.0181), cysteine and methionine metabolism (NES = 1.7277, adjusted p-value = 0.0195, q-value = 0.0134), p53 signaling pathway (NES = 1.5643, adjusted p-value = 0.0263, q-value = 0.0181) and DNA replication (NES = 1.9783, adjusted p-value = 0.0195, q-value = 0.0134), were found to be significantly enriched in high-risk MM patients (Supplementary Figure 9).

Since immune cell infiltration may have a differential impact on high and low-score patients, we next assessed the degree of immune infiltration using the ESTIMATE algorithm. The analysis showed that the high-risk MM in the training cohort had lower immune and stromal score but high tumor purity (Supplementary Figures 10A–C), which was also confirmed in the validation cohort (Supplementary Figures 9D–F). Of interest, we found that immune and stromal score were negatively correlated with risk score, whereas tumor purity was positively correlated with risk score in the training cohort (Supplementary Figures 10G–I). To further investigate the influence of immune cell population alternation, we built cox proportional hazards regression models based on the enrichment level of 28 immune infiltration-related gene sets via ssGSEA analyses, and focused on whether the alternation of these gene sets was related with poor outcome. In the training cohort, activated CD4+T cells, regulatory T cells, and type 1 T helper cells were significantly negatively associated with OS (P<0.05) (Supplementary Figure 11A), whereas follicular T helper cells and immature B cells were significantly positively associated with OS (P<0.05). Meanwhile, in the validation cohort (Supplementary Figure 11B), activated CD4+T cells and type 2 T helper cells were significantly negatively associated with OS (P<0.05), whereas type 17 T helper cells were significantly positively associated with OS (P<0.05). Thus, we noticed that activated CD4+T cells was significantly negatively associated with OS in both cohorts (Figure 2C). Interestingly, the enrichment degree of high-risk group was significantly higher than that of low-risk group in both cohorts (Figures 2D, E). Of significance, only activated CD4+T cells were
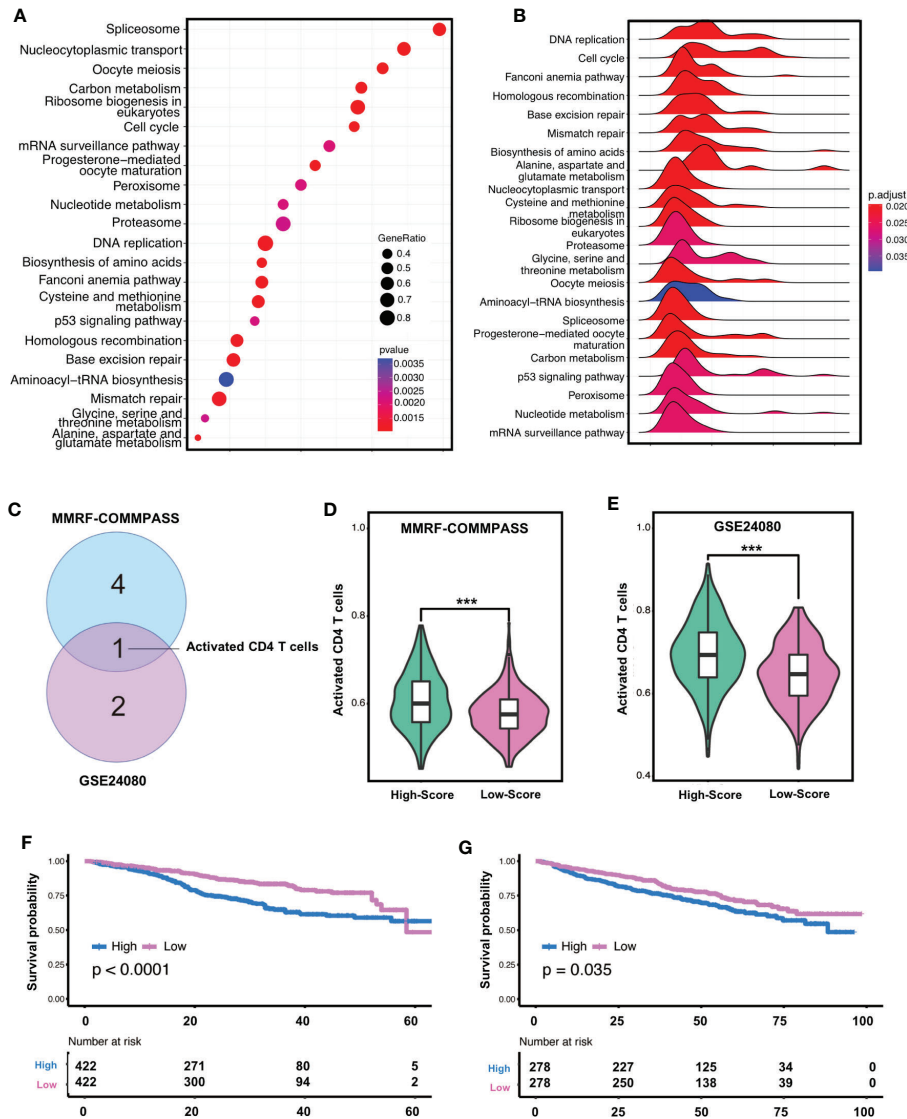
FIGURE 2
Gene enrichment and immunofiltration analysis confirmed the relevance of the signature in high-risk MM patients. **(A)** Bubble diagram shows gene counts and gene ratio of the significantly enriched KEGG pathway terms. **(B)** Ridgeline plot shows enrichment score of the significantly enriched KEGG pathway terms. **(C)** Immune cell population alternation associated with OS with statistically significant difference in both cohorts. **(D, E)** the enrichment degree of high-risk group was significantly higher than that of low-risk group in both cohorts by ssGSEA analyses *** indicates P-value < 0.001. **(F, G)** Activated CD4+T cells were relevant to survival in both the training cohorts. KEGG, kyoto encyclopedia of genes and genomes; GSEA, gene set enrichment analysis; ES, enrichment score.

relevant to survival in both the training cohort (p<0.001) and the validation cohort (p=0.035) (Figures 2F, G).

Oncogenic lncRNA CRNDE and signature genes display strong correlation

Since an increasing number of studies have indicated that non-coding RNAs may modulate the process of ferroptotic cell death (43–45). Herein, we also assessed the potential correlation

of obtained ferroptosis gene signature with the lncRNAs. Of interest, while we found only a few lncRNAs in the training cohort (KIFC1, DSCR4) and in the validation cohort (SLC44A4, PSMB1, LINC01398, LINC01213, LINC00851), while the oncogenic lncRNA CRNDE was significantly correlated in both cohorts (Figure 3A). We also observed that the risk score increased significantly with increasing expression of CRNDE in both cohorts, MMRF-COMMPASS cohort (left) and GEO cohort (right). (Figure 3B). Further analysis revealed that the lncRNA CRNDE and signature genes interact with each other at

both the mRNA level and the protein level (Figures 3C, D). Our analysis showed that all tested proteins were reasonably good interaction partners of the lncRNA CRNDE. However, a selected few proteins such as HELLS, SLC16A1, and CDKN2A were predicted to be the major interacting partners of the lncRNA CRNDE. With one exception (DDIT4), all other ferroptosis associated genes in the obtained signature were enriched in repetitive genomes, especially with Alu-related repeats (MIOX, HELLS, DAZAP1, TRIB3, PIK3CA, SUV39H1).

Discussion

Emerging evidence suggests that ferroptosis may be the target of innovative antitumor therapies (46, 47). Given this, there have been a multitude of studies that have defined several aspects of genes and mechanisms related to ferroptosis in cancers (48–50). However, the effects of genome organization (repetitive genome) in the proximity of these genes have not been investigated. In addition, only a few studies have investigated the aspect of ferroptosis in multiple myeloma (MM), a form of cancer characterized by excessive proliferation and dysfunction of certain plasma cells in the bone marrow (5). MM being a hematological malignancy

harbors biological complexity due to several disrupted cancer pathways resulting from multiple genetic abnormalities and epigenetic aberrations (4, 51, 52). A recent study showed that induction of Ferroptosis in MM cells triggers DNA methylation and histone modification changes associated with cellular senescence (4). Similarly, a study compared the kinomic activity profile of the natural anticancer agent withaferin A with apoptotic and ferroptotic signatures to predict the mode of cell death in MM cells (53). Considering this, herein, we investigated the genomic architecture of ferroptosis-related genes and independently constructed a prognostic signature for patient stratification in MM.

To this end, we first defined the ferroptosis-related genes and assessed the presence of the repetitive genome in their promoter region and specified the gene clusters with L1, Alu, and L1/Alu repeats. To mention, such repeats have been described by their regulatory role in gene expression (54)., however, the significance of their distribution or configuration remains unclear. Moreover, further clustering of these genes revealed high prevalence of LINE/L1, SINE/MIR, and SINE/Alu and low prevalence when these genes were combined or when LINE/L2 or others were included. The functional analysis revealed that the obtained clusters are involved in key cellular and molecular processes. For instance, the gene cluster associated with LINE/L1
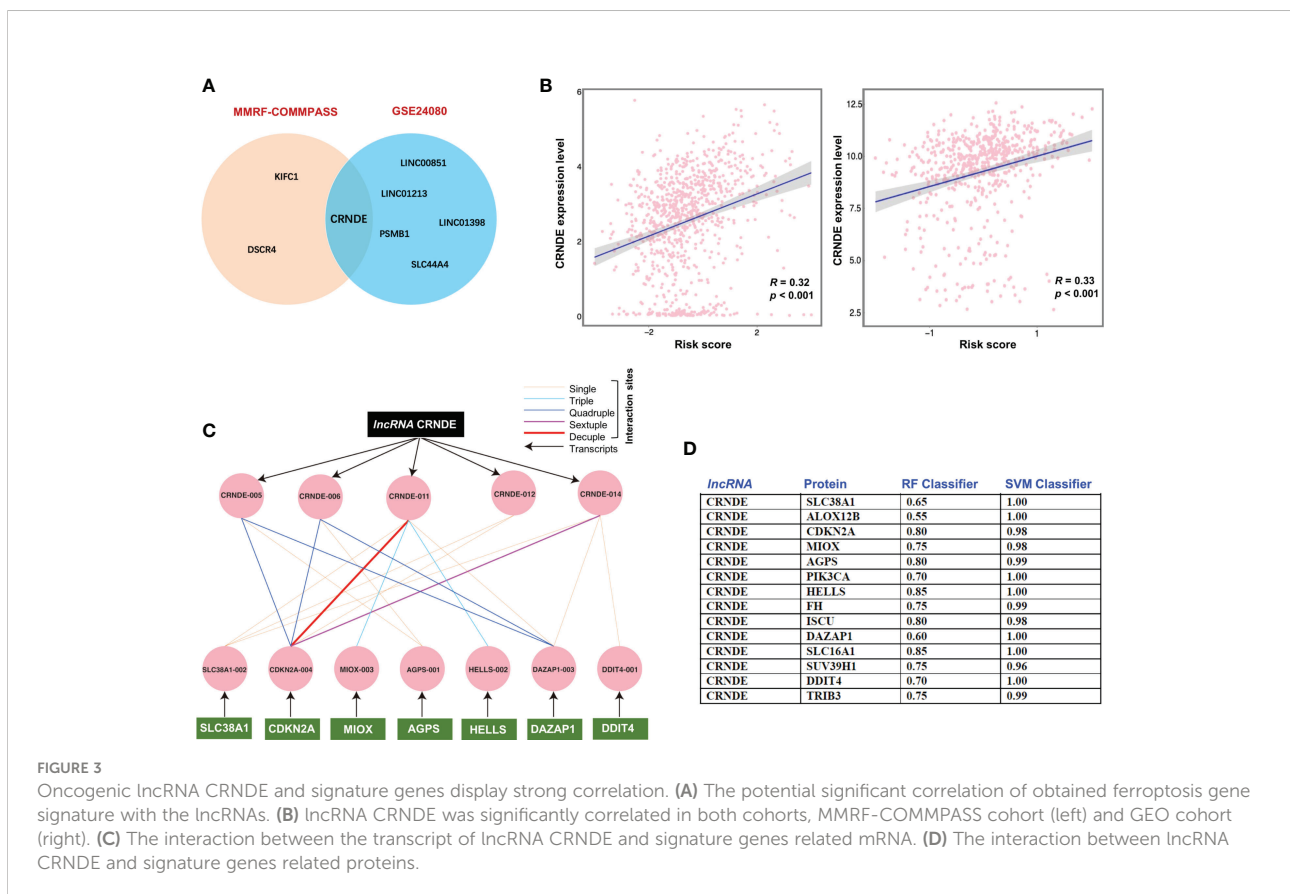
FIGURE 3

Oncogenic lncRNA CRNDE and signature genes display strong correlation. **(A)** The potential significant correlation of obtained ferroptosis gene signature with the lncRNAs. **(B)** lncRNA CRNDE was significantly correlated in both cohorts, MMRF-COMMPASS cohort (left) and GEO cohort (right). **(C)** The interaction between the transcript of lncRNA CRNDE and signature genes related mRNA. **(D)** The interaction between lncRNA CRNDE and signature genes related proteins.

showed involvement in cellular responses to external stimuli (cytokine production, nongenomic effect of vitamin D, metabolic-related processes). While, the gene clusters more associated with SINE/Alu showed standard metabolic processes and cellular adaptations to endogenous factors (response to starvation, autophagy, ferroptosis, fatty acid metabolism). Of interest, the clusters with Alu/L1-related genes show chromatin pathways primarily linked sirtulin 1 (SIRT1) and histone lysine methyltransferase (SUV39H1) genes.

Next, using the stringent strategy, we established the ferroptosis-related prognostic genes signature containing fourteen genes (SLC38A1, CDKN2A, MIOX, AGPS, HELLS, FH, DAZAP1, SLC16A1, SUV39H1, DDIT4, TRIB3, ALOX12B, PIK3CA, ISCU). We further classified patients into high-risk and low-risk groups based on the mean risk score according to signature. We also confirmed the prognostic power and independence of the obtained signature related to ferroptosis with other clinical characteristics (age, albumin, B2M, creatinine, CRP, hemoglobin, isotype, ISS stage, LDH, race, sex, risk) and found it to be a reliable indicator for patients with MM. Besides, we investigated the reliability of the obtained signature in a panel of 29 cancers and found that these genes are relatively highly expressed in most cancers. Importantly, we found superior performance and better prognostic ability of the obtained ferroptosis-gene signature compared to 10 already known biomarkers. The outcome of decision curve analysis (DCA) of the nomogram affirmed the possible use of this signature for clinical utility. As next, we utilized the ferroptosis-related gene signature for GSEA analysis and found that several KEGG terms significantly enriched in the high-risk group. Among them, four ferroptosis-related pathways, including proteasome, cysteine and methionine metabolism, p53 signaling pathway and DNA replication, were found to be significantly enriched in high-risk MM patients. In terms of clinical application, myeloma patients receiving proteasome inhibitor (ie, bortezomib) benefited in OS compared to those who did not receive proteasome inhibitor (55)., and proteasome inhibitor was commonly used to treat relapsed/refractory myeloma, either as single agent or combined with other therapies (56). Given that immune cell infiltration may have a differential impact on high and low-score patients, we also assessed the degree of immune infiltration and found that the high-risk MM (in the training cohort) had lower immune and stromal score but high tumor purity. Among several immune cell populations, we found that activated CD4+ T cells and activated CD8+ T cells were significantly upregulated in the high-score group. Of significance, only activated CD4+ T cells were relevant to survival in both the training cohort and the validation cohort. Since MM is an immunoproliferative disease, the increased frequency of Tregs and T cells possessing a regulatory function have already been discussed MM patients (57). An independent study also reported a higher proportion of activated CD4+ Tregs in MM patients compared to healthy

donors (58). The robust signature we used to establish the relationship between activated CD4+ T cell subsets and patient survival is concordant to these studies. However, the exact mechanism by which immune cells, especially activated CD4+ T cell subsets, affect MM remains unclear. To mention, some of the genes in our signature has already been implicated in MM, for instance, ALOX12B variants has been proposed as a biomarker for progression and resistance in MM (59). CDKN2A has previously been found to be differentially expressed in MM (60)., and its overexpression has been correlated with poor OS in MM (61). SUV39H1 and the contribution of other epigenetic modifiers has been implicated in MM development and disease progression (62). To mention, some studies have been conducted on prognostic gene signatures related to cell death mechanisms such as ferroptosis (63, 64) and autophagy (65, 66) seeking their potential role in cancer treatment. Of importance, the ferroptosis-related gene signature, we presented in the current study is the first for MM.

Next, we investigated whether the obtained signature shows any potential correlation with the lncRNAs implicated in cancers. Interestingly, we identified few lncRNAs (KIFC1, DSCR4) in the training cohort and (SLC44A4, PSMB1, LINC01398, LINC01213, LINC00851) in the validation cohort appears to correlate with the signature. Most importantly, we identified the oncogenic lncRNA CRNDE significantly correlated in both training and validation cohorts. LncRNA CRNDE has been found to be altered in several cancers, including colorectal cancer, glioma, hepatocellular carcinoma, lung cancer, breast cancer, gastric cancer, and renal cell carcinoma (67, 68). Of interest, a recent study performed CRISPR-mediated deletion of the lncRNA CRNDE and showed decrease in IL6 signaling and proliferation responses in multiple myeloma cells (69). Our analysis revealed that lncRNA CRNDE and signature genes interact with each other at both the mRNA level and the protein level. Hence, by using multiple myeloma, we support the potential use of non-coding genome based ferroptosis targeting, which has recently been suggested (23).

It is also important to mention the limitations of this study, such as: 1) we did not evaluate the impact of therapies (e.g., targeted therapy and/or chemotherapy, with or without steroids, etc.) on the defined high/low risk groups of MM patients. 2) Mutations in certain genes (including KRAS, NRAS, TP53, FAM46C, DIS3 and BRAF) have a high recurrence rate in MM, however, we did not calibrate our signature according to the mutation spectrum of patients. 3) The experimental validation of our signature is a requisite. 4) The current methodologies for the enrichment of plasma cells specially by using anti-CD138 immunomagnetic bead selection may lead to some potential bias for assessing the immune microenvironment components (e.g. memory B cells, CD4+ T cells, and activated NK cells), the composition of non-plasma cells may proportionally be lower/affected. Despite this, our study is the

first to define the effects of the repetitive genome on the proximity of ferroptosis related genes and their putative association with the oncogenic lncRNA CRNDE.

Conclusions

We showed that ferroptosis-related genes are enriched with the repetitive genome in their proximity, with a strong predominance of the SINE family, followed by LINE, of which the most significant discriminant values were SINE/Alu and LINE/L1, respectively. In addition, we developed an independent predictive model/signature comprising fourteen ferroptosis-related genes that can identify MM high-risk patients with lower immune/stromal score and higher tumor purity in their immune microenvironment.

Besides, we found that the oncogenic lncRNA CRNDE correlated with the risk score and was highly associated with most of the signature genes.

Data availability statement

The datasets presented in this study can be found in online repositories. The names of the repository/repositories and accession number(s) can be found in the article/ Supplementary Material.

Author contributions

Conceptualization, JQ, AS, YW, IS-W, and CJ. Data collection, JQ, AS, YW, FT-T,TD, HDL, HJL, BK, CK, TL, and CZ. Data curation, JQ, AS, YW, FT-T,TD, HDL, HJL, BK, CK, CZ, IS-W, and CJ. All authors contributed to the article and approved the submitted version.

Funding

Conflict of interest

The authors declare that the research was conducted in the absence of any commercial or financial relationships that could be construed as a potential conflict of interest.

Publisher's note

Supplementary material

The Supplementary Material for this article can be found online at: https://www.frontiersin.org/articles/10.3389/fonc.2022.1026153/full#supplementary-material

SUPPLEMENTARY FIGURE 1
Association of repetitive genome content in the upstream promoter region and their functional meaning for ferroptosis-related genes. **(A)** Hierarchical clustering of genes based on the normalized score of repeat quantity and length "Log (Repeat content)". **(B)** On top: k-means clustering of genes based on SINE/Alu and LINE/L1 (brain sections are from Allen Brain Atlas up-expression enrichment) and bottom: functional enrichment of each gene cluster.

SUPPLEMENTARY FIGURE 2
Flowchart of the study. LASSO, the least absolute shirankage and selection operator Cox regression model; ROC, receiver operating characteristic; MM, multiple myeloma.

SUPPLEMENTARY FIGURE 3
Construction of the prognostic gene signature using LASSO regression analysis. **(A)** Venn Diagram represents 17 potential prognostic genes composed from Intersecting 1669 univariate genes with 269 ferroptosis genes. **(B)** LASSO coefficient profiles of 17 ferroptosis-related potential prognostic genes. Each curve corresponds to a gene. **(C)** Selection of the optimal parameter in LASSO regression with 10-fold cross validation. LASSO, the least absolute shirankage and selection operator Cox regression model.

SUPPLEMENTARY FIGURE 4
The distribution of fourteen signature genes based on their mean risk score. **(A–L)** SLC38A1, CDKN2A, MIOX, AGPS, HELLS, FH, DAZAP1, SLC16A1, SUV39H1, DDIT4, TRIB3, ALOX12B. (M-N) PIK3CA, ISCU.

SUPPLEMENTARY FIGURE 5
Time-dependent dynamic AUC curves of the 14-gene signature risk score in the training **(A)** and validation **(B–G)** cohorts. The time-dependent dynamic AUC curve shows a comparison between the risk score and other independent factors. AUC, area under the ROC curve; ROC, receiver operating characteristic.

SUPPLEMENTARY FIGURE 6
Nomogram and its associated calibration curve analysis. **(A)** Ferroptosis-related fourteen-gene based nomogram predicting the 3- and 5-year survival probability in patients with multiple myeloma. **(B, C)** Calibration analysis of ferroptosis-related fourteen-gene containing nomogram at 3 years **(B)** and 5 years **(C)**.

SUPPLEMENTARY FIGURE 7
Decision curve analysis of the clinical use of ISS stage and the ferroptosis-related fourteen-gene based nomogram in multiple myeloma.

SUPPLEMENTARY FIGURE 8

Cell composition of tumor microenvironment investigated by CIBERSORT. **(A)** Cell composition of Bone marrow **(B)** Non-plasma cell composition.

SUPPLEMENTARY FIGURE 9

GSEA result of KEGG gene set based on the risk-score of each multiple myeloma patients. **(A)** Proteasome **(B)** Cysteine and methionine metabolism **(C)** p53 signaling pathway **(D)** DNA replication **(E)** Homologous recombination **(F)** Base excision repair **(G)** Mismatch repair **(H)** Fanconi anemia pathway **(I)** Spliceosome **(J)** Aminoacyl-tRNA biosynthesis **(K)** Cell cycle **(L)** Nucleotide metabolism. KEGG, kyoto encyclopedia of genes and genomes; GSEA, gene set enrichment analysis; NES, normalizedN enrichment score; FDR, false discovery rate.

SUPPLEMENTARY FIGURE 10

Relationship between immune infiltration level and ferroptosis-related fourteen-gene risk score. The distribution of immune score, stromal score and tumor purity upon different risk score in the training cohort **(A–C)** and validation cohort **(D–F)**. The correlation between risk score and the distribution of immune score **(G)**, stromal score **(H)** and tumor purity **(I)**, respectively. *p< 0.05, **p< 0.01, ***p< 0.001.

SUPPLEMENTARY FIGURE 11

Cox proportional hazards regression models based on the enrichment level of 28 immune infiltration-related gene sets *via* ssGSEA analyses in **(A)** MMRF-COMMPASS study and **(B)** GSE24080. Red stars indicate P<0.05.

References

1. Markowitsch SD, Schupp P, Lauckner J, Vakhrusheva O, Slade KS, Mager R, et al. Artesunate inhibits growth of sunitinib-resistant renal cell carcinoma cells through cell cycle arrest and induction of ferroptosis. *Cancers (Basel)* (2020) 12 (11):3150. doi: 10.3390/cancers12113150

2. Sharma P, Shimura T, Banwait JK, Goel A. Andrographis-mediated chemosensitization through activation of ferroptosis and suppression of B-Catenin/Wnt-Signaling pathways in colorectal cancer. *Carcinogenesis* (2020) 41 (10):1385–94. doi: 10.1093/carcin/bgaa090

3. Zhang H, Deng T, Liu R, Ning T, Yang H, Liu D, et al. Caf secreted mir-522 suppresses ferroptosis and promotes acquired chemo-resistance in gastric cancer. *Mol Cancer* (2020) 19(1):43. doi: 10.1186/s12943-020-01168-8

4. Logie E, Van Puyvelde B, Cuypers B, Schepers A, Berghmans H, Verdonck J, et al. Ferroptosis induction in multiple myeloma cells triggers DNA methylation and histone modification changes associated with cellular senescence. *Int J Mol Sci* (2021) 22(22):12234. doi: 10.3390/ijms222212234

5. Zhao Y, Huang Z, Peng H. Molecular mechanisms of ferroptosis and its roles in hematologic malignancies. *Front Oncol* (2021) 11:743006. doi: 10.3389/fonc.2021.743006

6. Zhou M, Zhu X. Construction and validation of a robust ferroptosis-associated gene signature predictive of prognosis in lung adenocarcinoma. *Med (Baltimore)* (2022) 101(16):e29068. doi: 10.1097/md.0000000000029068

7. Sun L, Li B, Wang B, Li J, Li J. Construction of a risk model to predict the prognosis and immunotherapy of low-grade glioma ground on 7 ferroptosis-related genes. *Int J Gen Med* (2022) 15:4697–716. doi: 10.2147/ijgm.S352773

8. Han C, Zheng J, Li F, Guo W, Cai C. Novel prognostic signature for acute myeloid leukemia: Bioinformatics analysis of combined cnv-driven and ferroptosis-related genes. *Front Genet* (2022) 13:849437. doi: 10.3389/fgene.2022.849437

9. Song S, Shu P. Expression of ferroptosis-related gene correlates with immune microenvironment and predicts prognosis in gastric cancer. *Sci Rep* (2022) 12 (1):8785. doi: 10.1038/s41598-022-12800-6

10. Sun Z, Li T, Xiao C, Zou S, Zhang M, Zhang Q, et al. Prediction of overall survival based upon a new ferroptosis-related gene signature in patients with clear cell renal cell carcinoma. *World J Surg Oncol* (2022) 20(1):120. doi: 10.1186/s12957-022-02555-9

11. Jiang M, Wang Z, He X, Hu Y, Xie M, Jike Y, et al. A risk-scoring model based on evaluation of ferroptosis-related genes in osteosarcoma. *J Oncol* (2022) 2022:4221756. doi: 10.1155/2022/4221756

12. Ping S, Wang S, Zhao Y, He J, Li G, Li D, et al. Identification and validation of a ferroptosis-related gene signature for predicting survival in skin cutaneous melanoma. *Cancer Med* (2022)11(18):3529-3541. doi: 10.1002/cam4.4706

13. Lu YJ, Gong Y, Li WJ, Zhao CY, Guo F. The prognostic significance of a novel ferroptosis-related gene model in breast cancer. *Ann Transl Med* (2022) 10 (4):184. doi: 10.21037/atm-22-479

14. Sharma A, Liu H, Tobar-Tosse F, Noll A, Chand Dakal T, Li H, et al. Genome organization in proximity to the Bap1 locus appears to play a pivotal role in a variety of cancers. *Cancer Sci* (2020) 111(4):1385–91. doi: 10.1111/cas.14319

15. Sharma A, Jamil MA, Nuesgen N, Dauksa A, Gulbinas A, Schulz WA, et al. Detailed methylation map of line-1 5'-promoter region reveals hypomethylated cpg hotspots associated with tumor tissue specificity. *Mol Genet genomic Med* (2019) 7 (5):e601. doi: 10.1002/mgg3.601

16. Criscione SW, Zhang Y, Thompson W, Sedivy JM, Neretti N. Transcriptional landscape of repetitive elements in normal and cancer human cells. *BMC Genomics* (2014) 15:583. doi: 10.1186/1471-2164-15-583

17. Jordà M, Díez-Villanueva A, Mallona I, Martín B, Lois S, Barrera V, et al. The epigenetic landscape of alu repeats delineates the structural and functional genomic architecture of colon cancer cells. *Genome Res* (2017) 27(1):118–32. doi: 10.1101/gr.207522.116

18. Aoki Y, Nojima M, Suzuki H, Yasui H, Maruyama R, Yamamoto E, et al. Genomic vulnerability to line-1 hypomethylation is a potential determinant of the clinicogenetic features of multiple myeloma. *Genome Med* (2012) 4(12):101. doi: 10.1186/gm402

19. Bollati V, Fabris S, Pegoraro V, Ronchetti D, Mosca L, Deliliers GL, et al. Differential repetitive DNA methylation in multiple myeloma molecular subgroups. *Carcinogenesis* (2009) 30(8):1330–5. doi: 10.1093/carcin/bgp149

20. Lee E, Iskow R, Yang L, Gokcumen O, Haseley P, Luquette LJ3rd, et al. Landscape of somatic retrotransposition in human cancers. *Sci (New York NY)* (2012) 337(6097):967–71. doi: 10.1126/science.1222077

21. Zuo YB, Zhang YF, Zhang R, Tian JW, Lv XB, Li R, et al. Ferroptosis in cancer progression: Role of noncoding rnas. *Int J Biol Sci* (2022) 18(5):1829–43. doi: 10.7150/ijbs.66917

22. Huang J, Wang J, He H, Huang Z, Wu S, Chen C, et al. Close interactions between lncrnas, lipid metabolism and ferroptosis in cancer. *Int J Biol Sci* (2021) 17 (15):4493–513. doi: 10.7150/ijbs.66181

23. Valashedi MR, Bamshad C, Najafi-Ghalehlou N, Nikoo A, Tomita K, Kuwahara Y, et al. Non-coding rnas in ferroptotic cancer cell death pathway: Meet the new masters. *Hum Cell* (2022) 35(4):972–94. doi: 10.1007/s13577-022-00699-0

24. Fu H, Zhang Z, Li D, Lv Q, Chen S, Zhang Z, et al. Lncrna pelaton, a ferroptosis suppressor and prognositic signature for gbm. *Front Oncol* (2022) 12:817737. doi: 10.3389/fonc.2022.817737

25. Tobar-Tosse F, Veléz PE, Ocampo-Toro E, Moreno PA. Structure, clustering and functional insights of repeats configurations in the upstream promoter region of the human coding genes. *BMC Genomics* (2018) 19(Suppl 8):862. doi: 10.1186/s12864-018-5196-6

26. Chen K-Y, Liu S-H, Chen B, Wang H-M, Jan E-E, Hsu W-L, et al. Extractive broadcast news summarization leveraging recurrent neural network language modeling techniques. *IEEE/ACM Trans Audio Speech Lang Process* (2015) 23 (8):1322–34. doi: 10.1109/TASLP.2015.2432578

27. Xie Z, Bailey A, Kuleshov MV, Clarke DJ, Evangelista JE, Jenkins SL, et al. Gene set knowledge discovery with enrichr. *Curr Protoc* (2021) 1(3):e90. doi: 10.1002/cpz1.90

28. Thorsson V, Gibbs DL, Brown SD, Wolf D, Bortone DS, Ou Yang TH, et al. The immune landscape of cancer. *Immunity* (2018) 48(4):812–30.e14. doi: 10.1016/j.immuni.2018.03.023

29. Newman AM, Steen CB, Liu CL, Gentles AJ, Chaudhuri AA, Scherer F, et al. Determining cell type abundance and expression from bulk tissues with digital cytometry. *Nat Biotechnol* (2019) 37(7):773–82. doi: 10.1038/s41587-019-0114-2

30. Jia Q, Wu W, Wang Y, Alexander PB, Sun C, Gong Z, et al. Local mutational diversity drives intratumoral immune heterogeneity in non-small cell lung cancer. *Nat Commun* (2018) 9(1):5361. doi: 10.1038/s41467-018-07767-w

31. Charoentong P, Finotello F, Angelova M, Mayer C, Efremova M, Rieder D, et al. Pan-cancer immunogenomic analyses reveal genotype-immunophenotype relationships and predictors of response to checkpoint blockade. *Cell Rep* (2017) 18 (1):248–62. doi: 10.1016/j.celrep.2016.12.019

32. Liu XP, Yin XH, Meng XY, Yan XH, Wang F, He L. Development and validation of a 9-gene prognostic signature in patients with multiple myeloma. *Front Oncol* (2018) 8:615. doi: 10.3389/fonc.2018.00615

33. Chen T, Berno T, Zangari M. Low-risk identification in multiple myeloma using a new 14-gene model. *Eur J Haematol* (2012) 89(1):28–36. doi: 10.1111/j.1600-0609.2012.01792.x

34. Zhu FX, Wang XT, Zeng HQ, Yin ZH, Ye ZZ. A predicted risk score based on the expression of 16 autophagy-related genes for multiple myeloma survival. *Oncol Lett* (2019) 18(5):5310–24. doi: 10.3892/ol.2019.10881

35. Flynt E, Bisht K, Sridharan V, Ortiz M, Towfic F, Thakurta A. Prognosis, biology, and targeting of Tp53 dysregulation in multiple myeloma. *Cells* (2020) 9 (2):287. doi: 10.3390/cells9020287

36. Zhang W, Zhang Y, Yang Z, Liu X, Yang P, Wang J, et al. High expression of Ube2t predicts poor prognosis and survival in multiple myeloma. *Cancer Gene Ther* (2019) 26(11-12):347–55. doi: 10.1038/s41417-018-0070-x

37. Goldsmith SR, Fiala MA, O'Neal J, Souroullas GP, Toama W, Vij R, et al. Ezh2 overexpression in multiple myeloma: Prognostic value, correlation with clinical characteristics, and possible mechanisms. *Clin Lymphoma Myeloma Leuk* (2019) 19(11):744–50. doi: 10.1016/j.clml.2019.08.010

38. Andersen NF, Vogel U, Klausen TW, Gimsing P, Gregersen H, Abildgaard N, et al. Polymorphisms in the heparanase gene in multiple myeloma association with bone morbidity and survival. *Eur J Haematol* (2015) 94(1):60–6. doi: 10.1111/ejh.12401

39. Zhang W, Lin Y, Liu X, He X, Zhang Y, Fu W, et al. Prediction and prognostic significance of Bcar3 expression in patients with multiple myeloma. *J Transl Med* (2018) 16(1):363. doi: 10.1186/s12967-018-1728-8

40. Lee BH, Park Y, Kim JH, Kang KW, Lee SJ, Kim SJ, et al. Pd-L1 expression in bone marrow plasma cells as a biomarker to predict multiple myeloma prognosis: Developing a nomogram-based prognostic model. *Sci Rep* (2020) 10(1):12641. doi: 10.1038/s41598-020-69616-5

41. Goyal B, Yadav SRM, Awasthee N, Gupta S, Kunnumakkara AB, Gupta SC. Diagnostic, prognostic, and therapeutic significance of long non-coding rna Malat1 in cancer. *Biochim Biophys Acta Rev Cancer* (2021) 1875(2):188502. doi: 10.1016/j.bbcan.2021.188502

42. Gu Y, Jin Y, Ding J, Yujie W, Shi Q, Qu X, et al. Low absolute Cd4(+) T cell counts in peripheral blood predict poor prognosis in patients with newly diagnosed multiple myeloma. *Leuk Lymphoma* (2020) 61(8):1869–76. doi: 10.1080/10428194.2020.1751840

43. Luo Y, Huang Q, He B, Liu Y, Huang S, Xiao J. Regulation of ferroptosis by Non–Coding rnas in the development and treatment of cancer (Review). *Oncol Rep* (2021) 45(1):29–48. doi: 10.3892/or.2020.7836

44. Balihodzic A, Prinz F, Dengler MA, Calin GA, Jost PJ, Pichler M. Non-coding rnas and ferroptosis: Potential implications for cancer therapy. *Cell Death Differ* (2022) 29(6):1094–106. doi: 10.1038/s41418-022-00998-x

45. Tang W, Zhu S, Liang X, Liu C, Song L. The crosstalk between long non-coding rnas and various types of death in cancer cells. *Technol Cancer Res Treat* (2021) 20:15330338211033044. doi: 10.1177/15330338211033044

46. Xia X, Fan X, Zhao M, Zhu P. The relationship between ferroptosis and tumors: A novel landscape for therapeutic approach. *Curr Gene Ther* (2019) 19 (2):117–24. doi: 10.2174/1566523219666190628152137

47. Su Y, Zhao B, Zhou L, Zhang Z, Shen Y, Lv H, et al. Ferroptosis, a novel pharmacological mechanism of anti-cancer drugs. *Cancer Lett* (2020) 483:127–36. doi: 10.1016/j.canlet.2020.02.015

48. Bebber CM, Müller F, Prieto Clemente L, Weber J, von Karstedt S. Ferroptosis in cancer cell biology. *Cancers (Basel)* (2020) 12(1):164. doi: 10.3390/cancers12010164

49. Zhu W, Li LL, Songyang Y, Shi Z, Li D. Identification and validation of hells (Helicase, lymphoid-specific) and Icam1 (Intercellular adhesion molecule 1) as potential diagnostic biomarkers of lung cancer. *PeerJ* (2020) 8:e8731. doi: 10.7717/peerj.8731

50. Qu C, Peng Y, Liu S. Ferroptosis biology and implication in cancers. *Front Mol Biosci* (2022) 9:892957. doi: 10.3389/fmolb.2022.892957

51. Alzrigat M, Párraga AA, Jernberg-Wiklund H. Epigenetics in multiple myeloma: From mechanisms to therapy. *Semin Cancer Biol* (2018) 51:101–15. doi: 10.1016/j.semcancer.2017.09.007

52. Garofano F, Sharma A, Abken H, Gonzalez-Carmona MA, Schmidt-Wolf IGH. A low dose of pure cannabidiol is sufficient to stimulate the cytotoxic function of cik cells without exerting the downstream mediators in pancreatic cancer cells. *Int J Mol Sci* (2022) 23(7):3783. doi: 10.3390/ijms23073783

53. Logie E, Novo CP, Driesen A, Van Vlierberghe P, Vanden Berghe W. Phosphocatalytic kinome activity profiling of apoptotic and ferroptotic agents in multiple myeloma cells. *Int J Mol Sci* (2021) 22(23):12731. doi: 10.3390/ijms222312731

54. Drongitis D, Aniello F, Fucci L, Donizetti A. Roles of transposable elements in the different layers of gene expression regulation. *Int J Mol Sci* (2019) 20 (22):5755. doi: 10.3390/ijms20225755

55. Scott K, Hayden PJ, Will A, Wheatley K, Coyne I. Bortezomib for the treatment of multiple myeloma. *Cochrane Database Syst Rev* (2016) 4:Cd010816. doi: 10.1002/14651858.CD010816.pub2

56. Cowan AJ, Green DJ, Kwok M, Lee S, Coffey DG, Holmberg LA, et al. Diagnosis and management of multiple myeloma: A review. *Jama* (2022) 327 (5):464–77. doi: 10.1001/jama.2022.0003

57. Giannopoulos K, Kaminska W, Hus I, Dmoszynska A. The frequency of T regulatory cells modulates the survival of multiple myeloma patients: Detailed characterisation of immune status in multiple myeloma. *Br J Cancer* (2012) 106 (3):546–52. doi: 10.1038/bjc.2011.575

58. Wang JN, Cao XX, Zhao AL, Cai H, Wang X, Li J. Increased activated regulatory T cell subsets and aging treg-like cells in multiple myeloma and monoclonal gammopathy of undetermined significance: A case control study. *Cancer Cell Int* (2018) 18:187. doi: 10.1186/s12935-018-0687-8

59. Montel RA, Gregory M, Chu T, Cottrell J, Bitasktsis C, Chang SL. Genetic variants as biomarkers for progression and resistance in multiple myeloma. *Cancer Genet* (2021) 252-253:1–5. doi: 10.1016/j.cancergen.2020.12.001

60. Katiyar A, Kaur G, Rani L, Jena L, Singh H, Kumar L, et al. Genome-wide identification of potential biomarkers in multiple myeloma using meta-analysis of mrna and mirna expression data. *Sci Rep* (2021) 11(1):10957. doi: 10.1038/s41598-021-90424-y

61. Elnenaei MO, Gruszka-Westwood AM, A'Hernt R, Matutes E, Sirohi B, Powles R, et al. Gene abnormalities in multiple myeloma: The relevance of Tp53, Mdm2, and Cdkn2a. *Haematologica* (2003) 88(5):529–37.

62. Caprio C, Sacco A, Giustini V, Roccaro AM. Epigenetic aberrations in multiple myeloma. *Cancers (Basel)* (2020) 12(10):2996. doi: 10.3390/cancers12102996

63. Luo L, Yao X, Xiang J, Huang F, Luo H. Identification of ferroptosis-related genes for overall survival prediction in hepatocellular carcinoma. *Sci Rep* (2022) 12 (1):10007. doi: 10.1038/s41598-022-14554-7

64. Wu S, Pan R, Lu J, Wu X, Xie J, Tang H, et al. Development and verification of a prognostic ferroptosis-related gene model in triple-negative breast cancer. *Front Oncol* (2022) 12:896927. doi: 10.3389/fonc.2022.896927

65. Wang Y, Ge F, Sharma A, Rudan O, Setiawan MF, Gonzalez-Carmona MA, et al. Immunoautophagy-related long noncoding rna (Iar-lncrna) signature predicts survival in hepatocellular carcinoma. *Biology* (2021) 10(12):1301. doi: 10.3390/biology10121301

66. Wang D, Jiang Y, Wang T, Wang Z, Zou F. Identification of a novel autophagy-related prognostic signature and small molecule drugs for glioblastoma by bioinformatics. *BMC Med Genomics* (2022) 15(1):111. doi: 10.1186/s12920-022-01261-5

67. Zhang J, Yin M, Peng G, Zhao Y. Crnde: An important oncogenic long non-coding rna in human cancers. *Cell Prolif* (2018) 51(3):e12440. doi: 10.1111/cpr.12440

68. Ellis BC, Molloy PL, Graham LD. Crnde: A long non-coding rna involved in cancer, neurobiology, and development. *Front Genet* (2012) 3:270. doi: 10.3389/fgene.2012.00270

69. David A, Zocchi S, Talbot A, Choisy C, Ohnona A, Lion J, et al. The long non-coding rna crnde regulates growth of multiple myeloma cells *Via* an effect on Il6 signalling. *Leukemia* (2021) 35(6):1710–21. doi: 10.1038/s41375-020-01034-y

3.4 Publication 4: Immunoautophagy-Related Long Noncoding RNA (IAR-lncRNA) Signature Predicts Survival in Hepatocellular Carcinoma

Yulu Wang[1,†], Fangfang Ge[1,†], Amit Sharma[1,2,†], Oliver Rudan[1], Maria F. Setiawan[1], Maria A. Gonzalez-Carmona[3], Miroslaw T. Kornek[3], Christian P. Strassburg[3], Matthias Schmid[4] and Ingo G. H. Schmidt-Wolf[1],*

1Center for Integrated Oncology (CIO), Department of Integrated Oncology, University Hospital of Bonn, 53127 Bonn, Germany
2 Department of Neurosurgery, University Hospital of Bonn, 53127 Bonn, Germany
3 Department of Internal Medicine I, University Hospital of Bonn, 53127 Bonn, Germany
4 Institute of Medical Biometry, Informatics and Epidemiology, University Hospital of Bonn, 53127 Bonn, Germany

biology

Article

Immunoautophagy-Related Long Noncoding RNA (IAR-lncRNA) Signature Predicts Survival in Hepatocellular Carcinoma

Yulu Wang [1,†], Fangfang Ge [1,†], Amit Sharma [1,2,†], Oliver Rudan [1], Maria F. Setiawan [1], Maria A. Gonzalez-Carmona [3], Miroslaw T. Kornek [3], Christian P. Strassburg [3], Matthias Schmid [4] and Ingo G. H. Schmidt-Wolf [1,*]

1. Center for Integrated Oncology (CIO), Department of Integrated Oncology, University Hospital of Bonn, 53127 Bonn, Germany; Yulu.Wang@ukbonn.de (Y.W.); Fangfang.Ge@ukbonn.de (F.G.); Amit.Sharma@ukbonn.de (A.S.); oliver.rudan@ukbonn.de (O.R.); Maria_fitria.setiawan@ukbonn.de (M.F.S.)
2. Department of Neurosurgery, University Hospital of Bonn, 53127 Bonn, Germany
3. Department of Internal Medicine I, University Hospital of Bonn, 53127 Bonn, Germany; maria.gonzalez-carmona@ukbonn.de (M.A.G.-C.); Miroslaw_theodor.kornek@ukbonn.de (M.T.K.); christian.strassburg@ukbonn.de (C.P.S.)
4. Institute of Medical Biometry, Informatics and Epidemiology, University Hospital of Bonn, 53127 Bonn, Germany; matthias.schmid@ukbonn.de
* Correspondence: ingo.schmidt-wolf@ukbonn.de; Tel.: +49-(0)-228-287-17050
† These authors have contributed equally as co-first authors.

Simple Summary: Hepatocellular carcinoma (HCC) is the most common type of primary liver cancer, which is more prevalent in adults. Herein, we established the first immuno-autophagy-related long non-coding RNA (IARlncRNA) signature displaying a prognostic ability among HCC patient groups.

Abstract: Background: The dysregulation of autophagy and immunological processes has been linked to various pathophysiological conditions, including cancer. Most notably, their particular involvement in hepatocellular carcinoma (HCC) is becoming increasingly evident. This has led to the possibility of developing a prognostic signature based on immuno-autophagy-related (IAR) genes. Given that long non-coding RNAs (lncRNAs) also play a special role in HCC, a combined signature utilizing IAR genes and HCC-associated long noncoding RNAs (as IARlncRNA) may potentially help in the clinical scenario. Method: We used Pearson correlation analysis, Kaplan–Meier survival curves, univariate and multivariate Cox regression, and ROC curves to generate and validate a prognostic immuno-autophagy-related long non-coding RNA (IARlncRNA) signature. The Chi-squared test was utilized to investigate the correlation between the obtained signature and the clinical characteristics. CIBERSORT algorithms and the Wilcoxon rank sum test were applied to investigate the correlation between signature and infiltrating immune cells. GO and KEGG analyses were performed to derived signature-dependent pathways. Results: Herein, we build an IAR-lncRNA signature (as first in the literature) and demonstrate its prognostic ability in hepatocellular carcinoma. Primarily, we identified three IARlncRNAs (MIR210HG, AC099850.3 and CYTOR) as unfavorable prognostic determinants. The obtained signature predicted the high-risk HCC group with shorter overall survival, and was further associated with clinical characteristics such as tumor grade (t = 10.918, $p = 0.001$). Additionally, several infiltrating immune cells showed varied fractions between the low-risk group and the high-risk HCC groups in association with the obtained signature. In addition, pathways analysis described by the signature clearly distinguishes both risk groups in HCC. Conclusions: The immuno-autophagy-related long non-coding RNA (IARlncRNA) signature we established exhibits a prognostic ability in hepatocellular carcinoma. To our knowledge, this is the first attempt in the literature to combine three determinants (immune, autophagy and LnRNAs), thus requiring molecular validation of this obtained signature in clinical samples.

Keywords: liver cancer; hepatocellular carcinoma; lncRNAs; autophagy; biomarker; kyoto encyclopedia of genes and genomes; prognosis; signature; immune genes

1. Introduction

Autophagy as a conserved process captures and degrades intracellular components primarily to maintain metabolism and cellular homeostasis. Dysregulation of this process has been linked to several pathophysiological conditions, such as cancer and neurodegenerative diseases [1,2]. Particularly in hepatocellular carcinoma (HCC), autophagy has been shown to play a role by promoting the metastatic colonization of HCC cells [3].

HCC, the most common malignancy of the liver, is currently the fourth leading cause of cancer-related death worldwide [4]. Primary risk factors for the development of HCC include chronic liver disease and cirrhosis, most of which are caused by chronic viral hepatitis (B + C) and excessive alcohol consumption. Several genetic and epigenetic factors have also been implicated in the molecular pathogenesis of HCC [5]. Considering the overlap of mutational pathways in cancers [6], studies have also prompted the analysis of the prognostic potential of certain genes across the spectrum of multiple cancers, including HCC [7]. Likewise, the relative contribution of autophagy in HCC is becoming increasingly apparent; for instance, Wu et al. showed that autophagic degradation machinery and the cell-cycle regulator cyclin D1 are linked to HCC tumorigenesis [8]. It has also been discussed that activation of autophagy decreases the expression of oncogenic microRNA-224, and thus impedes tumorigenesis in hepatitis B virus-related HCC [9]. Of interest, several compounds have been shown to exert antitumor effects in liver cancer via autophagy [10–12]. In the context of autophagy-related genes (ATG), lower expression was previously observed in HCC, which was predicted to contribute to tumor growth and the poor prognosis of the disease [13,14]. Of interest, there have been few recent attempts to identify a prognostic signature of ATGs in HCC [15,16]. Besides this, immunoautophagy-related genes (IARGs) were also recently evaluated for their potential prognostic significance in HCC patients [17]. Considering that long non-coding RNAs (lncRNAs) also play a special role in cancer, their ability to regulate tumor growth by modulating autophagy in liver, bladder, and pancreatic cancers has already been implicated [18,19]. In HCC, a study discussed the potential involvement of lncRNA HULC (highly upregulated in liver cancer) in the autophagy and chemoresistance of HCC cells [20]. Similarly, the lncRNA SNHG1 has been shown to induce resistance to the drug sorafenib in HCC through activation of the Akt pathway [21]. Recently, the prognostic value of an autophagy-related lncRNA signature in HCC has been discussed [22].

Considering this plethora of literature, we have attempted to combine immune-, autophagy, and noncoding RNAs to generate immunoautophagy-related long noncoding RNA (IAR-lncRNA). Herein, we build an IAR-lncRNA signature (first in the literature) and demonstrate its prognostic ability in hepatocellular carcinoma.

2. Materials and Methods

2.1. Gene Expression Data and Clinicopathological Characteristics

Gene expression data (workflow type: HTSeq—FPKM) and associated clinical information of patients with hepatocellular carcinoma of the liver (HCC) were downloaded from UCSC Xena (https://xena.ucsc.edu/, accessed on 22 October 2021). The reference database was the GDC TCGA Liver Cancer (LIHC) dataset, which contains 374 tumor samples with comprehensive gene expression data. Of these, 371 samples were from primary tumors (mainly used in this study), and the remaining 3 samples were from recurrent tumors (3 samples from 2 patients), which were excluded from the analysis. Only 365 samples have both gene expression data and survival data (survival time and survival status). Based on the available clinical characteristics, only 163 samples were further processed for the clinical comparisons. In total, 210 genes involved in autophagy were retrieved from the Human Autophagy Database (HADb, http://autophagy.lu/clustering/index.html, accessed on 22 May 2021). A total of 1344 immune-related genes were retrieved from Immport Shared Data (https://www.immport.org/shared/home, accessed on 27 June

57

2021). We focused our analysis on 371 HCC samples, excluding recurrent samples due to their peculiar clinical/biological characteristics. Log2(FPKM + 1) gene expression data were applied to obtain AR genes, IR genes and lncRNAs. Due to the sizes of genes and lncRNAs, the average gene expression (log2(FPKM + 1)) of AR genes and IR genes (no more than 0) and lncRNAs (no more than 0.5) was excluded. Log2 was further applied for the gene expression data (log2(FPKM + 1)) in order to obtain fitting normalized distribution. Since lncRNAs were expressed at relatively low levels, the correlation of gene (AR and IR) expression (Log2(log2(FPKM + 1) + 1)) and lncRNA expression (log2(FPKM + 1)) was used to establish AR- and IR-related lncRNAs. LncRNA expression (Log2(log2(FPKM + 1) + 1)) data were subsequently used in statistical analyses.

2.2. Development of the Prognostic Immuno-Autophagy-Related lncRNAs Signature

Univariate Cox regressions were applied to select survival-related autophagy genes and immune genes, which were based on p-values < 0.01. Then the correlation between lncRNAs and survival-related autophagy genes was determined by Pearson correlation analysis. LncRNAs with correlation coefficients |R| > 0.4 and p values < 0.01 were considered autophagy-related. The correlation between lncRNAs and survival-related immune genes was determined by Pearson correlation analysis. LncRNAs with correlation coefficients |R| > 0.6 and p values < 0.01 were defined as immune-related. Thus, we obtained autophagy-related lncRNAs (ARlncRNAs) and immune-related lncRNAs (IRlncRNAs) for the further steps. Next, we determined the lncRNA was associated with immunoautophagy (IARlncRNA) if the lncRNA belonged to both ARlncRNAs and IRlncRNAs concurrently. Then, univariate Cox regression was performed to select survival-related IARlncRNA. Subsequently, multivariate Cox regression analysis was performed based on the lowest Akaike information criterion (AIC) to determine the optimal prognostic signature. Risk scores were calculated using the following formula: (βgene 1 × expgene 1) + (βgene 2 × expgene 2) + --- + (βgene n × expgene n). Here, expgene represents the expression of lncRNA. Of note, the cutoff value for the high-risk group and the low-risk group was the median risk score. The differential expressions of the lncRNAs in signature between high- and low-risk groups were assessed by Wilcoxon rank sum test.

2.3. Prognostic Ability of Immuno-Autophagy-Related lncRNAs Signature

The Kaplan–Meier survival curve was applied to investigate the survival rate between high-risk and low-risk groups, and p < 0.05 was considered as a significant difference. Subsequently, an ROC curve was performed to test the predicting value of the signature. Univariate Cox regression and multivariate Cox regression were used to assess the independent ability of the signature, primarily based on p < 0.05 when clinical features (age, gender, Child–Pugh classification, AFP, fibrosis, grade and stage) were considered.

2.4. Correlation between Immune Cells and Signature

CIBERSORT analysis was performed to explore the percentages of 22 immune cells in each patient. Wilcoxon rank-sum test was used to determine the varying of immune cells in low- and high-risk groups (p < 0.05).

2.5. GO and KEGG Analysis

Differential genes were found between the low-risk group and the high-risk group based on log2 fold change (logFC) > 1 and false discovery rate (FDR) < 0.05 using the Wilcoxon rank sum test. Subsequently, these genes were included in GO and KEGG analyses using the R package "clusterProfiler" to explore pathways, which were selected with a q value < 0.05.

2.6. Statistical Analysis

Pearson correlation analysis, Chi-squared test, Wilcoxon rank sum test, Cox regression, Kaplan–Meier curves, survival status, heat map, ROC curve, cibersort algorithm, GO

analysis and KEGG analysis were performed using R software. The coexpression network between genes (ARgenes and IRgenes) along with an lncRNA coexpression network was illustrated using CYTOSCAPE software.

3. Results

3.1. Correlating Autophagy-Related Genes and Immune-Related Genes with lncRNAs

We first derived autophagy-related genes from the Human Autophagy Database (HADb, http://autophagy.lu/clustering/index.html, accessed on 22 May 2021) and immune-related genes from the Immport Shared Data (https://www.immport.org/shared/home, accessed on 27 June 2021). Subsequently, the gene expression datasets of LIHC (GDC TCGA Liver Cancer (LIHC)) were downloaded from the UCSC Xena. Next, we extracted the lncRNA genes, autophagy-related (AR) genes and immune-related (IR) genes corresponding to HCC from the TCGA data. First, univariate Cox regressions were performed to select survival-related AR genes and IR genes. Subsequently, Pearson correlation was used to confirm the correlation between autophagic genes and lncRNA ($|R| > 0.4$ and p-value < 0.01), in addition to the correlation between immune-related genes and lncRNA ($|R| > 0.6$ and p-value < 0.01). Using these parameters, a total of 244 ARlncRNAs (Supplementary File S1) and 36 IRlncRNAs (Supplementary File S2) was identified. When combined, the ARlncRNAs and IRlncRNAs yielded 36 IARlncRNAs. The overview of the complete strategy is shown in a flowchart (Figure S1).

3.2. A Signature Involving 3 Immuno-Autophagy-Related lncRNAs with Prognostic Potential

The aforementioned 36 immuno-autophagy-related lncRNAs were analyzed in combination with clinical survival data. Univariate Cox regression analysis was performed with a p-value of less than 0.01, resulting in the mapping of 10 lncRNAs (BACE1-AS, MIR210HG, AC073896.4, AC099850.3, AC026401.3, MAPKAPK5-AS1, LINC01018, CYTOR, AC115619.1, and F11-AS1) (Figure 1A). In addition, we used a multivariate Cox regression analysis based on the lowest Akaike information criterion (AIC) to determine the β-values that were subsequently used to calculate the risk scores. The analysis revealed three immunoautophagy-related lncRNAs (MIR210HG, AC099850.3, and CYTOR) as the strongest candidates with prognostic potential (Table S1). The correlation between the IARlncRNA of the obtained signature and the genes (AR genes and IR genes) is shown in Figure 1C. Of interest, all these genes showed high expression in the high-risk group (Figure 1B), and were considered unfavorable prognostic determinants (Figure 1D).

3.3. Validating the Prognostic Potential of Immuno-Autophagy-Related lncRNA Signature in Low- and High-Risk HCC Groups

Next, we determined the functionality of the obtained signature within the low-risk group and high-risk group HCC patients (Figure 2). The scatter plot shows that both survival rates and survival time were lower in the high-risk group compared to the low-risk group (Figure 2A).

Additionally, an expression pattern between lncRNAs and signature risk was observed in the heat map (Figure 2A). The Kaplan–Meier survival curve showed a significant difference in overall survival between the low-risk and high-risk groups (Figure 2B). Notably, the high-risk group showed shorter overall survival compared with the low-risk group. In addition, we performed univariable (Figure 2C) and multivariable Cox (Figure 2D) regression analyses to identify independent prognostic factors with clinical characteristics, and found that age, stage, and risk score were independent predictive determinants of survival in HCC patients. Additionally, an ROC curve was used to confirm the model, for which the AUC values of the risk score for the prediction times of 1, 2, and 3 years were 0.746, 0.700, and 0.674, respectively, for each prediction time (Figure 2E).
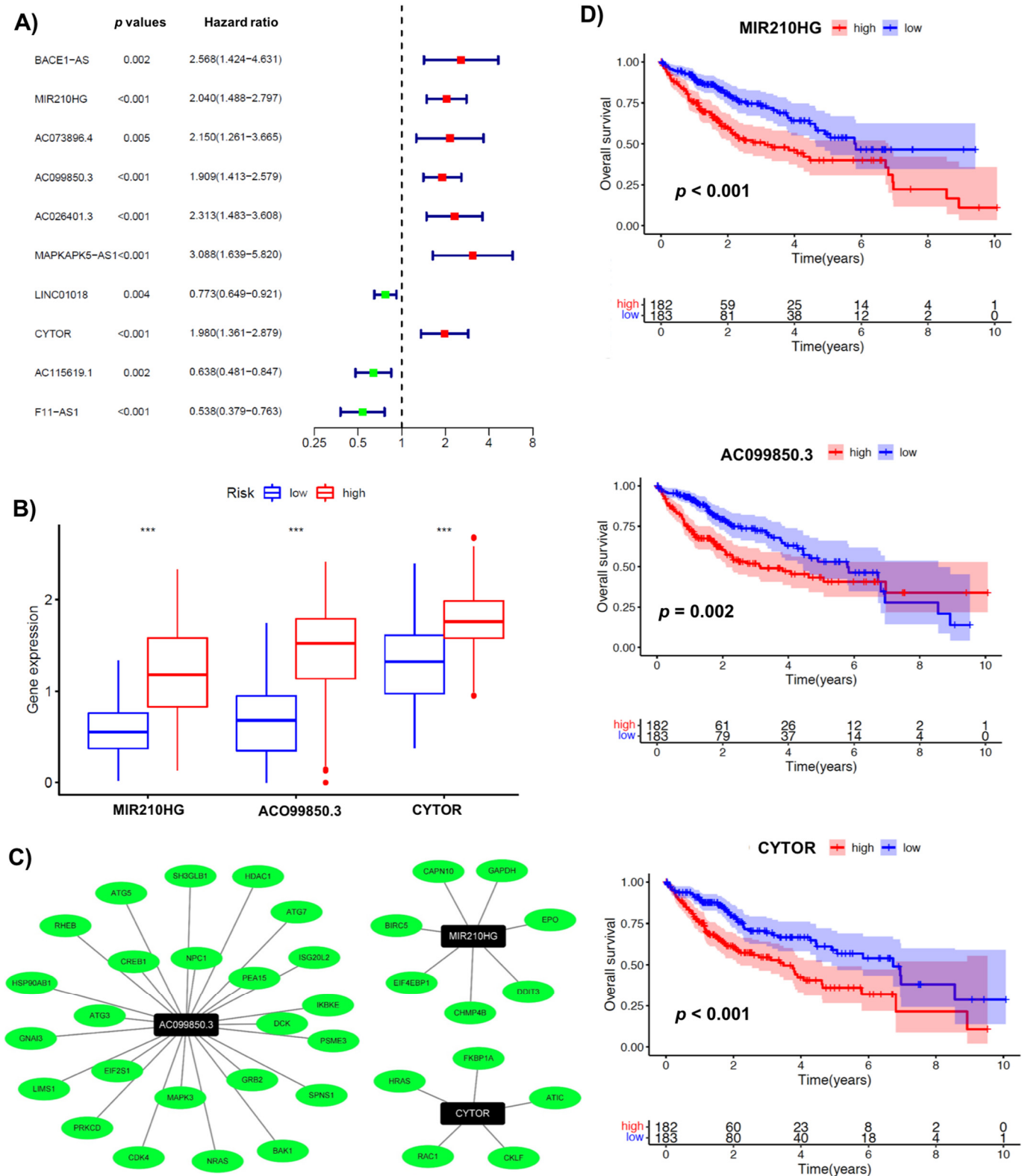
Figure 1. Identification of immuno-autophagy-related lncRNAs with prognostic potential. (**A**) Univariate Cox regression analysis: ten survival-related IARlncRNAs. (**B**) The differential gene expression of IARlncRNAs between high- and low-risk groups. (**C**) A network of prognostic lncRNA (black nodes) with co-expressed genes (green) in HCC. (**D**) Kaplan–Meier survival curves for 3 IARlncRNAs (MIR210HG, AC099850.3, and CYTOR) associated with HCC. *** $p < 0.001$.
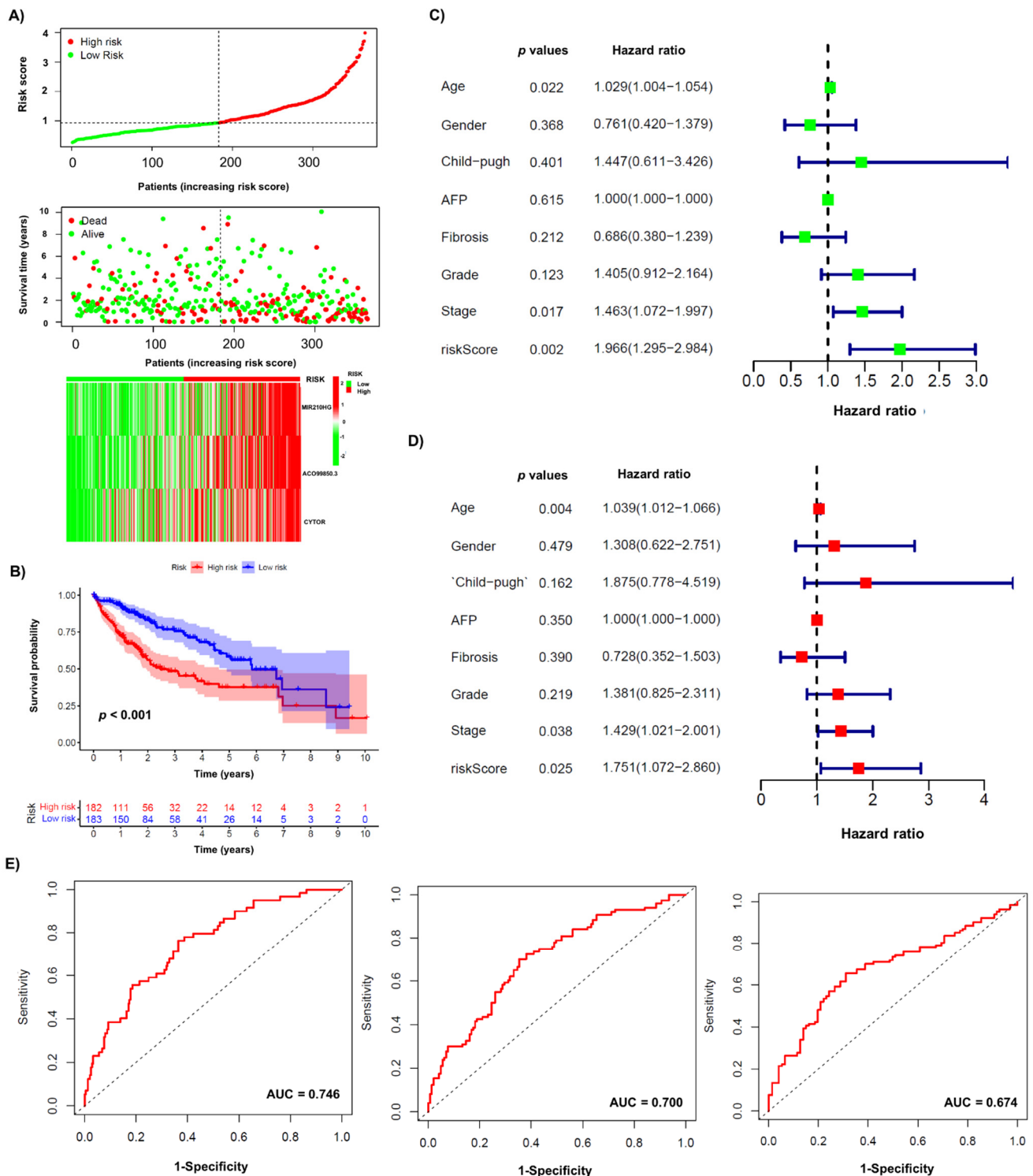
Figure 2. Immunoautophagy-related lncRNA risk score analysis in HCC patients. (**A**) Patient data with low- and high-risk scores (top section), survival status and survival time (middle), and a heatmap of 3 major lncRNAs expressions are shown. (**B**) Kaplan–Meier survival curves for immunoautophagy-related lncRNA risk score for the HCC in TCGA dataset. (**C**) Univariable Cox regression. (**D**) Multivariable Cox regression. (**E**) ROC curve for 1 year (left), 2 years (middle) and 3 years (right).

3.4. Association of Immuno-Autophagy-Related lncRNA Signature with Clinical Characteristics

To determine the association between immuno-autophagy-related lncRNA signature and clinical characteristics, we divided each feature into two groups, such as age (over/under 65 years), gender (male/female), grade (GI–G2/G3–G4), stage (I–II/III–IV), Child–Pugh classification (A/B + C), AFP/alpha-fetoprotein (over/under 400 ng/mL) and fibrosis (with/without) status of patients (Table 1). The analysis showed that a high-risk score was associated significantly with the higher grade (t = 10.918, *p* = 0.001).

Table 1. The relation between risk of signature with clinical features.

|	Risk	Total	High Risk	Low Risk	t	*p* Value
Age	<65	95 (58.28%)	46 (63.89%)	49 (53.85%)	1.280	0.258
	≥65	68 (41.72%)	26 (36.11%)	42 (46.15%)		
Gender	Female	50 (30.67%)	24 (33.33%)	26 (28.57%)	0.234	0.629
	Male	113 (69.33%)	48 (66.67%)	65 (71.43%)		
Child–Pugh	A	147 (90.18%)	64 (88.89%)	83 (91.21%)	0.053	0.819
	B + C	16 (9.82%)	8 (11.11%)	8 (8.79%)		
AFP	≥400	30 (18.4%)	17 (23.61%)	13 (14.29%)	1.748	0.186
	<400	133 (81.6%)	55 (76.39%)	78 (85.71%)		
Fibrosis	Fibrosis	113 (69.33%)	50 (69.44%)	63 (69.23%)	0	1
	No Fibrosis	50 (30.67%)	22 (30.56%)	28 (30.77%)		
Grade	G1–G2	99 (60.74%)	33 (45.83%)	66 (72.53%)	10.918	0.001 **
	G3–G4	64 (39.26%)	39 (54.17%)	25 (27.47%)		
Stage	Stage I–II	131 (80.37%)	57 (79.17%)	74 (81.32%)	0.021	0.885
	Stage III–IV	32 (19.63%)	15 (20.83%)	17 (18.68%)		

** *p* < 0.01.

3.5. Association of Infiltrating Immune Cells and Obtained Signature

Considering the obtained signature involved both immune and autophagy determinants, its relationship with immune infiltration cells was investigated. The relative percentages of 22 immune cells in each patient are shown in Figure S2. The distribution of these cells in risk groups is shown in Figure 3A. The Wilcoxon rank sum test was applied to determine the difference between each immune cell in the low- and high-risk groups (Figure 3B). Interestingly, B cells (naïve, *p* < 0.01; memory, *p* < 0.01), T cells CD4 memory (resting, *p* = 0.007; activated, *p* < 0.001), T cells follicular helpers (*p* < 0. 001), NK cells resting (*p* = 0.018), macrophages M0 (*p* < 0.001), macrophages M2 (*p* = 0.034) and mast cells resting (*p* = 0.015) were significantly different between low- and high-risk groups.

3.6. GO and KEGG Pathway Enrichment Analysis of the Obtained Signature

We further investigated the cellular and molecular pathways associated with the obtained signature. The differential genes between high- and low-risk groups are listed in Supplementary File S3. The biological/cellular processes obtained from GO analysis (Figure S3) show that the signature is mainly associated with mitosis and chromosome segregation. Additionally, the molecular function of the signature was related to tubulin binding and kinase activity. The KEGG analysis shows that the signature is clearly associated with seven signaling pathways, including cell cycle, oocyte meiosis, progesterone-mediated oocyte maturation, p53 signaling pathway, human T-cell leukemia virus 1 infection, cellular senescence, and human immunodeficiency virus 1 (Figure 3C).
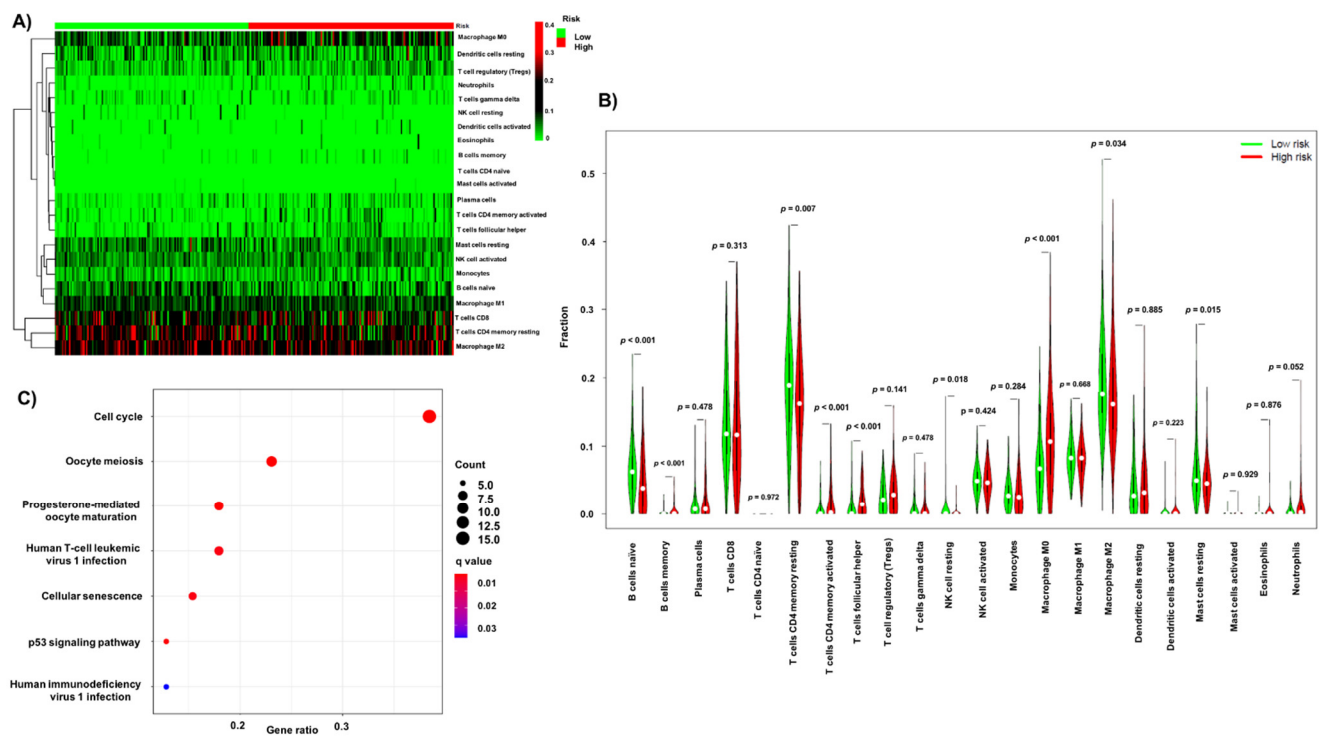
Figure 3. The relationship between immuno-autophagy-related lncRNA signature, infiltration immune cells and potential pathways. (**A**) Heatmap of 22 immune cells in high/low-risk group. (**B**) The fractions of immune cells in high- and low-risk group. (**C**) KEGG analysis.

4. Discussion

Cancer is a relatively complex disease [6,23], driven primarily by genetic/epigenetic processes that help these cells to proliferate and fuel cancer progression. Overall, the dynamics of dysregulated mechanisms involving several key cellular signaling pathways act as a critical factor for the slow to fast progression of this disease. Among them, autophagy and immune-related processes also play a crucial role in both promoting and suppressing tumor growth. Likewise, the peculiar contribution of long non-coding RNA (IARlncRNA) can also not be excluded. To date, several prognostic signatures involving autophagy-related (AR) and immune-related (IR) genes have been shown [24–26], and some have even attempted to combine them with lncRNAs [27,28]. However, to date, no combinatorial signature utilizing IR, AR and lncRNAs has been shown.

With a special focus on hepatocellular carcinoma (HCC), herein, we sought to investigate a possible immuno-autophagy-related long non-coding RNA (IARlncRNA) signature, primarily to predict survival in HCC patients. At first, we selected survival-related IR and AR genes, and combined them lncRNAs to identify ARlncRNAs and IRlncRNAs datasets. Following this, specific sets of ARlncRNAs (*n* = 244) and IRlncRNAs (*n* = 36) were generated, and then a preliminary signature of IARlncRNAs (*n* = 36) was derived from the aforementioned data sets. Among them, 10 IARlncRNAs (BACE1-AS, MIR210HG, AC073896.4, AC099850.3, AC026401.3, MAPKAPK5-AS1, LINC01018, CYTOR, AC115619.1, and F11-AS1) were found to be associated with survival. Of importance, three of them (MIR210HG, AC099850.3, and CYTOR) displayed a robust prognostic signature with unfavorable prognosis. Previously, these three IARlncRNAs had all been implicated in HCC; for instance, it has been shown that the silencing of MIR210HG expression leads to the inhibition of HCC tumor growth [29]. Similarly, CYTOR has been shown to promote HCC proliferation, and its disruption inhibited HCC growth [30,31]. Additionally, AC099850.3 has been shown to increase proliferation and migration in HCC [32], thus providing strong evidence for the utility of our prognostic signature in the clinical spectrum of HCC patients.

We next determined the functionality of the obtained signature within the HCC patient groups, and found that both survival rates and survival time were significantly low in the high-risk group. In addition, an inverse expression pattern was observed in lncRNAs and risk groups. Of interest, among several clinical characteristics, risk score was found to be an independent predictive determinant of survival in HCC patients. We also examined the relationship between the obtained signature and the infiltrating immune cells. The analysis showed that a higher proportion of naïve B cells, resting memory CD4 T cells, resting NK cells, M2 macrophages, and resting mast cells predominated in the low-risk group, whereas the proportion of memory B cells, activated memory CD4 T cells, follicular helper T cells, and M0 macrophages was specific for the high-risk group. GO analysis showed that differential gene expressions between risk groups were significantly enriched in biological processes (mitosis and chromosome segregation), cellular components (chromosomes), and molecular functions (tubulin binding and kinase activity). In addition, seven defined signaling pathways (cell cycle, oocyte meiosis, progesterone-mediated oocyte maturation, p53 signaling pathway, human T-cell leukemia virus 1 infection, cellular senescence, and human immunodeficiency virus 1) were found to be associated with the obtained signature. To our knowledge, we have presented for the first time an immuno-autophagy-related long non-coding RNA (IARlncRNA) signature prognostic ability in hepatocellular carcinoma. It is worth mentioning that molecular validation of this obtained signature using clinical samples is required. Prognostic models for HCC based on lncRNAs have also been reported previously. For instance, a recent study identified five autophagy-related long non-coding RNAs (AR-lncRNAs) (including TMCC1-AS1, PLBD1-AS1, MKLN1-AS, LINC01063, and CYTOR) for HCC patients from the TCGA database [27]. Likewise, one independent study described four-immune-related-LncRNA signatures for predicting the prognosis and guiding the application of immunotherapy in HCC [33]. However, it is worth mentioning that the heterogeneity within clinical samples submitted to repositories (as previously described by Sharma et al. [34]) and especially the selection of different computational analytical methods makes these predictive markers less effective in the clinical environment. In the present study, we have provided a detailed description of the methods used in our analysis, which offers a platform for methodological compression to enable similar analyses in HCC or in other cancers.

5. Conclusions

The immuno-autophagy-related long non-coding RNA (IARlncRNA) signature we established exhibits a prognostic ability in hepatocellular carcinoma.

Conflicts of Interest: The authors declare no conflict of interest.

References

1. Chavez-Dominguez, R.; Perez-Medina, M.; Lopez-Gonzalez, J.S.; Galicia-Velasco, M.; Aguilar-Cazares, D. The Double-Edge Sword of Autophagy in Cancer: From Tumor Suppression to Pro-tumor Activity. *Front. Oncol.* **2020**, *10*, 578418. [CrossRef] [PubMed]
2. Nixon, A.R. The role of autophagy in neurodegenerative disease. *Nat. Med.* **2013**, *19*, 983–997. [CrossRef]
3. Peng, Y.-F.; Shi, Y.-H.; Shen, Y.-H.; Ding, Z.-B.; Ke, A.-W.; Zhou, J.; Qiu, S.-J.; Fan, J. Promoting Colonization in Metastatic HCC Cells by Modulation of Autophagy. *PLoS ONE* **2013**, *8*, e74407. [CrossRef] [PubMed]
4. O'Connor, S.; Ward, J.W.; Watson, M.; Momin, B.; Richardson, L.C. Hepatocellular carcinoma–United States, 2001–2006. *MMWR Morb. Mortal. Wkly. Rep.* **2010**, *59*, 517–520.
5. Liu, M.; Jiang, L.; Guan, X.-Y. The genetic and epigenetic alterations in human hepatocellular carcinoma: A recent update. *Protein Cell* **2014**, *5*, 673–691. [CrossRef] [PubMed]
6. Liu, H.; Li, H.; Luo, K.; Sharma, A.; Sun, X. Prognostic gene expression signature revealed the involvement of mutational pathways in cancer genome. *J. Cancer* **2020**, *11*, 4510–4520. [CrossRef]
7. Sharma, A.; Biswas, A.; Liu, H.; Sen, S.; Paruchuri, A.; Katsonis, P.; Lichtarge, O.; Dakal, T.C.; Maulik, U.; Gromiha, M.M.; et al. Mutational Landscape of the BAP1 Locus Reveals an Intrinsic Control to Regulate the miRNA Network and the Binding of Protein Complexes in Uveal Melanoma. *Cancers* **2019**, *11*, 1600. [CrossRef]
8. Wu, S.-Y.; Lan, S.-H.; Wu, S.-R.; Chiu, Y.-C.; Lin, X.-Z.; Su, I.-J.; Tsai, T.-F.; Yen, C.-J.; Lu, T.-H.; Liang, F.-W.; et al. Hepatocellular carcinoma-related cyclin D1 is selectively regulated by autophagy degradation system. *Hepatology* **2018**, *68*, 141–154. [CrossRef]
9. Lan, S.; Wu, S.; Zuchini, R.; Lin, X.; Su, I.; Tsai, T.; Lin, Y.; Wu, C.; Liu, H. Autophagy suppresses tumorigenesis of hepatitis B virus-associated hepatocellular carcinoma through degradation of microRNA-224. *Hepatology* **2014**, *59*, 505–517. [CrossRef]
10. Chu, Y.-L.; Ho, C.-T.; Chung, J.-G.; Rajasekaran, R.; Sheen, L.-Y. Allicin Induces p53-Mediated Autophagy in Hep G2 Human Liver Cancer Cells. *J. Agric. Food Chem.* **2012**, *60*, 8363–8371. [CrossRef]
11. Liu, X.-W.; Cai, T.-Y.; Zhu, H.; Cao, J.; Su, Y.; Hu, Y.-Z.; He, Q.-J.; Yang, B. Q6, a novel hypoxia-targeted drug, regulates hypoxia-inducible factor signaling via an autophagy-dependent mechanism in hepatocellular carcinoma. *Autophagy* **2013**, *10*, 111–122. [CrossRef]
12. Hsieh, S.-L.; Chen, C.-T.; Wang, J.-J.; Kuo, Y.-H.; Li, C.-C.; Wu, C.-C. Sedanolide induces autophagy through the PI3K, p53 and NF-?B signaling pathways in human liver cancer cells. *Int. J. Oncol.* **2015**, *47*, 2240–2246. [CrossRef] [PubMed]
13. Shi, Y.-H.; Ding, Z.-B.; Zhou, J.; Qiu, S.-J.; Fan, J. Prognostic significance of Beclin 1-dependent apoptotic activity in hepatocellular carcinoma. *Autophagy* **2009**, *5*, 380–382. [CrossRef] [PubMed]
14. Ding, Z.-B.; Shi, Y.-H.; Zhou, J.; Qiu, S.-J.; Xu, Y.; Dai, Z.; Shi, G.-M.; Wang, X.-Y.; Ke, A.-W.; Wu, B.; et al. Association of Autophagy Defect with a Malignant Phenotype and Poor Prognosis of Hepatocellular Carcinoma. *Cancer Res.* **2008**, *68*, 9167–9175. [CrossRef]
15. Luo, Y.; Liu, F.; Han, S.; Qi, Y.; Hu, X.; Zhou, C.; Liang, H.; Zhang, Z. Autophagy-Related Gene Pairs Signature for the Prognosis of Hepatocellular Carcinoma. *Front. Mol. Biosci.* **2021**, *8*, 670241. [CrossRef]
16. Song, Z.; Zhang, G.; Yu, Y.; Li, S. A Prognostic Autophagy-Related Gene Pair Signature and Small-Molecule Drugs for Hepatocellular Carcinoma. *Front. Genet.* **2021**, *12*, 689801. [CrossRef] [PubMed]
17. Sun, Z.; Lu, Z.; Li, R.; Shao, W.; Zheng, Y.; Shi, X.; Li, Y.; Song, J. Construction of a Prognostic Model for Hepatocellular Carcinoma Based on Immunoautophagy-Related Genes and Tumor Microenvironment. *Int. J. Gen. Med.* **2021**, *14*, 5461–5473. [CrossRef]
18. Xin, X.; Wu, M.; Meng, Q.; Wang, C.; Lu, Y.; Yang, Y.; Li, X.; Zheng, Q.; Pu, H.; Gui, X.; et al. Long noncoding RNA HULC accelerates liver cancer by inhibiting PTEN via autophagy cooperation to miR15a. *Mol. Cancer* **2018**, *17*, 1–16. [CrossRef]
19. Ying, L.; Huang, Y.; Chen, H.; Wang, Y.; Xia, L.; Chen, Y.; Liu, Y.; Qiu, F. Downregulated MEG3 activates autophagy and increases cell proliferation in bladder cancer. *Mol. BioSyst.* **2012**, *9*, 407–411. [CrossRef]
20. Xiong, H.; Ni, Z.; He, J.; Jiang, S.; Li, X.; Gong, W.; Zheng, L.; Chen, S.; Li, B.; Zhang, N.; et al. LncRNA HULC triggers autophagy via stabilizing Sirt1 and attenuates the chemosensitivity of HCC cells. *Oncogene* **2017**, *36*, 3528–3540. [CrossRef]
21. Li, W.; Dong, X.; He, C.; Tan, G.; Li, Z.; Zhai, B.; Feng, J.; Jiang, X.; Liu, C.; Jiang, H.; et al. LncRNA SNHG1 contributes to sorafenib resistance by activating the Akt pathway and is positively regulated by miR-21 in hepatocellular carcinoma cells. *J. Exp. Clin. Cancer Res.* **2019**, *38*, 1–13. [CrossRef]
22. Yang, S.; Zhou, Y.; Zhang, X.; Wang, L.; Fu, J.; Zhao, X.; Yang, L. The prognostic value of an autophagy-related lncRNA signature in hepatocellular carcinoma. *BMC Bioinform.* **2021**, *22*, 1–16. [CrossRef] [PubMed]
23. Sharma, A.; Liu, H.; Herwig-Carl, M.C.; Dakal, T.C.; Schmidt-Wolf, I.G.H. Epigenetic Regulatory Enzymes: Mutation Prevalence and Coexistence in Cancers. *Cancer Investig.* **2021**, *39*, 257–273. [CrossRef] [PubMed]
24. Mao, D.; Zhang, Z.; Zhao, X.; Dong, X. Autophagy-related genes prognosis signature as potential predictive markers for immunotherapy in hepatocellular carcinoma. *PeerJ* **2020**, *8*, e8383. [CrossRef] [PubMed]
25. Li, L.; Xia, S.; Shi, X.; Chen, X.; Shang, D. The novel immune-related genes predict the prognosis of patients with hepatocellular carcinoma. *Sci. Rep.* **2021**, *11*, 1–14. [CrossRef]
26. Dai, Y.; Qiang, W.; Lin, K.; Gui, Y.; Lan, X.; Wang, D. An immune-related gene signature for predicting survival and immunotherapy efficacy in hepatocellular carcinoma. *Cancer Immunol. Immunother.* **2020**, *70*, 967–979. [CrossRef]

27. Deng, X.; Bi, Q.; Chen, S.; Chen, X.; Li, S.; Zhong, Z.; Guo, W.; Li, X.; Deng, Y.; Yang, Y. Identification of a Five-Autophagy-Related-lncRNA Signature as a Novel Prognostic Biomarker for Hepatocellular Carcinoma. *Front. Mol. Biosci.* **2021**, *7*. [CrossRef]

28. Xu, Q.; Wang, Y.; Huang, W. Identification of immune-related lncRNA signature for predicting immune checkpoint blockade and prognosis in hepatocellular carcinoma. *Int. Immunopharmacol.* **2021**, *92*, 107333. [CrossRef]

29. Wang, Y.; Li, W.; Chen, X.; Li, Y.; Wen, P.; Xu, F. MIR210HG predicts poor prognosis and functions as an oncogenic lncRNA in hepatocellular carcinoma. *Biomed. Pharmacother.* **2019**, *111*, 1297–1301. [CrossRef]

30. Hu, B.; Yang, X.-B.; Yang, X.; Sang, X.-T. LncRNA CYTOR affects the proliferation, cell cycle and apoptosis of hepatocellular carcinoma cells by regulating the miR-125b-5p/KIAA1522 axis. *Aging* **2020**, *13*, 2626–2639. [CrossRef]

31. Tian, Q.; Yan, X.; Yang, L.; Liu, Z.; Yuan, Z.; Zhang, Y. lncRNA CYTOR promotes cell proliferation and tumor growth via miR-125b/SEMA4C axis in hepatocellular carcinoma. *Oncol. Lett.* **2021**, *22*, 1–12. [CrossRef] [PubMed]

32. Wu, F.; Wei, H.; Liu, G.; Zhang, Y. Bioinformatics Profiling of Five Immune-Related lncRNAs for a Prognostic Model of Hepatocellular Carcinoma. *Front. Oncol.* **2021**, *11*, 667904. [CrossRef] [PubMed]

33. Li, M.; Liang, M.; Lan, T.; Wu, X.; Xie, W.; Wang, T.; Chen, Z.; Shen, S.; Peng, B. Four Immune-Related Long Non-coding RNAs for Prognosis Prediction in Patients with Hepatocellular Carcinoma. *Front. Mol. Biosci.* **2020**, *7*, 566491. [CrossRef] [PubMed]

34. Sharma, A.; Reutter, H.; Ellinger, J. DNA Methylation and Bladder Cancer: Where Genotype does not Predict Phenotype. *Curr. Genom.* **2020**, *21*, 34–36. [CrossRef]

4. Discussion

The epigenetic regulation plays a crucial role in the treatment and prognosis of cancers (Cheng et al., 2019; Lu et al., 2020). Epigenetic inhibitors, such as DNMT1 inhibitors and HDACs inhibitors, have been developed and proven effective in influencing cancer survival (Eckschlager, Plch, Stiborova, & Hrabeta, 2017; Y. Li & Seto, 2016; Lim et al., 2022; Wong, 2021). While combination therapy of epigenetic inhibitors with other chemotherapy has shown promising results, it is important to consider the side effects associated with both epigenetic inhibitors and chemotherapy agents. Non-oncology drugs with anticancer properties have been shown to impact epigenetic processes (Bezu, Kepp, & Kroemer, 2022; Bridgeman, Ellison, Melton, Newsholme, & Mamotte, 2018).To mitigate side effects associated with epigenetic drugs, exploring the synergistic effects of non-oncology drugs in combination with epigenetic inhibitors can be advantageous for minimizing overall side effects in combination therapy. Additionally, non-coding RNAs (ncRNAs), especially long non-coding RNAs (lncRNAs), have emerged as potential prognostic biomarkers or potential targets for some cancers (Cao et al., 2023; Gao et al., 2023; Khanmohammadi & Fallahtafti, 2023; Zhang et al., 2023). Therefore, exploring potential lncRNAs can contribute to predicting patient risk and identifying novel cancer targets. In summary, this cumulative dissertation focus on the following questions in hematological malignancies (leukemia and myeloma) and liver cancer: 1) Exploring potential non oncology drugs that synergize with epigenetic drugs, minimizing side effects. 2) Investigating the correlation between the epigenetics and the survival of cancer patients, particularly focusing on lncRNAs as potential prognostic markers.

In the first publication, our study focuses on exploring the potential of a non oncology drug in combination with epigenetic drugs in hematologic malignancies (leukemia and multiple myeloma) and liver cancer. In our investigation, we studied meticrane, a thiazide diuretic drug commonly used for essential hypertension. Previous studies have shown improved survival in mesothelioma mice through the combination of meticrane with CTLA-4 treatment (Lesterhuis et al., 2015), however the anticancer effect of meticrane remains unclear. Therefore, this study represents the first investigation of meticrane's anti-cancer abilities in hematologic malignancies and liver cancer cell lines. Our findings revealed that meticrane exhibited anticancer activity against leukemia and

liver cancer cells, while showing limited or no effect on myeloma cells. Subsequently, we examined the combination effect of meticrane with several established epigenetic drugs. The combination of meticrane with epigenetic inhibitors demonstrated additive or synergistic effects on leukemia and liver cancer cells, potentially reducing the toxicity associated with epigenetic drugs for patients. Furthermore, we conducted molecular docking studies to assess the binding affinity of meticrane with epigenetic targets, specifically DNMT1 and HDACs. Notably, the results indicated significant binding affinity scores of meticrane against most HDACs. Overall, our study investigated meticrane, a clinical non-oncology drug, as a potential candidate for combination therapy with epigenetic inhibitors. The synergy observed between meticrane and epigenetic inhibitors may help reduce the side effects associated with epigenetic inhibitor treatment in clinical settings.

In the second publication, we focused on the role of G protein-coupled receptors (GPCRs) in the tumorigenesis and development of hepatocellular carcinoma (HCC), a type of liver cancer (Peng et al., 2018). Additionally, the regulatory gene RGS20 has been associated with several cancers in previous studies (Huang, He, & Wei, 2018; Jiang, Shen, Zhang, He, & Wan, 2021; G. Li et al., 2019; Shi, Tong, Han, & Hu, 2022; L. Yang, Lee, Leung, & Wong, 2016; Zhao et al., 2018). We aimed to evaluate the prognostic ability of RGS20 in HCC. Our findings revealed that the expression of the RGS20 gene was significantly upregulated in HCC tissue compared to adjacent tissue. Moreover, we confirmed its prognostic capability in predicting outcomes for HCC patients. Additionally, we observed that RGS20 was associated with five long intergenic non-coding RNAs (lincRNAs): LINC00511, PVT1, MIR4435-2HG, BCYRN1, and MAPKAPK5-AS1. These lincRNAs have previously been implicated in the proliferation, survival, and progression of HCC (Ding, Jin, Hao, Kang, & Ma, 2020; Gou, Zhao, & Wang, 2017; Kong et al., 2019; L. Wang et al., 2021; R. P. Wang, Jiang, Jiang, Wang, & Chen, 2019). Our results suggest that lincRNAs may contribute to the role of RGS20 in HCC patients, potentially influencing disease progression and outcomes.

In the third publication, we established a ferroptosis-related signature in multiple myeloma based on ferroptosis genes, which showed good performance in predicting the survival of myeloma patients. By investigating the correlation of this signature with long

non-coding RNAs (lncRNAs), we found a strong association with the oncogenic lncRNA CRNDE, which has been implicated in many cancers (Ghafouri-Fard, Safarzadeh, Hussen, Taheri, & Mokhtari, 2023; C. Yang, Jiang, Hu, Li, & Qi, 2023), including multiple myeloma (David et al., 2021). CRNDE also exhibited potential interactions with a majority of ferroptosis genes and proteins, suggesting its involvement in the prognostic signature for myeloma survival. While lncRNAs have been shown to affect prognostic genes and signatures in cancers, further evaluation of the direct interaction between lncRNAs and patient survival is warranted. In light of these findings, we proceeded to investigate the role of lncRNAs in relation to the survival of liver cancer patients.

In the fourth publication, we focused on autophagy and immune-related long non-coding RNAs (lncRNAs) in liver cancer. Based on these lncRNAs, we constructed a signature consisting of three specific lncRNAs: MIR210HG, AC099850.3, and CYTOR. This signature proved to be an independent and robust prognostic factor for clinical hepatocellular carcinoma (HCC) patients. Interestingly, these three lncRNAs (MIR210HG, AC099850.3, and CYTOR) within the signature were found to impact the proliferation and growth of liver cancer (Hu, Yang, Yang, & Sang, 2020; Tian et al., 2021; Y. Wang et al., 2019; Wu, Wei, Liu, & Zhang, 2021). Overall, our findings demonstrate the interaction between lncRNAs and the survival of cancer patients, suggesting their potential as targets for improving outcomes in cancer patients.

4.1 Strengths and limitations

This dissertation has several strengths, as outlined below: 1) The utilization of meticrane, a thiazide diuretic drug, as a potential anticancer agent is advantageous due to its lower side effects compared to traditional chemotherapy. When combined with epigenetic drugs, meticrane demonstrates synergistic anticancer effects, which can contribute to reducing the side effects and toxicity associated with epigenetic drugs. 2) The strategy of drug repositioning, or repurposing, is an effective and cost-efficient approach for developing new anti-tumor drugs. In this study, meticrane, an already available drug used for treating essential hypertension, is repurposed for potential cancer treatment. This approach saves time and resources by leveraging existing drug knowledge and clinical data. 3) By utilizing publicly available RNA sequencing and clinical data, the dissertation establishes a set of lncRNAs that are related to cancer survival. These

lncRNAs have the potential to aid in the classification of cancer patients at the time of diagnosis. Additionally, they provide valuable insights into potential targets for cancer therapies at the epigenetic level, offering new avenues for treatment development. Overall, these strengths enhance the dissertation's impact and potential contributions to the field of cancer research and therapy.

This dissertation also has certain limitations, which are as follows: 1) The observed anticancer ability of meticrane was achieved at a relatively high concentration. Therefore, it is recommended to conduct screening with variable concentrations ranging from the minimum to the maximum effective dose. Additionally, synthesizing next-generation compounds based on the structure of meticrane that have a stronger tendency to inhibit the proliferation of cancer cells may partially address this limitation. 2) The anticancer effect of meticrane was only observed in vitro. To fully evaluate its potential as a cancer treatment, further studies are needed to assess its efficacy in vivo, using animal models or clinical trials. 3) Although the relationship between lncRNAs and the survival of cancer patients was observed, the underlying mechanisms through which these lncRNAs contribute to cancer development and progression remain unclear. Further research is necessary to elucidate the specific roles and mechanisms of action of these lncRNAs in cancer, which will provide valuable insights for future investigations. Acknowledging these limitations highlights areas for future research and refinement, ensuring the advancement of knowledge and potential improvements in cancer treatment approaches.

4.2 Implication for Practice and Research

The investigation of drugs with reduced toxicity to normal tissues and their synergistic effects with epigenetic drugs is crucial, considering the potential side effects associated with current cancer treatments. Drug repositioning, as an alternative strategy, offers a cost-effective approach to evaluate the anticancer potential of known drugs used for other diseases (Turabi et al., 2022). In our study, we demonstrated that meticrane, a non-oncology drug used for essential hypertension, exhibits anticancer abilities against cancer cells. Importantly, meticrane has shown a synergistic effect when combined with epigenetic drugs. This combination therapy has the potential to reduce the required dosage of epigenetic drugs, thereby limiting side effects for cancer patients. Additionally, meticrane is readily available on the market, saving time and costs associated with new

drug development. Furthermore, the advantages of meticrane extend beyond epigenetic drugs and can benefit other chemotherapies as well. Notably, based on the information gained from meticrane's anticancer ability and structure, it is possible to design more effective and sensitive drugs with limited toxicity. This approach holds promise for the development of novel anticancer treatments. Increasing evidence supports the significant role of the epigenetics, particularly lncRNAs, in cancer (Gao et al., 2023; Xia et al., 2023). Several lncRNAs have emerged as potential prognostic markers for cancer patients (Chen et al., 2023; W. Li, Hong, & Lai, 2023; Lin et al., 2023). Moreover, with the advancements in RNA-based therapy, FDA and/or EMA-approved RNA-based therapeutics such as antisense oligonucleotides and small interfering RNAs have paved the way for lncRNA-based therapeutics, which are gaining attention as alternative treatment options (Winkle, El-Daly, Fabbri, & Calin, 2021). Therefore, investigating lncRNAs holds great potential for predicting prognosis and identifying cancer targets for patients. In this dissertation, we have identified several lncRNAs associated with the survival of liver cancer or multiple myeloma. As their prognostic capabilities have been confirmed in these specific cancers, they may serve as predictive factors for classifying patients into good or poor prognosis categories at the time of diagnosis. Among these lncRNAs, some have been demonstrated to be involved in cancer proliferation and growth, while others have not. For the lncRNAs that have been implicated in cancer proliferation and growth, their effects on tumors may be mediated through specific tumor-related genes or pathways, thus providing potential therapeutic targets. Further investigation into the mechanisms of lncRNAs that have not yet been proven to be associated with cancer proliferation and growth is warranted. Exploring their potential roles may uncover novel targets for cancer treatment and intervention.

4.3 References

Bezu, L., Kepp, O., & Kroemer, G. (2022). Impact of local anesthetics on epigenetics in cancer. *Front Oncol, 12*, 849895. doi:10.3389/fonc.2022.849895

Bridgeman, S. C., Ellison, G. C., Melton, P. E., Newsholme, P., & Mamotte, C. D. S. (2018). Epigenetic effects of metformin: From molecular mechanisms to clinical implications. *Diabetes Obes Metab, 20*(7), 1553-1562. doi:10.1111/dom.13262

Cao, J., Liu, L., Xue, L., Luo, Y., Liu, Z., & Guo, J. (2023). Long non-coding RNA TTTY14 promotes cell proliferation and functions as a prognostic biomarker in testicular germ cell tumor. *Heliyon, 9*(5), e16082. doi:10.1016/j.heliyon.2023.e16082

Chen, L., Zhang, L., He, H., Shao, F., Gao, Y., & He, J. (2023). Systemic Analyses of Cuproptosis-Related lncRNAs in Pancreatic Adenocarcinoma, with a Focus on the Molecular Mechanism of LINC00853. *Int J Mol Sci, 24*(9). doi:10.3390/ijms24097923

Cheng, Y., He, C., Wang, M., Ma, X., Mo, F., Yang, S., . . . Wei, X. (2019). Targeting epigenetic regulators for cancer therapy: mechanisms and advances in clinical trials. *Signal Transduct Target Ther, 4*, 62. doi:10.1038/s41392-019-0095-0

David, A., Zocchi, S., Talbot, A., Choisy, C., Ohnona, A., Lion, J., . . . Garrick, D. (2021). The long non-coding RNA CRNDE regulates growth of multiple myeloma cells via an effect on IL6 signalling. *Leukemia, 35*(6), 1710-1721. doi:10.1038/s41375-020-01034-y

Ding, S., Jin, Y., Hao, Q., Kang, Y., & Ma, R. (2020). LncRNA BCYRN1/miR-490-3p/POU3F2, served as a ceRNA network, is connected with worse survival rate of hepatocellular carcinoma patients and promotes tumor cell growth and metastasis. *Cancer Cell Int, 20*, 6. doi:10.1186/s12935-019-1081-x

Eckschlager, T., Plch, J., Stiborova, M., & Hrabeta, J. (2017). Histone Deacetylase Inhibitors as Anticancer Drugs. *Int J Mol Sci, 18*(7). doi:10.3390/ijms18071414

Gao, N., Jiang, G., Gao, Z., Cui, M., Li, J., Liu, H., & Fan, T. (2023). Long non-coding RNA LINC00707, a prognostic marker, regulates cell proliferation, apoptosis, and

EMT in esophageal squamous cell carcinoma. *Am J Transl Res, 15*(4), 2426-2442.

Ghafouri-Fard, S., Safarzadeh, A., Hussen, B. M., Taheri, M., & Mokhtari, M. (2023). Contribution of CRNDE lncRNA in the development of cancer and the underlying mechanisms. *Pathol Res Pract, 244*, 154387. doi:10.1016/j.prp.2023.154387

Gou, X., Zhao, X., & Wang, Z. (2017). Long noncoding RNA PVT1 promotes hepatocellular carcinoma progression through regulating miR-214. *Cancer Biomark, 20*(4), 511-519. doi:10.3233/CBM-170331

Hu, B., Yang, X. B., Yang, X., & Sang, X. T. (2020). LncRNA CYTOR affects the proliferation, cell cycle and apoptosis of hepatocellular carcinoma cells by regulating the miR-125b-5p/KIAA1522 axis. *Aging (Albany NY), 13*(2), 2626-2639. doi:10.18632/aging.202306

Huang, G., He, X., & Wei, X. L. (2018). lncRNA NEAT1 promotes cell proliferation and invasion by regulating miR- 365/RGS20 in oral squamous cell carcinoma. *Oncol Rep, 39*(4), 1948-1956. doi:10.3892/or.2018.6283

Jiang, L., Shen, J., Zhang, N., He, Y., & Wan, Z. (2021). Association of RGS20 expression with the progression and prognosis of renal cell carcinoma. *Oncol Lett, 22*(3), 643. doi:10.3892/ol.2021.12904

Khanmohammadi, S., & Fallahtafti, P. (2023). Long non-coding RNA as a novel biomarker and therapeutic target in aggressive B-cell non-Hodgkin lymphoma: A systematic review. *J Cell Mol Med*. doi:10.1111/jcmm.17795

Kong, Q., Liang, C., Jin, Y., Pan, Y., Tong, D., Kong, Q., & Zhou, J. (2019). The lncRNA MIR4435-2HG is upregulated in hepatocellular carcinoma and promotes cancer cell proliferation by upregulating miRNA-487a. *Cell Mol Biol Lett, 24*, 26. doi:10.1186/s11658-019-0148-y

Lesterhuis, W. J., Rinaldi, C., Jones, A., Rozali, E. N., Dick, I. M., Khong, A., . . . Lake, R. A. (2015). Network analysis of immunotherapy-induced regressing tumours identifies novel synergistic drug combinations. *Sci Rep, 5*, 12298. doi:10.1038/srep12298

Li, G., Wang, M., Ren, L., Li, H., Liu, Q., Ouyang, Y., . . . Li, F. (2019). Regulator of G protein signaling 20 promotes proliferation and migration in bladder cancer via NF-kappaB signaling. *Biomed Pharmacother, 117*, 109112. doi:10.1016/j.biopha.2019.109112

Li, W., Hong, G., & Lai, X. (2023). INKA2-AS1 Is a Potential Promising Prognostic-Related Biomarker and Correlated with Immune Infiltrates in Hepatocellular Carcinoma. *Mediators Inflamm, 2023*, 7057236. doi:10.1155/2023/7057236

Li, Y., & Seto, E. (2016). HDACs and HDAC Inhibitors in Cancer Development and Therapy. *Cold Spring Harb Perspect Med, 6*(10). doi:10.1101/cshperspect.a026831

Lim, B., Yoo, D., Chun, Y., Go, A., Cho, K. J., Choi, D., . . . Choi, G. (2022). The preclinical efficacy of the novel hypomethylating agent NTX-301 as a monotherapy and in combination with venetoclax in acute myeloid leukemia. *Blood Cancer J, 12*(4), 57. doi:10.1038/s41408-022-00664-y

Lin, K., Zhou, Y., Lin, Y., Feng, Y., Chen, Y., & Cai, L. (2023). Senescence-Related lncRNA Signature Predicts Prognosis, Response to Immunotherapy and Chemotherapy in Skin Cutaneous Melanoma. *Biomolecules, 13*(4). doi:10.3390/biom13040661

Lu, Y., Chan, Y. T., Tan, H. Y., Li, S., Wang, N., & Feng, Y. (2020). Epigenetic regulation in human cancer: the potential role of epi-drug in cancer therapy. *Mol Cancer, 19*(1), 79. doi:10.1186/s12943-020-01197-3

Peng, W. T., Sun, W. Y., Li, X. R., Sun, J. C., Du, J. J., & Wei, W. (2018). Emerging Roles of G Protein-Coupled Receptors in Hepatocellular Carcinoma. *Int J Mol Sci, 19*(5). doi:10.3390/ijms19051366

Shi, D., Tong, S., Han, H., & Hu, X. (2022). RGS20 Promotes Tumor Progression through Modulating PI3K/AKT Signaling Activation in Penile Cancer. *J Oncol, 2022*, 1293622. doi:10.1155/2022/1293622

Tian, Q., Yan, X., Yang, L., Liu, Z., Yuan, Z., & Zhang, Y. (2021). lncRNA CYTOR promotes cell proliferation and tumor growth via miR-125b/SEMA4C axis in hepatocellular carcinoma. *Oncol Lett, 22*(5), 796. doi:10.3892/ol.2021.13057

Turabi, K. S., Deshmukh, A., Paul, S., Swami, D., Siddiqui, S., Kumar, U., . . . Aich, J. (2022). Drug repurposing-an emerging strategy in cancer therapeutics. *Naunyn Schmiedebergs Arch Pharmacol, 395*(10), 1139-1158. doi:10.1007/s00210-022-02263-x

Wang, L., Sun, L., Liu, R., Mo, H., Niu, Y., Chen, T., . . . Liu, Q. (2021). Long non-coding RNA MAPKAPK5-AS1/PLAGL2/HIF-1alpha signaling loop promotes hepatocellular carcinoma progression. *J Exp Clin Cancer Res, 40*(1), 72. doi:10.1186/s13046-021-01868-z

Wang, R. P., Jiang, J., Jiang, T., Wang, Y., & Chen, L. X. (2019). Increased long noncoding RNA LINC00511 is correlated with poor prognosis and contributes to cell proliferation and metastasis by modulating miR-424 in hepatocellular carcinoma. *Eur Rev Med Pharmacol Sci, 23*(8), 3291-3301. doi:10.26355/eurrev_201904_17691

Wang, Y., Li, W., Chen, X., Li, Y., Wen, P., & Xu, F. (2019). MIR210HG predicts poor prognosis and functions as an oncogenic lncRNA in hepatocellular carcinoma. *Biomed Pharmacother, 111*, 1297-1301. doi:10.1016/j.biopha.2018.12.134

Winkle, M., El-Daly, S. M., Fabbri, M., & Calin, G. A. (2021). Noncoding RNA therapeutics - challenges and potential solutions. *Nat Rev Drug Discov, 20*(8), 629-651. doi:10.1038/s41573-021-00219-z

Wong, K. K. (2021). DNMT1: A key drug target in triple-negative breast cancer. *Semin Cancer Biol, 72*, 198-213. doi:10.1016/j.semcancer.2020.05.010

Wu, F., Wei, H., Liu, G., & Zhang, Y. (2021). Bioinformatics Profiling of Five Immune-Related lncRNAs for a Prognostic Model of Hepatocellular Carcinoma. *Front Oncol, 11*, 667904. doi:10.3389/fonc.2021.667904

Xia, A., Yue, Q., Zhu, M., Xu, J., Liu, S., Wu, Y., . . . Sun, B. (2023). The cancer-testis lncRNA LINC01977 promotes HCC progression by interacting with RBM39 to prevent Notch2 ubiquitination. *Cell Death Discov, 9*(1), 169. doi:10.1038/s41420-023-01459-1

Yang, C., Jiang, Y., Hu, F., Li, Q., & Qi, B. (2023). Implications of CRNDE in prognosis, tumor immunity, and therapeutic sensitivity in low grade glioma patients. *Cancer Cell Int, 23*(1), 93. doi:10.1186/s12935-023-02930-w

Yang, L., Lee, M. M., Leung, M. M., & Wong, Y. H. (2016). Regulator of G protein signaling 20 enhances cancer cell aggregation, migration, invasion and adhesion. *Cell Signal, 28*(11), 1663-1672. doi:10.1016/j.cellsig.2016.07.017

Zhang, Y., Wang, Y., He, X., Yao, R., Fan, L., Zhao, L., . . . Pang, Z. (2023). Genome instability-related LINC02577, LINC01133 and AC107464.2 are lncRNA prognostic markers correlated with immune microenvironment in pancreatic adenocarcinoma. *BMC Cancer, 23*(1), 430. doi:10.1186/s12885-023-10831-4

Zhao, J., Cheng, W., He, X., Liu, Y., Li, J., Sun, J., . . . Gao, Y. (2018). Construction of a specific SVM classifier and identification of molecular markers for lung adenocarcinoma based on lncRNA-miRNA-mRNA network. *Onco Targets Ther, 11*, 3129-3140. doi:10.2147/OTT.S151121

5. Acknowledgements